University of Messina

University of Reggio Calabria

DOCTORATE COURSE IN

CIVIL, ENVIRONMENTAL AND SAFETY ENGINEERING

XXXV CICLE

Curriculum: Science and technology, materials, energy, and complex systems for distributed computing and networks (ICAR/03 – CHIM/07)

DEVELOPMENT OF HETEROGENEOUS CATALYTIC SYSTEMS FOR CHEMICAL AND ENVIRONMENTAL ENGINEERING PROCESSES

Head of Doctoral School:
Prof. Gaetano Bosurgi

PhD:
Mariachiara Miceli

Supervisor:
Prof. Francesco Mauriello

Co-Supervisor:
Ing. Angela Malara
Dott.ssa Emilia Paone

A.A 2021/2022

Index

Abstract

The energy transition is the shift from an energy model based on fossil fuels to one based on renewable and clean energy sources (photovoltaic, wind, hydroelectric, geothermal). This is not a simple replacement of energy sources, but rather the radical transformation of a system for the generation, distribution, and consumption of energy. Heterogeneous catalysis is a crucial tool for achieving a sustainable use of resources for energy, chemicals, and materials production, as well as for preserving the environment. The use of heterogeneous catalysts to produce fuels and chemicals reduces energy demand and minimizes the formation of non-recyclable wastes, by increasing the activity and selectivity of the conversion of fossil and renewable resources.

The design, implementation, and testing of catalytic systems for three selected reactions have been investigated in detail in this thesis, namely the reforming of H_2, the CO_2 methanation and the exploitation of lignin through a waste-derived catalyst.

Introduction

Environmental degradation, global warming, and dwindling fossil resources are formidable challenges that the 21st century will inherit for humankind. All these issues coincide with the rapid economic expansion in China and India, home to 2.3 billion people.

The latest IPCC (International Panel Climate Change) report (Climate Change 2022: Mitigation of Climate Change) argues that stabilizing the climate will require fast actions, highlighting that the issue of climate change, due to greenhouse gas (GHG) emissions, is now broadly acknowledged as one of the major challenges facing humankind, that requires urgent attention. Then, considerable efforts on clean energy processes and technologies should be recommended to address this issue.

The energy transition is the shift from an energy production and consumption model based on fossil fuels (such as coal, oil, and methane) to one based on renewable and clean energy sources (photovoltaic, wind, hydroelectric, geothermal).

This is not a simple replacement of energy sources, but rather the radical transformation of a system for the generation, distribution, and consumption of energy. Industrial, tertiary, residential, and public sectors will undergo a profound and intricate transformation towards a more sustainable and efficient model.

The ecological transition is one of the pillars of the Next Generation EU project and, consequently, of the PNRR (National Recovery and Resilience Plan), constituting one of the most important directives for the development and recovery of Italian SMEs and the national economy.

In this context is placed the research developed for the doctoral dissertation, with three main focuses:

- Production of "blue hydrogen", namely the hydrogen from natural gas with carbon capture and storage. Hydrogen is indicated to be an important energy vector during (and after) the transition to GHG emission-free economies. The requirement is that its production results in extremely low greenhouse gas emissions, such that the entire process of hydrogen production and use could be made net-zero with a feasible level of carbon dioxide removal from the atmosphere.
- Methanation of carbon dioxide captured from flue gases into synthetic natural gas (SNG) aims to create a closed carbon cycle in which the excess of H_2 produced from renewables is used to convert CO_2 released from existing conventional power plants into a reliable and high-energy-density carrier, namely CH_4. Re-use of waste through a circular economy.
- The exploitation of lignocellulosic residues and waste with a view to a circular economy that aims to preserve the value of products, materials, and resources for as long as possible by returning them to the product cycle at the end of their useful lives, while minimizing waste production.

Thus, in this work three highly important heterogeneous catalytic reactions have been chosen as case studies. The thesis consists of three separate and independent parts, treating each of these reactions.

The common thread of the work research in this dissertation is the advancement of heterogeneous catalytic systems for the aforementioned processes.

Heterogeneous catalysis is a crucial tool for achieving a sustainable use of resources for energy, chemicals, and materials production, as well as for preserving and rehabilitating the environment.

Using heterogeneous catalysts to produce fuels and chemicals reduces energy demand and minimizes the formation of non-recyclable wastes by increasing the activity and selectivity of the conversion of fossil and renewable resources.

In the past, heterogeneous catalysts were developed through trial and error. The development of the ammonia synthesis process in the early twentieth century exemplifies how empirical screening can result in a robust catalytic process. This example also illustrates the enormous potential global impact of heterogeneous catalysis; in this case, the dramatic increase in agricultural production enabled by synthetic fertilizers was estimated to provide food for nearly half of the world's population in 2008.

This study focuses on the design, the implementation, and the testing of heterogeneous catalysts, characterized by the formation of at least two phases, reactants and products. The catalyst materials studied in this dissertation include monometallic/bimetallic catalysts, metal-supported zeolite catalysts and catalyst derived from waste, that have been adapted to targeted applications: the reforming of H_2, the methanation of CO_2 and the lignin exploitation.

In the first chapter, the selected processes are described, and the current state of the art is analysed. In the second chapter, the development of each catalytic system and an extensive discussion of their characterization are detailed. The third chapter describes the outcomes of the catalytic activity and

the discussion of the research activities. Finally, the fourth chapter presents future perspectives and concluding remarks.

Chapter 1

Background of the research

1.1 **Agenda 2030 and 12 Green Chemistry Principles**

On 25 September 2015, world leaders of 193 countries met in New York to define the Sustainable Development Goals for 2030, the so-called SDGs or "Global Goals"; SDGs face issues that are crucial for achieving sustainable development [1]. Among challenges: health and education, economic growth, social inclusion, clean water and sanitation, energy availability and affordability, responsible consumption and production of resources, and actions against climate change. All states, and not just the developing countries, are called to address and achieve the SDGs since they are intended to reflect the complete spectrum of sustainability concerns on a global level [2].

These 17 goals (Table 1.1) structured around five pillars (5Ps) - people, planet, prosperity, peace and partnership - aim to improve the world welfare by social, environmental, and economic sustainability [3]. The first pillar, "People", aims to eradicate poverty and hunger, the second, "Planet", claims the preservation of the environment; the third, "Prosperity", ensures that all people can live prosperous and fulfilling lives; the fourth, "Peace", urges the promotion of peaceful and inclusive societies; and the fifth, "Partnership", aids in the establishment of a network and the mobilization of resources to carry out these goals [4]. Each SDG includes a set of targets and indicators: targets describe the goals; indicators are the metrics by which the world attempts to monitor the attainment of these goals [5].

The SDG7, "Affordable and Clean Energy", in particular, specifies the steps that must be taken so that everyone has access to "affordable, reliable, sustainable, and modern energy". The access to energy shall be considered a fundamental need for human development and therefore a human right, although it is not specifically mentioned in the SDG7 [6]. A better accessibility to sustainable energy services is necessary to improve people's health and

quality of life and to achieve other SDGs such as SDG 1 (no poverty) and SDG 10 (reduced inequality). Nevertheless, depending on the source, producing energy may be a very polluting and damaging activity to the environment, just think of greenhouse gases, responsible for the global warming released by thermal power plants that use coal as raw material [7]. Given that energy-related carbon dioxide (CO_2) emissions account for two-thirds of all greenhouse gases, a shift away from fossil fuels toward low-carbon solutions will be necessary [8]. It is for that reason that the SDG7's second target calls for a considerable rise in the proportion of renewable energy by the year 2030.

The Intergovernmental Panel on Climate Change (IPCC) estimates that by 2050, 70-85% of the world's electricity will come from renewable sources [9]. Although the renewable energy generation sources present different disadvantages such as dependence on weather conditions or low energy efficiency, the amount of greenhouse gases or pollutants emitted into the air during combustion is lower than that emitted from fossil fuel technologies. This translates into a lower carbon footprint and a positive impact on the preservation of the environment. The third and last target of SDG7 aims at doubling the rate of improvement in energy efficiency by 2030. Energy efficiency reduces energy uses and, as a result, the greenhouse gases emissions, resolves the issue of dependence on energy imports and the conflicts caused by energy distribution. Therefore, the targets of the SDG 7 also contribute to the achievement of the SDG13 that focuses on climate change and the SDG16, that promotes peaceful and inclusive societies.

Table 1.1. The 17 Sustainable Development Goals of Agenda 2030.

17 Sustainable Development Goals		
	No poverty	End poverty in all its forms everywhere
	Zero hunger	End hunger, achieve food security and improved nutrition and promote sustainable agriculture
	Good health and well-being	Ensure healthy lives and promote well-being for all at all ages
	Quality education	Ensure inclusive and equitable quality education and promote lifelong learning opportunities for all
	Gender equality	Achieve gender equality and empower all women and girls
	Clean water and sanitation	Ensure availability and sustainable management of water and sanitation for all
	Affordable and clean energy	Ensure access to affordable, reliable, sustainable and modern energy for all
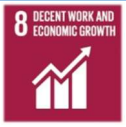	Decent work and economy growth	Promote sustained, inclusive and sustainable growth, full and productive employment and decent work for
	Industry, innovation and infrastructure	Build resilient infrastructure, promote inclusive and sustainable industrialization and foster innovation
	Reduced inequalities	Reduce inequality within and among countries
	Sustainable cities and communities	Make cities and human settlements inclusive, save, resilient and sustainable
	Responsible consumption and production	Ensure sustainable consumption and production patterns

	Climate action	Take urgent action to combat climate change and its impacts
	Life below water	Conserve and sustainably use the oceans, seas and marine resources for sustainable development
	Life on land	Protect, restore and promote sustainable use of terrestrial ecosystems, sustainably manage forests, combat desertification, and halt and reverse land degradation and halt biodiversity
	Peace, justice and strong institutions	Promote peaceful and inclusive societies for sustainable development, provide access to justice for all and build effective, accountable and inclusive institutions at all levels
	Partnership for the goals	Strengthen the means of implementation and revitalize the Global Partnership for Sustainable Development

The Green Chemistry has a key role in achieving sustainable development and its principles are highly related to SDGs.

The concept of Green Chemistry was first introduced in the U.S. at the beginning of the 1990s as a response to the Pollution Prevention Act of 1900, a federal act that led the U.S. to adopt a national policy based on the prevention or reduction of pollution at its source, wherever feasible. The term "Green Chemistry", coined by Paul Thomas Anastas, a Professor of Chemistry and Chemical Engineering at Yale University in the United States, indicates a branch of chemistry and chemical engineering focused on producing the chemicals we need on a daily basis using processes and chemical reactions that produce and use fewer (or, ideally, no) hazardous substances. But since no chemical process can be considered perfectly "green", the negative impact of the chemistry on the environment can be minimized by applying, wherever possible, the so- called "Twelve Principles of Green Chemistry", developed and published in 1998 by Paul Anastas and John Warner in their publication

"Green Chemistry, Theory and Practice", and below described in Table 1.2. These guiding principles, still in use today, represent essentially a checklist on how to lessen the harms that chemicals and chemical synthesis may cause to the environment and human health [3] and may be the key to reach various SDGs, such as increased health and wellbeing, access to clean water, and the production and use of renewable energy. They can be used in practically every aspect of chemistry e.g. to catalyse a process, create less polluting reaction conditions, and synthesize molecules with desired structures and properties). According to these principles, the use of more environmentally friendly chemicals and more efficient processes, planned ahead, will prevent or reduce the production of wastes and their effect on the environment. The aphorism ''an ounce of prevention is worth a pound of cure'' is at the heart of the first of the Twelve Principles of Green Chemistry: "it is better to prevent waste than to treat or clean up waste after it is formed". The Green Chemistry, therefore, distances itself from the historic "command-and-control" approach toward environmental problems and prefer prevention of the wastes rather than their treatment, control and disposal. In Green Chemistry, prevention is the approach to be followed to reduce the risk, according to the relation:

$$\text{Risk} = f(\text{hazard} \times \text{exposure})$$

The risk of accidents such as explosions, fires, environmental spills, and other releases are less likely when the hazard component of the equation is minimized, and this is possible by using of innocuous chemicals and procedures [8]. A preventive approach preserves not only human and natural resources but will also often offer economic advantages. When wastes are eliminated, their treatment and disposal are not required. Decreased solvent usage and fewer processing steps result in lower production material and energy costs and higher material efficiency [10]. It was highlighted that eliminating waste at the source not only lowers the expense of its disposal but also boosts economic competitiveness by making better use of raw materials.

Table 1.2. The Twelve Principles of Green Chemistry proposed by Anastas and Warner [11].

The Twelve Principles of Green Chemistry			
I	Prevent waste instead of treating it	VII	Preferably use renewable raw materials
II	Design atom-efficient synthetic methods	VIII	Avoid unnecessary derivatisation
III	Choose synthetic routes using no-toxic compounds where possible	IX	Replace stoichiometric reagents with catalytic cycles
IV	Design new products that preserve functionality while reducing toxicity.	X	Design new products with biodegradable capabilities
V	Minimise the use of auxiliary reagents and solvents	XI	Develop real-time and on-line process analysis and monitoring methods
VI	Design processes with minimal energy requirements	XII	Choose feedstocks and design processes that minimise the chance of accidents.

To compare the efficiency or sustainability of different chemical processes, we need appropriate metrics and indicators that measure greenness of processes and products. The E(nvironmental) factor (kg waste/kg product) and atomic economy (mol wt of product/sum of mol wt of starting materials) are the two oldest green metrics, born in an effort to prompt synthetic organic chemists to pursue "greener chemistry". The E factor which Roger Sheldon first developed in 1994, takes into account the amount of waste produced in the process such as solvent losses, spent catalysts and catalyst supports, leftover reactants and anything else that can be regarded as a "waste". Higher

E values are generally less desirable since the E factor is linked to more waste production and, consequently, greater environmental impact. Zero is the ideal value since it fully encapsulates the first of Green Chemistry's twelve guiding principles [12]. The chemical industry, particularly the pharmaceutical business, has largely accepted the E factor as a helpful instrument for evaluating the environmental impact of production processes. However, this factor just considers the mass of wastes produced and not their nature, assigning all waste types the same weighting. While a few thousand tons of carbon dioxide produced yearly may not cause much concern since the amount released into the atmosphere is insignificant in comparison to the millions of tons emitted when burning fossil fuels, a few kilograms of heavy metal wastes, instead, can cause alarm considering their toxicity. Hence, Sheldon introduced a new metric, the "environmental quotient" (EQ), calculated by multiplying the E factor with a number Q assigned to a particular kind of waste. However, while E is simply assessed by straightforward weighing, Q is far more arbitrary and liable to change when new knowledge is learned about the potential impact of specific types of wastes [12].

The Atom Economy first proposed by Barry Trost in 1991, is similar to the E-factor. It takes into account the quantity and type of reactant atoms that make up the final product. If all components employed in a reaction are incorporate into the final product, the depletion of raw resources and the production of waste are minimized. Since the most significant environmental issue now plaguing our planet is global warming caused by greenhouse gases, particularly carbon dioxide, Christensen et al. proposed the usage of the climate factor (C-factor), to measure the carbon footprint of chemicals and therefore, the CO_2 burden of chemical processes, calculated as the total mass of CO_2 released, divided by the amount of product generated (kg CO_2/kg product).

Green strategies in chemicals manufacture concern all aspects of the process life-cycle, and include, other than prevention of waste production, the design of chemicals which can be recycled or safely disposed. It also concerns the use of catalysts rather than stoichiometric reagents, the elimination or the recycling of solvents in chemical processes, when it is possible, or the replacement of toxic solvents with environmentally benign solvents such as water, fluorous and ionic liquids, supercritical media, and their various combinations. The implementation of green chemistry is essential if the expanding global population is to enjoy an increased standard of living without having a negative impact on the health of the planet; two requirements must be met for a technology to be considered sustainable: natural resources should be consumed at rates that do not deplete supply over time, and waste must be produced to rates that are easily assimilable by the natural environment.

The Brundtland Commission (1987) defined ***sustainable development*** as "development that meets the needs of the present without compromising the ability of future generations to meet their own needs" [13]. The sustainable development can be reached using various approaches, and this is where green chemistry comes in. Green Chemistry uses various monitoring tools (such as life-cycle assessment) and operational tools (such as catalysis).

Life-cycle assessment is one instrument that aids in assessing the environmental effect of a chemical product or process (LCA). LCA methodology is based on ISO 14040 and consists of four distinct analytical steps: defining the scope and the goal of the study, developing an inventory of all the environmental interventions, analysing the impact, and lastly interpreting the results in order to identify the process components that may be modified [12].

Catalysis is one of the very important concepts of green chemistry. The biggest contribution of chemistry to sustainable development is made through

catalysts, which enables reactions to be carried out in the most effective, economical, and environmentally friendly manner. A catalyst is a substance that makes a chemical reaction go faster (by reducing the activation energy or changing the reaction mechanism) without being consumed in the process. Since it remains unchanged after reaction, the same catalyst molecule can participate in many consecutive cycles of reaction, called catalytic cycles. The catalyst turnover number (TON) and the turnover frequency (TOF) are two important parameters widely used for comparing catalyst efficiency. If the reaction conditions are well defined, these parameters enable a quantitative comparison of the performance of various catalysts. TON is a dimensionless number that represents the number of cycles that a catalyst can run before becoming inactive or more simply, the number of molecules that one molecule of catalyst can convert into molecules of product. The TOF is TON/time. Since it is impossible to know exactly how many "catalyst molecules" there are on the surface, TON and TOF are often calculated as the amount of product formed per active site, or per gram catalyst.

The key benefit of catalysis is that the required product may be produced more quickly while using less resources and producing less waste. By selectivity, we refer to a catalyst's capacity to steer a reaction toward the formation of specific products while excluding others. We define the selectivity for product P, the proportion (or percentage) of the converted reagent that has transformed into product P. High selectivity reduces waste and makes the separation simpler and less expensive. Other indicators of the efficiency of a catalytic process are the reactant conversion and the product yield over time. The conversion is the proportion of reactant molecules that have changed into product molecules (regardless of which product it is). The yield of P is equivalent to conversion x selectivity.

Catalysis applications include photocatalysis [14] [15], environmental catalysis [16][17], metal-catalysis [18][19], electrocatalysis [20][21], and green catalysis, all of which are concerned with sustainability.

There are several types of catalysts and catalysis mechanisms. Most solid catalysts are metals dispersed on a solid surface or inside a liquid matrix, known as supported catalysts. The presence of the support allows its recovery and reuse and, therefore, it is of considerable interest. In addition to high catalytic performance, an easy separation and efficient recycling of the catalyst after a chemical reaction are important in order to reduce the production costs and waste generation, particularly in industrial applications.

Catalysts are traditionally classified as homogeneous or heterogeneous. Homogeneous catalysts are in the same phase as the reactants and products and due to their good solubility in reaction media, have advantages in terms of activity and stability. Homogeneous catalysts, on the other hand, are difficult to separate and recover from the reaction mixture, resulting in increased economic costs, pollution, and corrosion [22]. Because of the issue of metal contamination in metal-catalyzed synthesis, this problem restricts their applicability in industry, particularly in the pharmaceutical industries [23]. In heterogeneous catalysis, the catalyst and the substrate are in different phases and the chemical reaction occurs on the heterogeneous interface between catalytic materials and reactive species (such as a solid/gas, solid/liquid, or solid/liquid/gas three phase contact). Although heterogeneous catalysis is often less efficient than homogeneous catalysis, it has the advantage of allowing a better recovery of the products.

In a heterogeneous catalytic process, reactants diffuse to the reactive interface, are adsorbed on the catalyst surface, and get activated. Adsorbed reactants then react to form adsorbed products, which desorb from the catalyst surface and diffuse away from the interface. Thus, the adsorption and

desorption of reactive species depends on the physical and chemical properties of the catalytic systems [24].

1.2 European Green Deal and bio-based economy in Europe: state of art and future perspectives

The global threats to Europe and the entire world are the climate change and the degradation of the environment. In this respect, the EU has put on the table, in 2019, a strategy for establishing the European Green Deal (EGD) with the aim of achieving carbon neutrality, resources efficiency and zero pollution by 2050. The vision of a competitive and sustainable Europe, no more depending on fossil-based resources, has been put in practice by the Bio-Based Industries Joint Undertaking 2021 (BBIJU) with public-private funds amounting to € 3.7 billion in the framework of EU's Bioeconomy Strategy and Activation (European Commission, EC, 2018) [25].

The challenges to be faced by the bio-based industry are the sustainable sourcing of feedstock and the innovation of economically practical technologies in the biorefining field. More particularly, BBIJU is acting to achieve substantial reduction of imported proteins by 50% and phosphorus and potassium by 25% in the next few years. Moreover, the EU bio-based industry is projected to create 700,000 jobs by 2030. An important goal of EC is "decoupling economic growth from resource use", as the BBIJU initiative exemplarily does. In addition, BBIJU aims at valorizing biowaste, such as the organic fraction of municipal solid waste, industrial as well as bio-based waste compounds [26].

Another EU priority aimed at increasing resource efficiency is operation under zero-waste biorefinery concepts maximizing, in such a way, the valorization of feedstock to obtain as much as possible value-added products.

Bioeconomy strongly contributes to EGD, also moving away from a linear to a circular economy, the former being based on consumption of fossil

and mineral resources. At present, an estimation of the contribution of bioeconomy to the labor force amounts to about 10%, with more than 2,300 bio-based plants being operative in the continent. EC contributed € 3.85 billion (public funds) into bioeconomy projects in the last seven years in the framework of Horizon 2020, and probably as many will be dedicated by Horizon Europe 2021-2027.

Bioeconomy contributes to EGD by many ways:

- climate pact and law (by generating significant carbon savings, about 55% by 2030);
- promotion of clean energy (biowaste converted into energy);
- investments in smart and sustainable transport (about 95% emission savings compared to fossil fuels);
- striving for green industries (production of high value-added products from waste streams);
- eliminating pollution (by maximization of the use of side- and residual streams);
- financing green projects (up to € 250 million planned in different bio-based projects);
- making homes energy efficient (through insulation of buildings with bio-based materials).

The Italian government has implemented in recent years an Action Plan (2020-2025) for the national bioeconomy strategy (BIT II). In particular, in this framework, a series of pilot actions to support bioeconomy are planned in the following areas:

- agri-food;
- bio-based industry;

- urban biowaste;
- blue bioeconomy (aquaculture);
- knowledge of national biodiversity and ecosystems;
- promotion of engagement and education across the bioeconomy.

The flagship projects to be deployed in the short-term amount to € 570 M [27].

Ultimately, the implementation of EU's climate and environmental goals should principally:

- provide a real strategy for the sectors that currently use and manage biomass;
- discourage actions that contribute to climate impacts;
- promote the ecological use of biomass;
- re-establish the high value (economical, environmental, social) of natural ecosystems.

1.3 Clean energy transition towards blue H_2 production

Given global energy consumption and the need to reduce GHG emissions, it is expected that hydrogen due to its high energy density, will become a carrier of renewable energy in the future [28]. However, the only hydrogen that can be retained completely sustainable is known as "green hydrogen" and it is produced by electrolysis or using renewable energy. Although the emissions are reasonably low, green hydrogen technologies are not yet cost-competitive.

At present, 98% of the world's hydrogen is produced from fossil fuel and, in particular, Steam Methane Reforming (SMR) is responsible for 48% of the hydrogen produced globally from natural gas due to its low cost and excellent efficiency [29]. However, this technology generates "grey hydrogen" since it leads greenhouse gas emissions into the atmosphere (9 kg of CO_2 is generated for every kg of H_2 produced using SMR) [30]. Currently, there is increasing interest in "blue hydrogen". Blue hydrogen is hydrogen produced from fossil fuels but such a way that some or nearly all the CO_2 emissions associated with its production are captured and sequestered. There are many proposed alternative technologies to produce blue hydrogen.

With the use of fuel cell technology, hydrogen energy may be released and transformed to electricity. Fuel cells are highly efficient electrochemical devices able to convert the chemical energy stored in fuels directly to electrical energy without adversely affecting the environment [31] [32]. Solid oxide fuel cells (SOFCs) represent an excellent alternative for reaching a sustainable energy future, especially when compared to conventional energy conversion technologies now in use. To be considered sustainable, a technology must

overcome three challenges: (i) energy demand reduction, (ii) enhancing the efficiency of energy producing technologies, and (iii) deploying renewable energy and replacing fossil fuels [28]. Solid oxide fuel cells allow us to overcome the second and third challenge: they are characterized by high electrical efficiency and an high degree of flexibility since they can be fed with a wide variety of fuels, not only hydrogen, but also methane, propane, ethanol and natural gas and many other conventional and alternative fuels [33] [34].

Conventional SOFCs employ Ni-yttria stabilized zirconia (YSZ) as the anode and hydrogen as the fuel [35] [36]. However, due to the high costs associated with transporting and storing hydrogen, fuel cells utilizing pure hydrogen are currently unsuitable. On the other hand, solid oxide fuel cells suffer from the direct utilization of fuels different from hydrogen. Carbon deposits at the anode in the absence of an appropriate pre reforming step with consequent anode catalyst poisoning and delamination is a well-known drawback.

Therefore, when diesel, natural gas, or methanol are utilized as raw fuels, a fuel reformer is required to convert the hydrocarbons into a hydrogen-rich gas so that the fuel cell carries out the electrochemical conversion [32].

In SOFC-based power generating systems, hydrogen can be generated by a hydrocarbon reforming process in an "external reforming." Due to their high operating temperature, SOFCs may be utilized to internally reform hydrocarbons into hydrogen, which means that hydrocarbons enter the SOFC directly and hydrogen is recovered immediately. Therefore, SOFC anode has the dual function of catalysing the fuel reforming reaction and the fuel electrochemical oxidation reaction [37].

This procedure is known as "internal reforming". By Internal reforming an high efficiency for hydrogen production and a greater simplification of the system can be achieved [32]. According Eric et al. the internal reforming in the

same SOFC system is 8% more efficient than the external reforming [38]. This procedure is known as "internal reforming". By Internal reforming an high efficiency for hydrogen production and a greater simplification of the system can be achieved [32].

Reforming of natural gas is the most widely used method for syngas (a mixture of CO and H_2) generation. The reforming methods to obtain hydrogen-rich fuel gas usually include steam reforming (SR), dry reforming (DR), partial oxidation (POx), autothermal reforming (ATR) or a combination of two or more approaches [39]. Each approach uses a different oxidizing agent (steam, oxygen, or carbon dioxide) and different operating conditions to produce syngas with different H_2/CO ratios and different chemical compositions [39].

Steam Reforming (SRM)

Steam reforming is a well-established industrial technique aimed to produce hydrogen. It is an endothermic reaction between water steam and methane that it is carried out at a high temperatures (800 e 1000 °C) with a high pressure of 35 bar in the presence of a Ni based catalysts [37]. During the process, the water-gas shift reaction (WGS) could occur, which would increase the amount of H_2 produced [40].

$$CH_4 + H_2O \leftrightarrow CO + 3\,H_2 \qquad \Delta H°_{298°K} = 206\ kJmol^{-1} \qquad \text{(Eq. 1)}$$

$$H_2O + CO \leftrightarrow CO_2 + H_2 \qquad \Delta H°_{298°K} = -41\ kJmol^{-1} \qquad \text{(Eq. 2)}$$

The syngas obtained by steam reforming is high in hydrogen and low in carbon monoxide (the ratio H_2:CO is of 3:1). Currently, Ni based catalysts are the most commonly used catalysts due to their low cost and high activity. Several strategies have been developed to improve the catalytic activity and coking resistance of Ni catalysts including the addition of promoters, development of advanced supports, and structural modification, etc. [40].

Dry Reforming (DRM)

Dry reforming is the reaction that converts two green gases (CH_4 and CO_2) to syngas with a theorical ratio H_2:CO of 1:1 in the presence of a catalyst. The process of DRM of natural gas occurs via the following reaction:

$$CH_4 + CO_2 = 2H_2 + 2\,CO \qquad \Delta H°_{298°K} = 247{,}3\ kJmol^{-1} \qquad \text{(Eq. 3)}$$

The idea of using two greenhouse gases to make something useful, makes dry reforming a good option to think about [41]. Due to its endothermic nature, DRM needs to be carried out at high temperatures (> 600°C) [42]. High temperatures promote several side reactions such as the reverse water gas shift reaction, RWGS, (Eq.4), leading to a higher conversion of CO_2 than that of CH_4 and a ratio H_2/CO in the products of reaction lower than the unity [43] but suitable for use in Fischer–Tropsch (FT) synthesis process for the production of of liquid fuel and valuable chemicals [42].

$$CO_2 + H_2 \leftrightarrow CO + H_2O \qquad \Delta H°_{298°K} = 41{,}2\ kJmol^{-1} \qquad \text{(Eq. 4)}$$

Noble metals are active metals for DRM but their industrial application is limited due to their high costs [43]. On the other hand, although Ni based catalysts are readily available and economical, they tend to become deactivated as a result of sintering of Ni particles and carbon deposition (coking). Several literature studies have shown that these problems can be overcome by the use of perovskites with Ni at the B site as catalysts precursors [44][45]. In particular, Ni exsolution process on the perovskite surface allows to stop the growing of particles and carbon deposition on the transition metal anodes of direct hydrocarbon solid oxide fuel cells [46] [47][48].

Partial Oxidation (POx)

Partial oxidation of natural gas is an exothermic reaction that involves the use of pure oxygen. It is a more energy efficient process than steam reforming and dry reforming and since it needs lower temperature, it can also

be carried out in absence of a catalyst [49][50]. Partial oxidation of natural gas (Eq.5) is an exothermic reaction that involves the use of pure oxygen.

$$CH_4 + 1/2\ O_2 \leftrightarrow CO + 2\ H_2 \qquad \Delta H°_{298°K} = 36\ kJmol^{-1} \qquad (Eq.5)$$

POx produces the syngas with a ratio H_2/CO that allows its direct utilization for various chemical production processes such as Fischer-Tropsch and also for solid oxide fuel cells [51].

Autothermal Reforming (ATR)

Combined reforming allows to take advantage of the benefits of each reforming method while minimizing the negatives. In particular, the autothermal reforming (ATR) of methane involves a thermal energy balance between the endothermic reaction of steam reforming, (Eq. 6) and the exothermic reaction of partial oxidation, (Eq. 7). The heat generated by partial oxidation is utilized to compensate the heat absorbed by steam reforming [49].

$$CH_4 + H_2O \rightleftharpoons CO + 3H_2 \qquad (Eq.6)$$

$\Delta H° \simeq 226\ kJmol^{-1}$; $\Delta G° \simeq -45\ kJmol^{-1}$ @ 800 °C

$$CH_4 + ½O_2 \rightleftharpoons CO + 2H_2 \qquad (Eq.7)$$

$\Delta H° \simeq -22\ kJmol^{-1}$; $\Delta G° \simeq -234\ kJmol^{-1}$ @ 800 °C

Therefore, the overall reaction equation for the autothermal process is:

$$CH_4 + xH_2O + 2(1-x)\ H_2O \rightleftharpoons CO_2 + 2(2-x)\ H_2 \qquad (Eq.8)$$

$$\Delta H° \simeq 0\ J; \Delta G° \simeq -192\ kJ\ mol^{-1} @ 800\ °C$$

The produced H_2/CO ratio from ATR depends on the feed composition and operating conditions and can vary from 1 to 2 [52].

Due to their extraordinary properties, Perovskite-type mixed oxides could be used as suitable supports for nickel catalysts in autothermal reforming of hydrocarbons.

1.4 The methanation of CO_2 as storage of renewable energy in a gas distribution system

In recent years, the increased renewable capacity, together with the need to minimize the carbon emissions have encouraged researchers to develop new energy supply technologies that could be used to replace definitely traditional energy sources like nuclear power or fossil fuels with renewable energy sources, like wind or solar energy [53][54]. However, due to the intermittent nature of renewable energy sources, the development of appropriate storage devices is required to address the gap between power supply and immediate consumption [54].

The Power to X technology (P2X) currently represents a promising approach to solve the energy storage problems and to reduce greenhouse gas emissions. This technology converts electricity into gaseous fuels like hydrogen and methane (power-to-gas) or liquid hydrocarbons like methanol (power-to-liquid). Unlike the PTG process, the PTL process generates liquid fuels, which are preferred in terms of energy density and added value, as well as storage and transportation [55].

The Power-to-Methane or P2M system, in particular, offers a pathway to convert the surplus electrical energy into chemical energy in form of methane, using hydrogen produced by water electrolysis and carbon dioxide sourced from a variety of industrial processes, including biomass combustion and gasification, biogas facilities, power plants, oil refineries, and cement kilns [54]. Depending on the source of the electricity used, generally renewable, it can result in a process with no harmful gas emissions [56]**.** Since that methane can be produced by recycling carbon dioxide, P2M technology can potentially promote the abatement of polluting gas emissions. Indeed, carbon oxides are

recognized as the principal pollutants in the atmosphere, and their reduction constitutes an urgent problem in detecting and limiting their negative impacts [57]**.** Currently, Carbon Capture and Sequestration (CCS) is the most commonly studied technology to reduce CO_2 emissions and consists of CO_2 capture, transportation and underground storage. Alternatively, the CO_2 generated from industrial processes could be captured and then converted into fuels and chemicals, just as it happens in Power to X technologies. From the environmental point of view, thus, the deployment of the P2G technology allows to avoid the impact of further ambient temperature increases on global warming.

The conversion of energy to methane occurs via two main reactions*:* *electrolysis* (Eq. 9) that uses electrical power to split water into its components (hydrogen and oxygen) and *CO_2 methanation* (Eq. 10) that uses carbon-dioxide from the air (CO_2-extraction) or from biomass to transform hydrogen to methane. The effectiveness and efficiency of power-to-gas plants strongly depend on the latter reaction [54].

Electrolysis: surplus electricity + $H_2O_{(l)} \leftrightarrow H_{2(g)}+1/2\ O_{2(g)}$ (Eq. 9)

Methanation: $CO_{2(g)}+4H_{2(g)} \leftrightarrow CH_{4(g)}+2H_2O_{(g)}$ (Eq. 10)

A typical plant P2M is characterised by at least four components as shown in Figure 1.1: - An electrolyser, which allows H_2 to be produced - a CO_2 capture section for separating CO_2 from the carbon-intensive industries - A methanation process device for producing liquid fuels and/or SNG - Storage facilities, to allow the H_2, CH_4 and CO_2 to be stored safely and buffered [53].

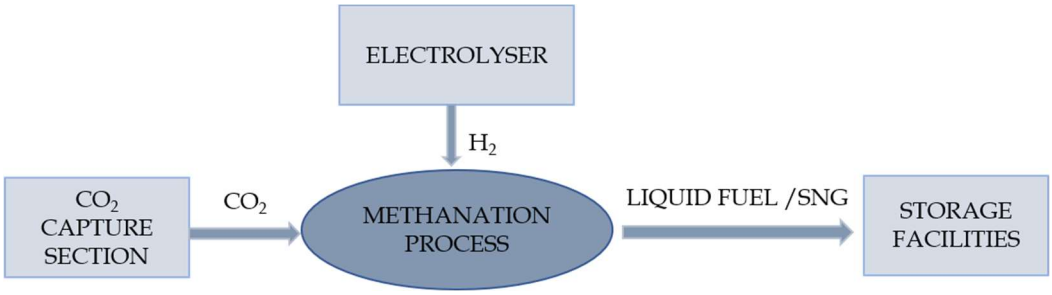

Figure 1.1. Block diagram of a typical plant Power- to-Methane.

The methane obtained, is called Synthetic Natural Gas and represents a more appropriate medium for the storage applications than hydrogen gas because it is much easier to handle (especially in the form of Liquid Synthetic Natural Gas) and it could be directly transported through the already existing pipeline networks or storage infrastructures [56]. Because of the substantial compression (>100 bar) necessary to achieve a modest energy density, hydrogen is not an acceptable medium for a storage application. Instead, the Natural gas (methane) has the energy density three times higher than hydrogen [57] [58] and, therefore, it needs much less space to produce the same amount of energy. On the other hand, with its large underground storage, it is a fully established energy carrier in all parts of the world [58], particularly in Europe [59][60].

Recent studies examined the installation costs of PtG technologies. Currently, the costs are regarded high and the efficiency of individual processes needs to be improved [61]. Many plants are now under construction or even in operation. The most representative plants are in the north-west of Germany (50-100 MW_{el}) and in the North Sea (up to 30 GW_{el}) [62].

Even if the investment expenses are not negligible, Power-to-Gas technology will have a significant influence on a future energy scenario at zero CO_2 emissions, in particularly in Europe where interest in this approach has begun

to grow due to increasing share of renewable resources [61]. This technology offers high flexibility and the potential to implement electricity grids with a high share of renewable resources, allowing a long-term decarbonization [63].

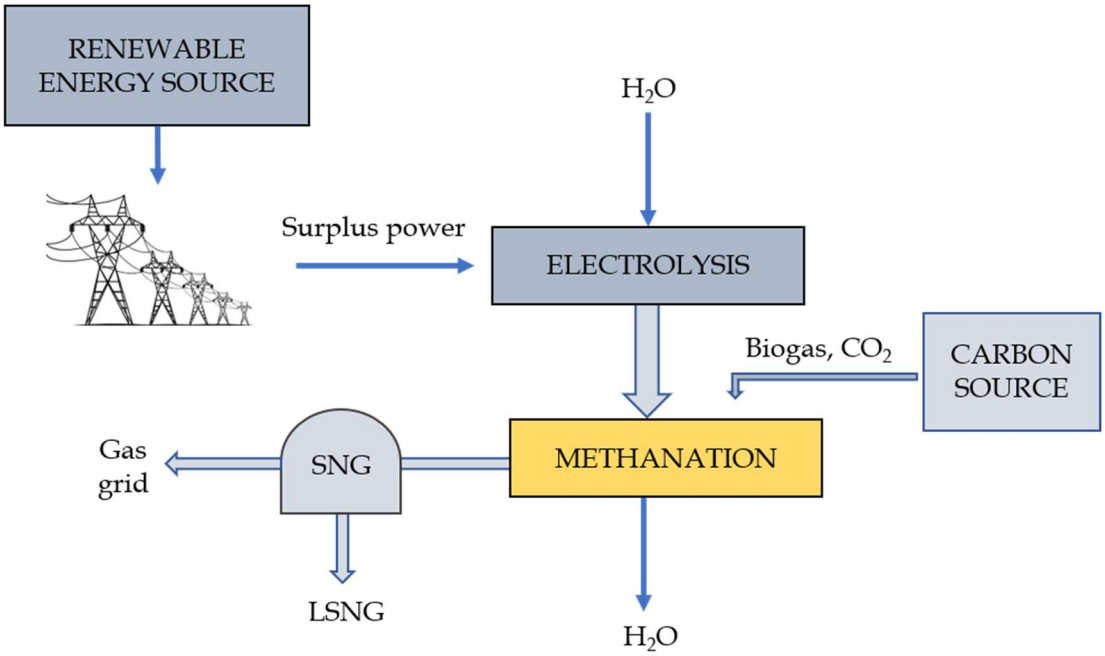

Figure 1.2. Schematic representation of a power-to-SNG system.

2.2.1 Description of the methanation reaction

Carbon dioxide methanation is the core of the P2M process but it could be also used in the biogas upgrading [62]. The reaction discovered by Sabatier and Senderens in 1902 and, for this reason generally known as Sabatier's reaction, is commonly applied in ammonia synthesis to remove small traces of CO_2 and CO from ammonia [64].

Since biogas contains approximately 60 mol% methane and 40 mol% CO_2 together with minor components like H_2S (0.4%), siloxanes (20 mg/m^3), nitrogen, oxygen, ammonia, etc. [65], it could be converted directly or indirectly (by first separating CO_2 from biogas) into high-grade methane in

order to meet natural gas grid standards. The upgrading of biogas technology reduces the cost associated with carbon dioxide removal and increases the methane yield and carbon utilization from biological sources [66].

The process includes the removal from biogas of contaminants such as sulphur-containing molecules to avoid catalyst deactivation and the dehydration in order to obtain pure methane. The plant used to upgrade biogas (Figure 1.3), therefore, consists of a biogas pre-treatment section, a methanation reactor and a water separation/gas drying section [58].

Recent studies have demonstrated that CO_2 methanation could be carried out using hydrogen came from the exit-streams of the solid oxide electrolysis cells (SOECs). Recent studies have demonstrated that CO_2 methanation could be carry out using hydrogen came from the exit-streams of the solid oxide electrolysis cells (SOECs) [57].

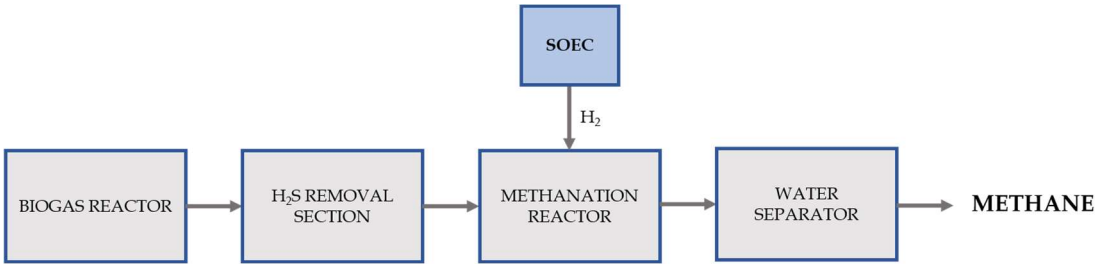

Figure 1.3. Block diagram of the plant used to upgrade biogas.

CO_2 methanation is a highly exothermic reaction and is thermodynamically favoured ($\Delta G_{298°K}$ = – 130.8 kJmol^{-1}) at low temperatures [54]. The reaction stoichiometry is shown in (Eq.11). The high temperatures limit the CO_2 conversion and favour the competitive reverse water-gas shift reaction (Eq.12) according to Le Chatelier's principle. Therefore, a higher reaction temperature produces more CO, whereas a lower temperature

produces more methane, implying that the product composition may be changed based on which component is in more demand.

$$CO_2+4H_2 \leftrightarrow CH_4+2H_2O_{(g)} \quad \Delta H_{298°K}=-165{,}1\ kJmol^{-1} \qquad (Eq.11)$$

$$CO_2+H_2 \leftrightarrow CO + H_2O_{(g)} \quad \Delta H_{298°K}= +\ 41{,}2\ kJmol^{-1} \qquad (Eq.12)$$

On the other hand, for the same reasons, an increase in pressure shifts the thermodynamic equilibrium to the reaction products involving an enhancement of the reaction performance.

Several experimental studies have shown that the fraction of the end product varies differently with different H_2/CO_2 ratios. In particular, when the ratio is increased from 1 to 4 at the same temperature and pressure, CH_4 yield increases, when it increases to 6 it is not observed to be an effective improvement in terms of CO_2 conversion and CH_4 selectivity [67].

Therefore, the methanation reaction generally operates at temperatures between 200°C and 550°C depending on the catalyst, at pressures ranging from 1 to 100 bar and with a H_2/CO_2 ratio equal to the stoichiometric ratio.

In addition to the reverse water gas shift, other competing reactions might occur and lead to a lower product selectivity than desired. For example, temperatures above 500 °C might promote CO disproportionation according to Boudouard reaction (Eq.13) enhancing carbon deposition on the catalyst resulting in catalyst deactivation [66].

$$CO \leftrightarrow CO_2 + C \quad \Delta H_{298°K}= -\ 172{,}5\ kJmol^{-1} \qquad (Eq.13)$$

As shown in Eq.11, the reduction of fully oxidized carbon to methane is an eight-electron process with significant kinetic limitations that necessitates the use of a catalyst to achieve acceptable rates and selectivity [68].

Fixed-bed reactors are the main type of catalytic reactors used for CO_2 methanation [22]. A fixed bed methanation reactor consists of a cylindrical tube that is filled with either catalyst pellets or powder and reactant fluid (CO_2 and H_2) that flows uniformly across the bed and it is transformed into products. The illustration of this reactor is shown in Figure 1.4. A fixed-bed reactor allows the easy recovery of the solid catalyst. As a consequence, the catalyst's activity can be restored to or near its original level, decreasing the cost and time necessary to generate a new catalyst.

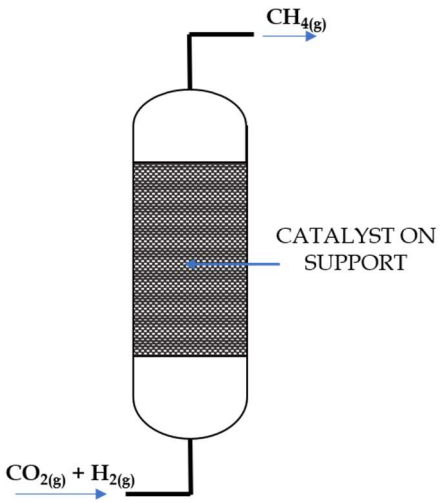

Figure 1.5. Schematic diagram of fixed bed reactor for CO_2 Methanation.

Despite multiple studies have been published on the subject recently, there is no broad agreement on the reaction's mechanism due to the difficulties in defining the intermediate chemical engaged in the rate determining step. Two different mechanisms have been proposed for CO_2 methanation. The first and most common mechanism concerns the conversion of CO_2 to CO, which is then hydrogenated to CH_4 via CO methanation. The second mechanism involves direct hydrogenation of CO_2 to CH_4, with no CO intermediates formed (Figure 1.6) [54].

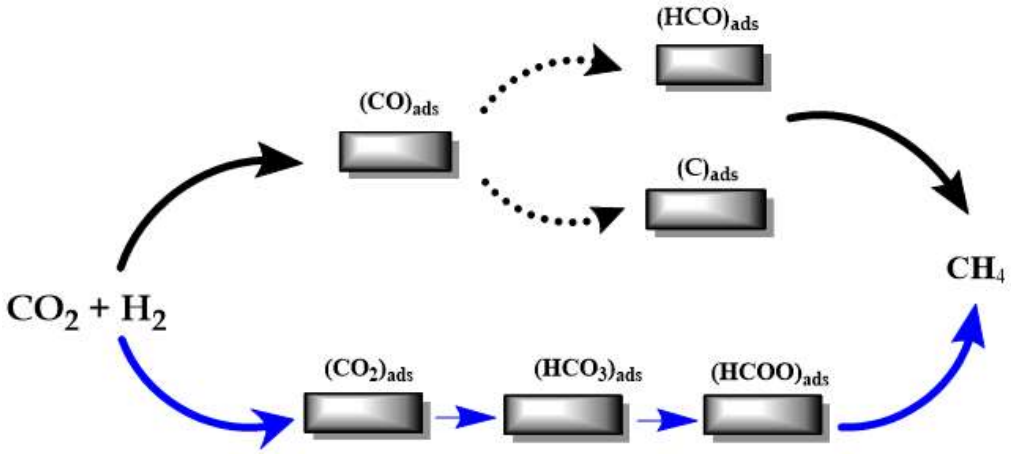

Figure 1.6. Schematic mechanism of CO_2 methanation.

2.1.2 State of art of catalytic systems

Due to competing reactions, the conversion of CO_2 into CH_4 requires an active catalyst at relatively low temperatures and selective towards methane. In the last three decades, several systems have been widely investigated as catalysts for CO_2 methanation [72]. The catalysts used in methanation reaction, are typically composed of active metal particles (e.g. Ni, Fe, Co, Ru, Rh, Pt, Pd, W or Mo) dispersed on a metal oxide support (e.g. Al_2O_3, SiO_2, TiO_2, SiC, ZrO_2, CeO_2, $Ce_xZr_{1-x}O_2$). The characterisation in terms of activity (intended as catalysts interaction with CO_2), and selectivity towards CH_4 of the most common metal catalysts used for the methanation process is shown in the **Table 1.3**.

However, it is important to note that the order is simply an indication of a trend that might vary based on different metal support interactions. These metals, in their reduced state, are able to effectively dissociate the hydrogen in order to react with CO_2 adsorbed on the support.

Table 1.3 Characterisation of common metal catalyst used for methanation process.

Characterisation	Catalyst
Activity:	Ru > Fe > Ni > Co > Rh > Pd > Pt > Ir
Selectivity:	Pd > Pt > Ir > Ni > Rh > Co > Fe > Ru

Even though Ru is evidenced to be an active and stable metal for CO_2 methanation, nickel, among the transition metals, is the most commonly used catalyst, due to its relatively low price and its high availability, characteristics which influence the metal's utilization for industrial purposes. Its price is comparatively 100 times cheaper than Ru with fairly good activity and selectivity towards CH_4. However, nickel-based catalysts need a high feed gas purity since they are easily deactivated by sintering or coke deposition when the reaction is carried out at elevated temperatures. Its low thermal stability leads to a short lifetime and low reusability of the catalyst.

As a result, in order to achieve high CO_2 conversion and CH_4 selectivity at low temperatures using Ni, the selection of catalyst support have all been thoroughly investigated. Alongside the active metal, the support of this phase plays a fundamental role. The support can improve the dispersion of active components and tunes the surface structure of the catalysts; these effects can influence the adsorption characteristics of the species involved and, consequently, the reaction pathways. The physico-chemical characteristics (structure, chemical composition, defect groups, and thermal stability) of supports are fundamental aspects to consider in metal-supported catalysts tuning because they affect the activity, productivity, and lifetime of the final heterogeneous catalyst.

The most common support materials for Ni-based methanation catalysts are Al_2O_3, SiO_2, ZrO_2, CeO_2, TiO_2, composite oxides (hexaaluminate, solid solution, perovskite), structured metal oxide, carbon and zeolite materials.

In the last years, different types of zeolites were used as metal supports to prepare active and stable catalysts since their properties are adjusted to meet the requirements of the CO_2 methanation. Zeolites are micro- or mesoporous aluminosilicate structures that include silicon and aluminium atoms linked by oxygen atoms. Despite their massive utilization is mainly related to other specific applications, such as molecular sieves and adsorbent materials, their use in catalysis has manifold reasons: (i) the zeolite confinement effects (zeolite cages and channels intersections really act like nanoreactors, boosting catalysts' activity); (ii) the possibility to adapt their basicity or acidity by both cationic exchange with alkaline metals and post-synthesis treatments (e.g., dealumination); and (iii) their hydrothermal stability that can be improved by steaming treatments. Recently, Bacariza et al. have reviewed several works about the use of zeolite-based catalysts for carbon dioxide methanation, showing the potentiality of zeolites as support catalysts in this reaction. The type of zeolites more investigated are Y, A, X and ZSM-5, which essentially differ for framework structure and aluminium content [57].

1.5 Catalytic Upgrading of lignocellulosic residues and waste

Biomass is a readily accessible renewable carbon- neutral resource that can be converted into a wide range of valuable chemicals with applications ranging from pharmaceuticals to fuel [73][74][75][76]. Catalytic conversion of biomass to fuels and/or chemicals is a promising option to reduce society's dependence on traditional fossil fuels and then, the accumulation of greenhouse gas in the atmosphere [77]. Lignocellulosic biomass is most abundantly raw material on the earth and it is composed of a combination of three main biopolymers: cellulose (30-50 wt%), hemicellulose (20-40%) and lignin (10-20 wt %) together components such as extractives, pectins, and minerals [78][79]. The contents of each component are variable among different plant species or the different parts of the same type of biomass. Lignin is the most prevalent aromatic polymer in nature and contains a wide variety of etheric aromatic monomers (p-coumaryl alcohol, coniferyl alcohol, and sinapyl alcohol) that are bonded with each other by C-C and C-O-C linkages and may be employed as alternative raw materials for the synthesis of different polymers. Cellulose and hemicellulose are commonly utilized as initial feedstocks for biofuel production because, being polysaccharides, they depolymerize into monosaccharides more easily than lignin. In particular, cellulose is a linear homopolymer consisting of D-glucopyranose units linked together by β-1,4 glycosidic bonds. Strong hydrogen bonds and Van der Waals forces hold these linear polymeric chains together to form a rigid crystalline structure. Hemicellulose is a short and highly branched heteropolymer of pentoses and hexoses, such as xylan, mannan, , β-glucans, and xyloglucans [80].

Since biomass (lignocellulosic) has a complex structure, to obtain the desired product selectively is difficult. On the contrary, breaking down of

lignocellulose and its conversion into simple C5-C6 sugars and subsequently to furan-based platform chemicals offers a simple and sustainable route to produce a diverse variety of value-added chemicals and fuels [81].

In particular, furanic platform molecules with short carbon chains like furfural (FUR) and 5-hydroxymethylfurfural (HMF), have rapidly emerged as preferred bio-based intermediates for biorefinery since from them, by extending the number of chain's carbon atoms, is possible to synthetize hydrocarbon fuels that fall within the range of standard transportation liquid fuels (C8-C22) [82].

In 2004, the US Department of Energy (DOE) named furfural and hydroxymethylfurfural (HMF) among the top 14 most significant biomass-derived platform molecules for the production of various industrially important value-added chemicals and fuel components, owing to their diverse functional groups and ease of production from cellulose and hemicellulose [83]. In particular, furfural is produced by acid-catalyzed dehydration of pentoses such as xylose and arabinose, while, 5- hydroxymethilfurfural by the acid-catalyzed dehydration of C6 sugars such as glucose and fructose [84]. Furfural is a heteroaromatic molecule conteining a heterocyclic five-membered ring with four carbon and one oxygen atoms and an aldehyde functional group. It can be used directly as an organic solvent in chemical synthesis to increase the selectivity of aromatics and unsaturated compounds. Hydroxymethilfurfural has a similar chemical structure to FUR with both an aldehydic and a hydroxymethyl group which can undergo oxidation processes.

Furfural and HMF's functional groups (-CHO and/or -CH_2OH group linked to the furan ring) are responsible for their high reactivity in a wide variety of chemical reactions including hydrogenation, oxidation, hydrodeoxygenation (HDO), dehydroxylation, deoxygenation, and decarbonylation [78].

Furfuryl alcohol, tetrahydrofurfuryl alcohol, furan, tetrahydrofuran (THF), 2-methyltetrahydrofuran (MTHF), dihydropyran, and acetylfuran are only a few of the compounds that may be produced by upgrading furfural.

HMF possesses a very strong chemical reactivity and for these reasons is a versatile precursor in the synthesis of a wide range of value-added compounds and liquid fuels. For example, it can be converted by selective oxidation into two important commodity chemicals: 2,5-diformylfuran (DFF) and 2,5-furandicarboxylic acid (FDCA). Molecules of FDCA can be used as starting building blocks in polymer synthesis of polyethylene furanoato (PEF), a 100% bio-based polymer that should replace in future petrochemical-derived terephthalic acid (PET) [85]. The 2,5-dimethylfuran (DMF) compound is produced by hydrogenation of HMF and it is often used as a fuel additive. The acid-catalyzed etherification of HMF with a simple alcohol such as methanol or ethanol can lead to the formation of two alkoxymethyl furfurals: 5-(methoxymethyl)furfural (MMF) and EMF. In particular, 5-(ethoxymethyl)furfural (EMF) is considered a promising second-generation biofuel due to its significant properties such as energy density (8.7 kW hL^{-1}), which is higher than that of ethanol (6.1 kW hL^{-1}) and comparable to that of gasoline (8.8 kW hL^{-1}) [86].

Hydrogenated derivates have gained significant attention in biomass exploitation for the production of liquid hydrocarbon fuels, fuel blenders, and a variety of industrially important chemicals. In presence of molecular hydrogen, FUR and HMF can lead to a variety of reactions including C=O and C=C hydrogenation, decarbonylation, and C-O and C-C hydrogenolysis [87].

Undoubtedly, the most significant and extensive use of furfural is centred on its hydrogenation, as around 62% of furfural is industrially employed for furfuryl alcohol (FA) manufacture [88]. Furfuryl alcohol is a key monomer in the polymer industry, where it is used to produce poly(furfuryl alcohol), a chemical-resistant resin widely applied in thermoset polymer

matrix composites, cements, adhesives, coatings, and casting/foundry resins [77]. The salt of FA is also used in the pharmaceutical field to produce lysine and vitamin C [88].

The hydrogenation of FUR and HMF is commonly carried out using highly pressurized H_2 gas as a reducing agent. This approach necessitates the use of specialized infrastructure for the transportation, storage, and handling of high-pressure H_2, which is very combustible and explosive when mixed with air. Alternatively, it can be performed by employing formic acid or alcohol as a hydrogen donor via catalytic transfer hydrogenation (CTH) process [77]. Transfer hydrogenation reaction, introduced more than a century ago by Knoevenagel [89], is a competitive and complementary strategy of the conventional molecular hydrogen-based processes such as the reductive catalytic fractionation (RCF) used to biomass fractionation and lignin valorization [78]. The application of CTH processes in lignocellulose biomass valorization has recently drawn significant research interest due to the ability of most H-donor organic molecules to dissolve biomass and the low cost of lignocellulose based biorefinery plants [78].

The CTH processes are simple and safe in terms of experimental facilities and operations. The use of an indirect H-source allows to adopt milder reaction conditions and reduces the complexity and cost of the experimental setup [89]. Moreover, H-donor molecules, due to their lower hydrogenation ability with respect to molecular H_2 increases the selectivity of the process and reduces, at the same time, costs linked to the purification from undesired products [78].

There are two main mechanisms for CTH reactions. One is the Meerwein–Ponndorf– Verley (MPV) mechanism which involves the direct transfer of hydrogen from the donor molecule to the acceptor molecule in a concerted step with formation of a six-membered cyclic transition state. The reaction needs the presence of a catalyst containing both acid and base Lewis

sites able to coordinate both the reducing alcohol and the carbonyl compound [78] [90].

According to the other mechanism, both the hydrogen of the hydroxyl group and the α-hydrogen atom of the H-donor molecule are transferred on the catalyst surface with the consequent formation of metal hydrides which subsequently react with carbonyl group to give the corresponding alcohol [78].

In Figure 1.7 are shown the two possible mechanisms for CTH reaction.

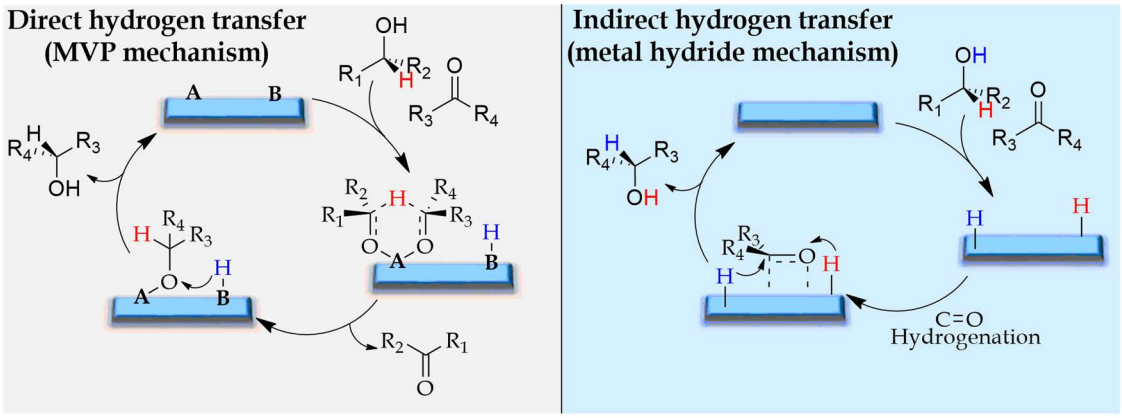

Figure **1.7.** Two possible mechanisms for CTH reaction: MVP mechanism and metal hydride mechanism.

In acid-base-catalyzed CTH reactions, alcohols have a dual role: they can act as both hydrogen donor molecules and solvents. In addition, they are easy to use, not too expensive and they can be recycled or used again [91]. In particular, the secondary alcohols, such as 2-propanol and 2-butanol, are considered more efficient H-donors than primary alcohols since that two alkyl groups have a stabilizing effect on the carbocation formed during the transfer of hydride. Tertiary alcohols can't donate hydrogen because they don't have atoms of hydrogen on the α-carbon [78].

As hydrogenated products of furfural and HMF have of great interest to many scientists and researchers thanks to their ability to produce biofuels,

fuel blenders and several industrially relevant chemicals several monometallic and bimetallic heterogeneous catalysts have been developed and tested for the upgradation of furfural and HMF via the hydrogen transfer approach. To be useful, the catalyst needs to be selective to the desired CTH products due to the highly functionalized nature of the furfural (i.e., C=C, C-O and C-O bonds) and heterogeneous for an easy separation and recovery of products without undesirable contamination by reaction wastes.

Numerous precious-metal-based catalysts have been reported for the CTH of furfural (FUR) to furfuryl alcohol (FAL); although they exhibit excellent catalytic performance under mild conditions, precious metals are expensive and have limited availability. On the other hand, the non-precious-metal catalysts are a good alternative to systems based on noble metals, particularly in the valorisation of biomass and production of molecules made from biomass. This is because they are easier to find, cheaper, and less harmful to the environment [78]. Among non-precious metal catalysts, Cu - based catalysts are the most used for the hydrogenation of FUR because generally they show low activity in furan ring hydrogenation and relatively high activity to C=O bonds hydrogenation. The Cu-based catalyst supported on sulfonate group grafted active carbon (Cu/AC-SO_3H) is a very efficient and selective system able to convert FUR into FAL with 100% yield [78]. Cu-based catalysts like $CuCr_2O_4$ are also very active, but they are not safe for the environment because the Cr species are toxic [92].

Several studies have focused on the use of Cu/MgO–Al_2O_3 catalyst. Lu and coworkers tested different Cu-based catalysts (10–50 wt% Cu supported on MgO–Al_2O_3) for the transfer hydrogenation of FUR at 210°C using 2-propanol as the H-donor solvent and observed that all of the FUR was converted but the yield of FAL first went up from 49% over a 10 wt% Cu/MgO-Al_2O_3 catalyst to 91% over a 20 wt% Cu/MgO-Al_2O_3 catalyst. After that, it started going down as the Cu loadings went up.

Ni-based catalysts have shown interesting results in the hydrogenation of biomass derived molecules because they are low cost and exhibit a good catalytic performance in CTH conditions. However, metallic Ni particles are too active and have the tendency to dehydrogenate and decompose the reactants. NiO nanoparticles are selective catalyst (~95%) when 2-propanol is used as both of solvent and H-donor at 130-170 C° [77]. According to proposed reaction mechanism the Lewis acidic site (Ni^{2+}) and Lewis basic site (O^{2-}) lead to the activation of 2-propanol and FUR [78]. Bimetallic catalysts such as the couples Ni–Cu and Ni–Fe are attractive systems since that they can be easily recovered magnetically from the reaction media. Recently, Mingwei Ma et al. used magnetic Fe_3O_4 nanoparticles as catalyst for the CTH reaction of FUR to FAL under relatively mild reaction conditions (120−160 °C) and what emerged at the conclusion of the experiment was that they had high catalytic activity and were easily separated from liquid using a magnet.

Even if cobalt-based catalysts are relatively little investigated, it has been shown that Co_3O_4 nanoparticles (3 nm) supported on mesoporous carbon can efficiently catalyze the CTH reaction with a complete conversion of FUR (100%) and 97% selectivity to FAL at 160 °C for 4 h using 2-PrOH as a solvent/H-donor [93].

Chapter 2

Synthesis and characterization of catalytic systems

2.1 Synthetic methodologies to produce heterogeneous catalysts

Catalysts are chemical species that facilitate chemical processes, accelerating them and allowing them to occur under milder conditions. Catalysts reduce the activation energy of a process, but do not alter its equilibrium; hence, a catalyst alters the kinetics of the reaction, but not its thermodynamic equilibrium. In addition to speeding processes, catalysts also have the ability to modify their selectivity. This means that distinct products can be derived from the same reagents by merely altering the catalyst. One of the most important characteristics of catalysts is that they act cyclically: they are not consumed during the reaction while interact with the reactants, generating an intermediate species that, once the transformation predicted by the reaction has occurred, generates the final product and returns the catalytic species to its original form, ready to begin a new cycle. Today, more than 90 percent of chemical industrial operations include catalysts, and without them, many processes would be unfeasible [94].

There are a number of ways to classify a catalyst (structure, composition, application area, etc.), but it is usually better to divide them based on their aggregation state inside the reaction environment. Therefore, we refer to catalysts as homogeneous if they exhibit phase homogeneity and as heterogeneous if they do not. Typically, homogeneous catalysts are chemical compounds, such as mineral or organic acids, or coordination complexes, such as transition metal ions coordinated by organic molecules. Typically, heterogeneous catalysts consist of solid materials, such as metal mesh or metal dispersion on inert substrates.

Heterogeneous and homogeneous catalysts have benefits and drawbacks in their applications: homogeneous catalysts are generally more active, selective, reproducible, and exploit the totality of the phase atoms active in the catalysis phase, but they are more difficult to recover, cost more on average, and are less resistant to thermal stresses. Heterogeneous catalysts, on the other hand, are more temperature-stable, manageable, recyclable, and regenerable, but less reproducible and less active.

The procedure to prepare a heterogeneous catalyst is delicate. Each step must be executed with the utmost care and attention, as even minute alterations can have a significant impact on the finished product's qualities. It is essential to differentiate between bulk and supported heterogeneous catalysts. The bulk catalysts are very porous metals or their oxides that are composed wholly of active phase, whereas the latter are finely dispersed metals on a porous substrate that is inert to reactions [95].

Generally, bulk catalysts are produced in following ways:

- melting at high temperatures and alloy leaching: two metals are melted together and then one is removed to create a porous mass with a large surface area, known as "sponge". The outcome is a fine, superficial powder with a high surface area that is a suitable catalyst for hydrogenation reactions;
- precipitation and co-precipitation: preparation of a solution containing a precursor of the desired metal (such as an aqueous solution of a salt) to which a precipitant agent (usually acids or bases) is added to generate the desired solid. Co-precipitation operates in the same way, except that there are two or more precursors. The obtained bulk catalyst or support is aged, filtered, washed, dried, and calcined;
- hydrothermal synthesis: in an autoclave, precipitates, flocculates, or gels are heated to temperatures between 100 and 300 °C in the presence

of water. There is a variation of the structure of the solid: it is possible to obtain ordered structures starting from amorphous solids.

The most frequent procedure for preparing a supported catalyst entails five steps [94,95]:

1. First, the substrate is prepared. This is typically precipitation or co-precipitation. Supports created in this manner include metal oxides such as silicon, titanium, and aluminium, as well as mixed oxides such as magnetite.

2. Substrate impregnation. A solution containing the metal precursor is introduced in contact with the porous support that absorbs it. It differs in dry impregnation, when the solution containing the precursor is even at the maximum quantity absorbed by the support, and in wet impregnation, when the solution of the precursor is in excess.

3. Post-preparation treatment. It consists of filtration, washing, drying and calcination. Drying is a straightforward procedure for crystalline solids, but complex for hydrogels and other supports precipitated by water: most of them must be removed slowly and consistently, otherwise the pores may collapse. The residual of the solvent is eliminated by calcination (300-800 °C), which also serves to eliminate the counter-ions of the metal precursor not removed by washing. At the conclusion of the procedure, the impregnated metal takes the form of oxide.

4. Forming. It serves to give the catalyst the necessary shape, so that the interior of the reactor has the required mechanical and physical qualities for the operation. It is possible that a binder is utilized throughout these operations to create the desired forms. Pelletizing and extrusion are typical techniques for shaping, from which pellets, cylinders, cones, etc., can be made.

5. Activation. As previously stated, once the catalyst has been calcined, the metal phase takes the form of an oxide. Reducing this oxide with hydrogen transforms it back into metal, yielding the active phase and the final catalyst.

2.2 Instrumental analytical techniques for the characterization of heterogeneous catalysts

Several techniques are usually employed for heterogeneous catalysts characterization. Among these, Scanning Electron Microscopy (SEM), X-ray diffraction (XRD) and thermogravimetry (TGA) are the most commonly used. In such a way, different and complementary information on sample morphology, crystalline structure and thermal stability can be extrapolated. Alongside, temperature programmed reduction in H_2 atmosphere (H_2-TPR) and equilibrium adsorption and desorption isotherms of N_2 at 77 K (surface area analysis) are also introduced in the following, being useful for the evaluation of metal oxide reduction behavior and porosity features of catalysts, respectively. Experimental conditions for catalysts characterizations are reported for each investigation technique.

2.2.1 Scanning Electron Microscopy (SEM)

Scanning electron microscopy provides information regarding topography, morphology, composition, and crystallography of samples. It is considered a versatile technique for micro- and nanostructures analysis with a large range of applications. A scanning electron microscope consists of an electron optical column, where a beam of electrons is generated by a suitable source, typically a tungsten filament, and accelerated through a high voltage between 20 and 60 kV. The electron beam is focused into a fine spot on the sample surface through appropriate lenses. This beam is scanned in a rectangular raster over the specimen and the intensities of various signals created by interactions between the beam electrons and the specimen are measured and mapped as variations in brightness on the image display. These

signals include backscattered electrons, secondary electrons, X-rays and Auger electrons and their creation mechanisms are shown in Figure 2.1. The penetration of electrons to different depths provides different signals and therefore each interaction can provide information on the material composition, surface topography and morphology [96].

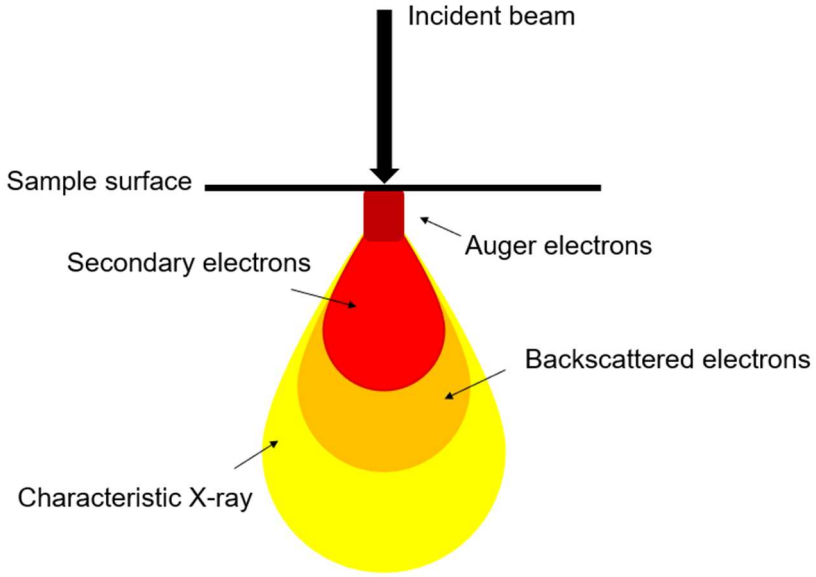

Figure 2.1. Schematic diagram of the interaction of radiation-matter: Auger electrons, secondary electrons, backscattered electrons, and X-rays.

SEM is generally coupled with Energy-dispersive X-ray spectroscopy (EDX), an analytical technique used for the elemental analysis or chemical characterization of a sample, generally referred to as microanalysis. It relies on the investigation of the interaction of X-rays with the sample. Its characterization capabilities are due in large part to the fundamental principle that each element has a unique atomic structure allowing a unique set of peaks on its X-ray spectrum. To stimulate the emission of characteristic X-rays from a specimen, a beam of X-rays is focused into the sample. The incident beam may excite an electron in an inner shell, ejecting it from the shell while creating an electron hole. An electron from an outer higher-energy shell then fills the

hole, and the difference in energy between the higher energy shell and the lower energy shell may be released in the form of characteristic X emission. The number and energy of the X-rays emitted from a specimen can be measured by an energy-dispersive spectrometer. Thus, the elemental composition of the sample is possible since the X-rays energy depends on the energy difference between the two shells and on the atomic structure of the element from which they are emitted.

A Phenom Pro-X scanning electron microscope equipped with an energy-dispersive X-ray spectrometer was utilized for SEM analysis. The EDX analysis was used to evaluate the content and dispersion of metal, acquiring for all samples at least 20 points of investigation at three different magnifications. The counting time for the EDX analysis was 120 s. The results were found to be reproducible to less than ±5% for all samples.

2.2.2 X-ray diffraction (XRD)

X-ray diffraction is an analytical technique mainly used to gather information on crystalline solids. This type of information includes variations in crystal structure, phase quantification and identification, shape and size of crystallite, distortion of lattice, size, and periodicity of non-crystalline and orientation. It is based on the interaction of X-radiation with matter, explained by Bragg's Law (Eq. 1):

$$2d\sin\theta=n\lambda \qquad \text{(Eq. 1)}$$

where d is the distance between crystal planes layers, ϑ is the incident angle, n is an integer (the diffraction order) and λ is the incident wavelength (Figure 2.2). When the path difference is equal to any integer value of the wavelength, a constructive interference will occur. X-ray sources are the commonly used tubes, in which a tungsten filament, made incandescent by the passage of a current, is brought to a negative potential of 30-60 kV and emits electrons,

which are directed, for effect of the electric field, to a target of pure metal (Cu, Cr, Fe, Co, etc.) acting as an anode. Copper is the most common target material, with λKα(Cu)=1.5418 Å, [97]. Characteristic X-ray spectra are produced and directed onto the sample (Figure 2.2).

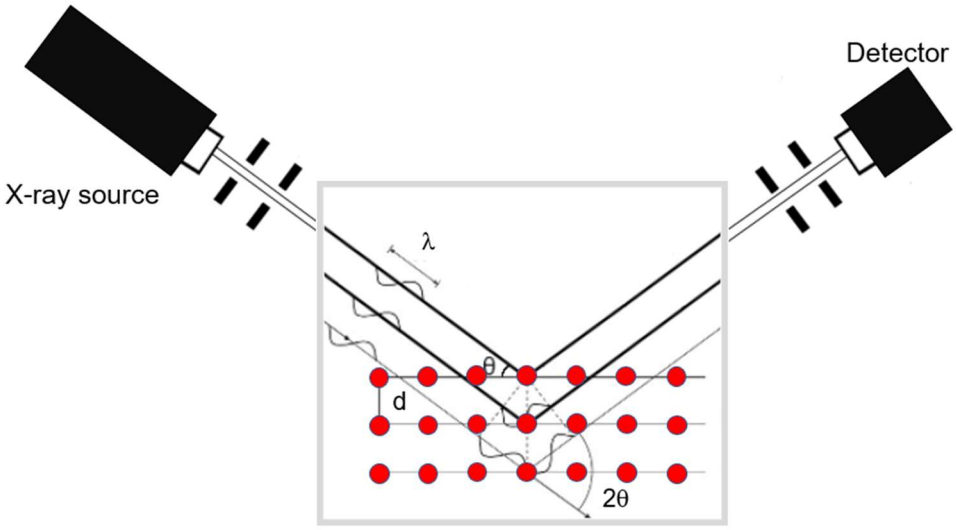

Figure 2.2. Instrumental sketch and geometry for interference of a wave scattered from two planes separated by d spacing.

Diffracted X-rays are then detected, processed and counted. By scanning the sample through a range of 2θ angles, all possible diffraction directions of the lattice can be obtained. The result is displayed in a diffractogram where the intensity of diffraction is reported versus the 2θ angle. Peaks can be unequivocally attributed allowing material identification.

To this purpose a Bruker D2 Phaser with CuKα radiation at 30 kV and 20 mA was used. Peaks attribution was made according to COD (Crystallographic Open Database). The diffraction angles 2θ were varied between 10° and 120° in steps of 0.02° and a count time of 5 s per step.

An x-ray diffraction analysis, with a temperature effect evaluation within the range 25-1000°C, was carried out by a Panalytical Empyrean S-2

diffractometer, using Cu Kα radiation (1.54056 Å) at 40 kV and 40 mA. The patterns were recorded in step scan mode from 10-60° 2θ angles in steps of 0.02° and a count time of 5 seconds per step.

2.2.3 Thermogravimetry (TGA)

Thermogravimetry (TGA) and coupled differential scanning calorimetry (DSC) are two characterization techniques that allow to investigate the transformations that occur in a sample as the temperature changes. In particular, thermogravimetry is a technique that allows to analyze the change in weight of a given sample while it is subject to heating through a controlled growth of temperature. During the thermogravimetric analysis of samples, heating causes chemical transformations with splitting of the bonds that usually lead to the formation of volatile products. Therefore, TGA is mainly used for understanding thermal events such as absorption, adsorption, desorption, vaporization, sublimation, decomposition, oxidation and reduction [98]. Alongside, the prediction of thermal stability for samples allows to study the kinetics of chemical reactions under various conditions. Indeed, thermal stability is determined for a substance using TGA based on its ability to maintain its characteristics as almost unaffected as likely upon exposure to heat. Upon increasing the temperature of a sample, it is certain that the sample undergoes weight loss. The information about weight loss remains significant in order to determine the composition of the sample such that it is possible to understand the reaction steps involved in the decomposition process. Through weight loss profile, it is also possible to identify the unknown compound present in the sample or evaluate the amount or percentage of a specific compound present among the mixture of different compounds present in the sample. The result of this analysis is expressed with a thermal decomposition curve, which reports in abscissa the

temperature or time and in ordinate the change in mass, as an absolute value or percentage.

Differential scanning calorimetry is instead an analysis that provides quantitative information about the energy exchanges that take place within the sample, studying in particular the difference in thermal flux between the sample under examination and a reference one. The heat flux between the sample to be examined and the reference sample is proportional to the temperature variation between them, which is due to the phenomena that occur within the sample.

The instrumentation for this type of investigation basically consists of a microbalance inserted into a furnace equipped with an accurate temperature regulation (Figure 2.3). The system is managed by a computer that simultaneously controls the weight and the heating or cooling of the sample, recording the mass and temperature values over time. The control of the pressure and the composition of the surrounding atmosphere is also allowed, through a gas system apparatus.

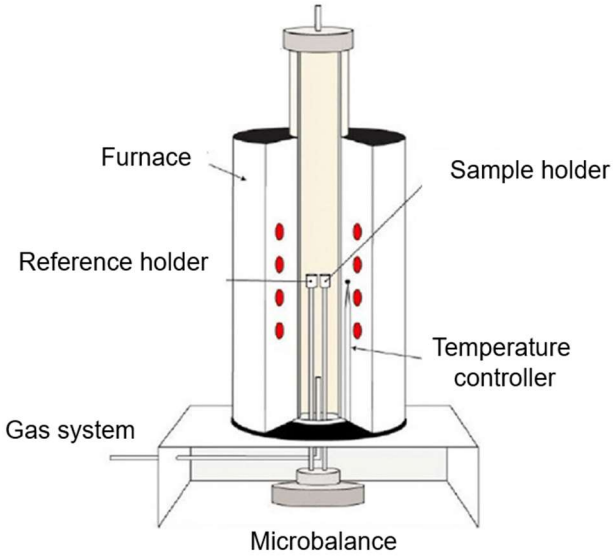

Figure 2.3. Schematic representation of TGA-DSC instrument.

Thermogravimetric TGA/DSC analysis was performed with a Netzsch instrument. The temperature-programmed experiments were carried out in the range 25–1000°C, under a total air flow rate of 100 cc/min with a heating rate of 2°C min^{-1}.

2.2.4 Temperature programmed reduction by hydrogen (TPR-H_2)

Temperature Programmed reduction (TPR) is a very useful characterization analysis used in the study of catalysts based on metal oxides, since it allows to obtain important information on the oxidation state of the reducible species present in the material, identify the most efficient reduction conditions and characterize complex systems, as bimetallic or doped catalyst, allowing to establish alloy formation or promotion effects [99].

In the TPR technique an oxide catalyst precursor undergoes a programmed temperature rise while a reducing gas mixture (usually hydrogen diluted with inert nitrogen) is flowed over its surface. The sample is placed inside a quartz reactor and placed in an electric furnace that heats it up to high temperatures. The reduction rates are continuously measured by monitoring the change in composition of the reactive mixture. Indeed, the decrease in H_2 concentration in the effluent gas with respect to the initial percentage monitors the reaction progress.

From the TPR spectrum it is possible to obtain qualitative information, since, based on the number of TPR peaks obtained, it is possible to determine not only the number of reducible species present but also their oxidation state and reduction temperatures. Graphically, the consumption of reducing agent (H_2) as a function of temperature is reported, obtaining a series of peaks each corresponding to a distinct reduction process concerning the metal oxide.

The reduction of metal oxides was carried out with a Chemisorb Micromeritics 2750 instrument under a flux of 50 cm^3 min^{-1} of 10 vol.% H_2/Ar in the temperature range 25–1000°Cat atmospheric pressure.

2.2.5 Transmission Electron Microscopy (TEM)

The transmission electron microscopy is a very powerful technique based on the interaction of a sample with a high energy beam of electrons, transmitted through it. This interaction can be used to observe features such as crystal structures, dislocations and grain boundaries as well as chemical compositions of samples. TEM microscopy operates on the same basic principles as the light microscope unless it makes use of electrons. Since the wavelength of electrons is much smaller than that of light, it can reveal the finest details as small as an individual atom. The beam of electrons, generated from an electron gun, is accelerated through a high voltage up to 200 kV, necessary to penetrate the specimen. It is then focused into a thin coherent beam by the use of appropriate lens over the sample and transmitted depending upon sample thickness and its transparency to the e-beam. The transmitted beam is focused by the objective lens into an image on a charge coupled device (CCD) camera. The image then passes down through a number of lenses and is finally enlarged to the desired magnification (Figure 2.4). Darker areas of the image represent those areas of the sample in which transmission of fewer electrons occurs and on the contrary lighter areas of the image represent the areas of the sample where electrons are mainly transmitted through.

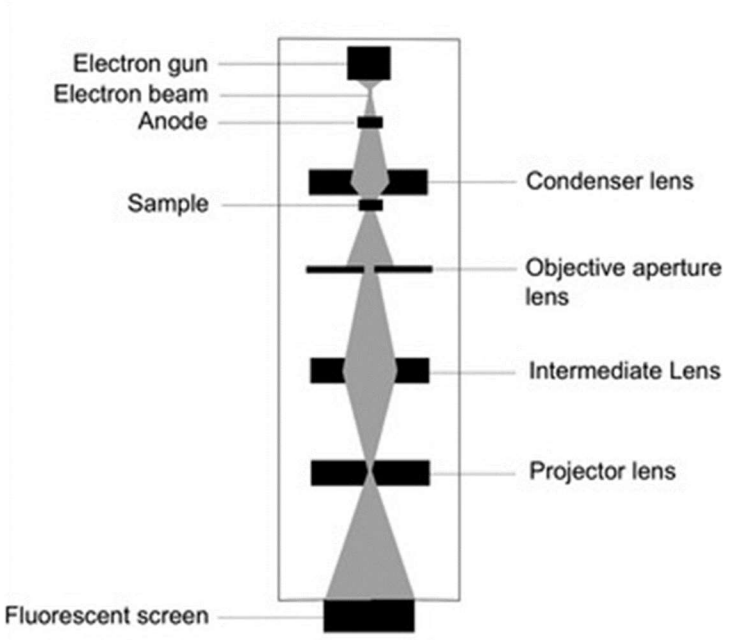

Figure 2.4. Schematic representation of TEM instrument.

The transmission electron microscopy analysis was carried out using a JEOL 1400 Plus instrument operated at 120 kV, able to achieve a 0.19 nm point-to-point resolution and a 0.14 nm line resolution.

2.2.6 Surface area analysis (BET)

The BET (Brunauer, Emmett, Teller) method is widely used for the calculation of surface areas of solids by physical adsorption of gas molecules. In detail, for the measurement of the specific surface of porous materials, the method of gas adsorption is used until the formation of a monolayer, so that the volume of the adsorbed gas is directly proportional to the specific surface of the material, according to the following relationship (Eq. 2):

$$S_s = \frac{V_m N A}{V W} \quad (m^2/g) \qquad \text{(Eq. 2)}$$

being V_m the volume of the gas monolayer (m^3), A the area of the gas molecule (m^2/molecules), V the molar volume (which under normal conditions is equal

to 22.414 l), *N* the Avogadro number (equal to $6.023 \cdot 10^{23}$ molecules), *W* the weight of the material (g).

The adsorption of the gas on the surface of the material is reversible and generally inert gases such as nitrogen N_2 and argon Ar are used for this purpose. The temperature at which the system operates is the liquefaction temperature of the gas, so that it works under conditions of equilibrium of liquid ↔ vapor condensation. Nitrogen gas is the most widely used adsorbate due to its low cost and easy to handle; moreover, liquid nitrogen is used as a cooling agent due to its liquefaction temperature, equal to 77 K, [100].

Under well-defined requirements and conditions, thanks to the BET equation, applying the equilibrium condition of the volumes of adsorbed and desorbed gas to the various layers, the following equation (Eq. 3) is reached:

$$\frac{V}{V_m} = \frac{cp}{p_0\left(1-\frac{p}{p_0}\right)} \cdot \frac{1}{\left(1-\frac{p}{p_0}+c\frac{p}{p_0}\right)} \qquad \text{(Eq. 3)}$$

where *c* is the c-BET constant that determines seven different adsorption curves; *p* and p_0 are the equilibrium and the saturation pressure of adsorbates at the temperature of adsorption, respectively. The BET equation is valid only in the range $0.05 \leq p/p_0 \leq 0.3$.

Surface area analysis of samples was determined by equilibrium adsorption and desorption isotherms of N_2 at 77 K with a Micromeritics ASAP 2020 instrument. Before the analysis, all samples were pre-treated in vacuum condition at 200°C for 12h. To determine the total surface area of samples, the data collected were modelled using the BET equation. The evaluation of microporous volumes, internal and external surface area, V–t curves were also interpreted by the 't-plot' method, using the Harkins–Jura reference isotherm [101].

2.3 Catalytic systems for the reforming of different fuels

The catalytic systems for the reforming of fuels are continuously under investigation, since the reforming of fuels represents a promising technology for low carbon and renewable hydrogen production. The most active species in these processes are noble metals and nickel-based catalysts [102–107]. The interest of researchers on Ni-based catalysts is due to their lower cost and higher availability as compared to noble metal catalysts, as well as their considerable intrinsic activity. The support is an important element in the catalyst design too, as it has the function of a skeletal framework that distributes the active metal particles. Sometimes, chemical modifications of support and metal active species can be necessary to avoid the deterioration of the reforming catalyst due to the presence of heavy hydrocarbon and sulphur compounds. High carbon deposition and sulphur resistance can be generally achieved by catalysts containing alkaline earth metal oxides and rare earth oxides in the support [108–111].

Among the different strategies to improve the catalytic performance and at the same time reducing carbon deposition, the development of composite materials is one of the most followed. Ceria-zirconia based catalysts have been shown to contribute to a better metal dispersion and to aid carbon tolerance, thanks to their oxygen storage capacity [112]. Literature data reported that the Ni-Ce-ZrO2 system was suitable as anode material for direct internal reforming of biogas by solid oxide fuel cells. In fact, the incorporation of cerium in ZrO_2 improved the bulk oxygen mobility and the oxygen storage capacity of composite material, mitigating the carbon deposition [113]. Other authors showed that lanthanum and neodymium ions incorporation in ceria

structure promoted a higher abundance of defects and oxygen vacancies, resulting in a less reducible oxygen-deficient material that improves the CO oxidation activity, as a result of the weakened cerium-oxygen bonds [114].

In this context, the activity was focused on the investigation of the reactivity of nickel-based catalytic systems supported over ceria-zirconia, undoped and doped with lanthanum and neodymium, towards the reforming reactions: steam reforming (SR), partial oxidation (POX) and autothermal reforming (ATR) of different fuels (methane, biogas and propane).

2.3.1 Production and characterization of catalysts for reforming

The catalytic system was realized using nickel metal dispersed over ceria-zirconia support, in both the undoped and lanthanum/neodymium doped forms. Supports were prepared with a surfactant assisted method according to literature data [115]. In particular, $Ce_{0.8}Zr_{0.2}O_2$ (CZ80) and $Ce_{0.8}Zr_{0.13}La_{0.5}Nd_{0.2}O_{2-x}$ (dpCZ80) were produced. Supports were impregnated with an alcoholic solution of nickel nitrate hexahydrate, with a nominal content of nickel equal to 3,5% in weight with respect to the support. Impregnated samples were then calcined at 500°C for 1 hour under air flux.

In Figure 2.5 XRD patterns of samples are reported. The bare support CZ80 showed visible peaks at about 28.4°, 32.9°, 47.3° and 56.2° which correspond to the indices of (1 1 1), (2 0 0) and (3 1 1) planes of CeO_2. The XRD profile of the support indicates that zirconia could be incorporated into the ceria lattice to form a solid solution maintaining the fluorite structure, indicating that the cubic Ce and Zr were highly homogenously distributed. According to previous studies, it was observed a shift of peaks relative to the cubic ceria phase to higher 2-theta ceria-zirconia positions.

The XRD of dpCZ80 had the same profile of CZ80 sample. In the XRD profile it was observed a shift of the peaks to higher 2-theta values with respect to the undoped phases, confirming the insertion of lanthanum and neodymium into the fluorite structure. In the detail of Figure 2.5 the peak at 2-theta 28.6 shifts to 29.3 after the incorporation of zirconia and to 2-theta equal to 29.8 after the incorporation of neodymium and lanthanum. The profile of calcined catalysts exhibits a cubic NiO phase as indicated from the (1 1 1), (2 0 0) and (2 2 0) diffraction peaks at 2-theta 37.4, 43.4 and 62.6 respectively.

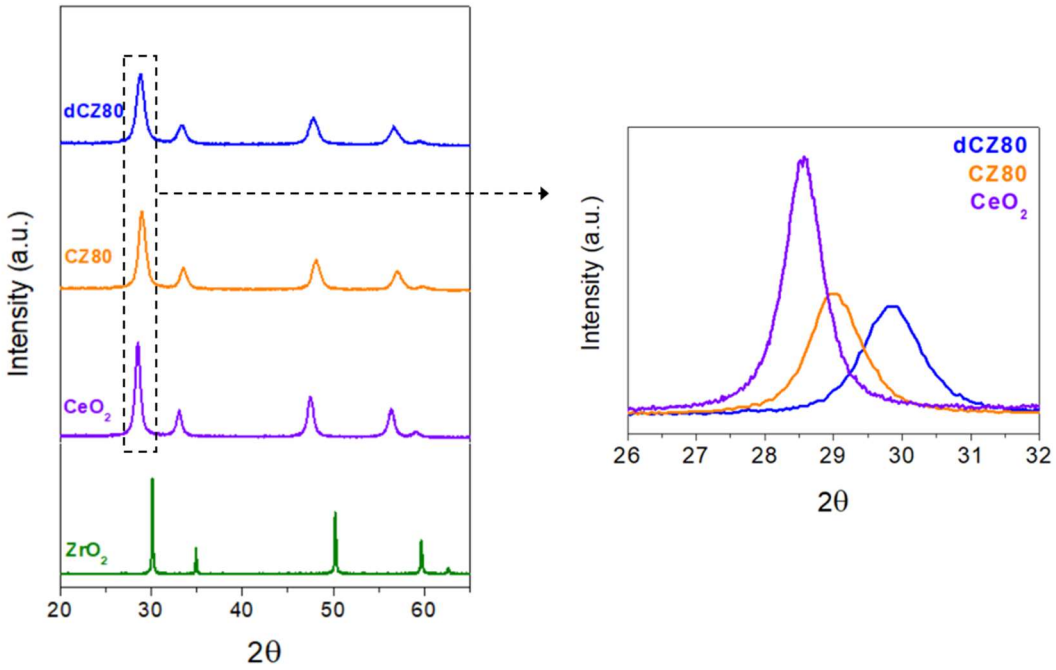

Figure 2.5. XRD spectra of ceria-zirconia supports, undoped and doped.

The thermal stability of the doped catalyst was investigated through the evaluation of XRD spectra recorded at increasing temperature from 25°C to 800°C indicating that the structure was retained (Figure 2.6). The absence of typical peaks of lanthanum and neodymium species confirmed a high thermal stability of powder without exsolution of doped elements.

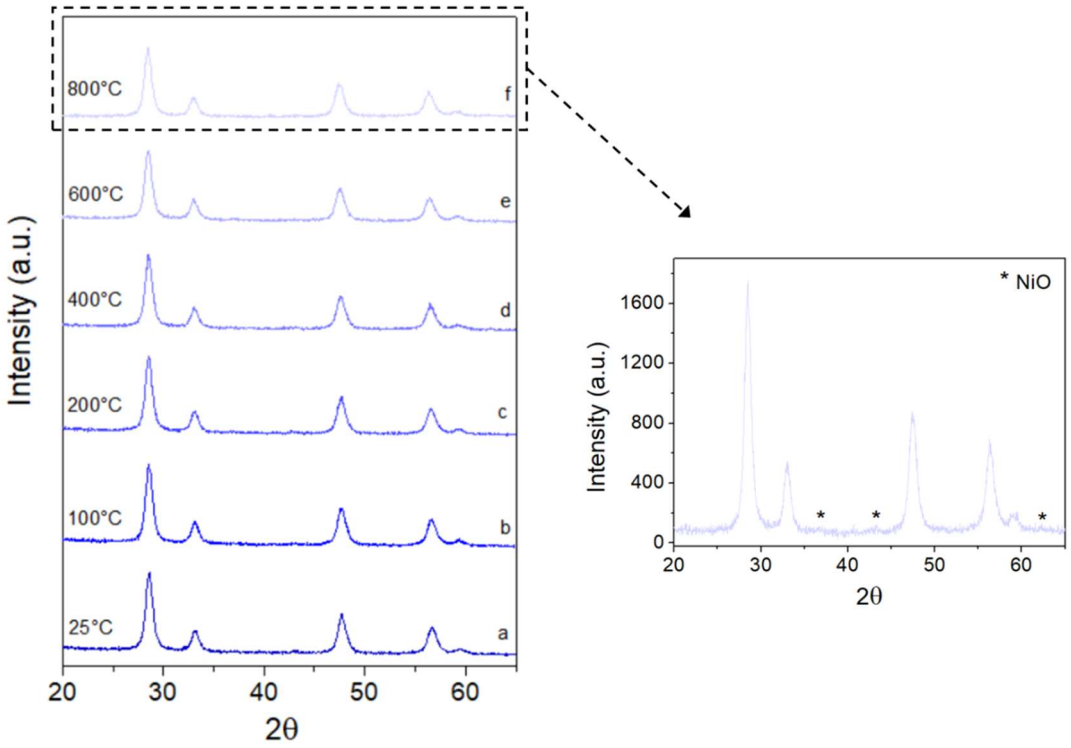

Figure 2.6. XRD spectra vs temperature of doped ceria-zirconia support.

Supports and catalysts were studied by SEM analysis (Figure 2.7). Particles distribution, heterogeneous shapes and morphologies were maintained, confirming that no significant modifications were caused after nickel impregnation and calcination treatments. In addition, EDX analysis showed the homogeneous distribution of the different elements in the catalyst (Figure 2.8) and the loading of the nickel metallic phase, which resulted very close to the nominal content (3.5 ± 0.2 %).

TEM images of Ni catalysts supported on undoped and doped support showed for both samples a well-defined cubic nanomorphology with slightly reduced dimension for the doped samples and the absence of the segregation related to doping of lanthanum and neodymium, confirming the reliability of results obtained by X-Ray diffraction analysis. Furthermore, an almost unimodal dispersion could be observed for both catalysts with slightly reduced dimensions for the doped sample. The difference can be explained

considering that the incorporation of dopant ions in ceria-zirconia structure hinder the crystal growth, fostering the formation of smaller nanocubes, (Figure 2.9).

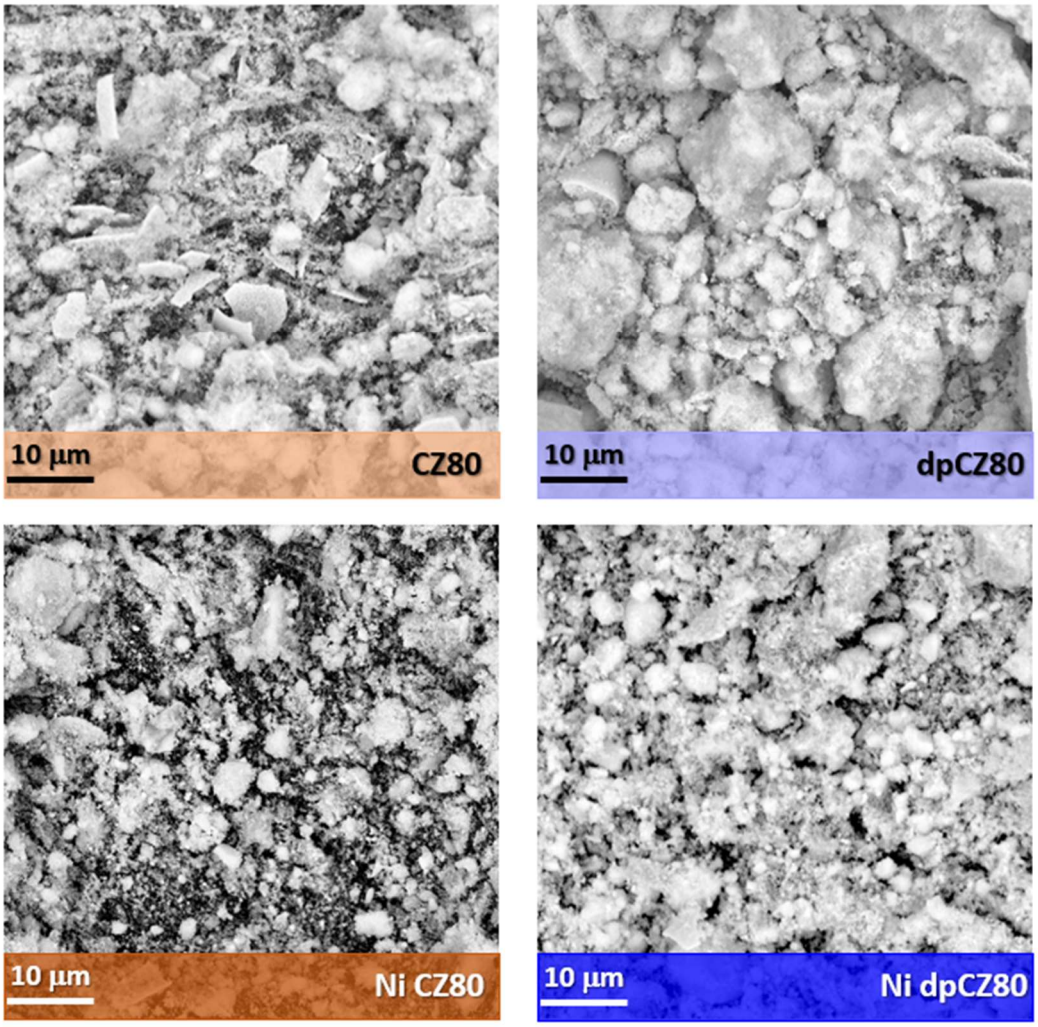

Figure 2.7. SEM micrographs of supports, undoped CZ80 and doped dpCZ80, and Ni supported catalysts, NiCZ80 and NidpCZ80.

The TPR-H_2 profiles of supports, undoped and doped, and Ni- catalysts are shown in Figure 2.10. For the undoped support the lower temperature was related to the reduction of superficial Ce^{4+} and Zr^{x+}, while the larger band up to 700°C was the result of the progressive release of the lattice oxygen from the bulk of the sample. The doped support was characterized by a similar profile, in agreement with Sartoretti et al. [114]. In addition, the effect of doping

appeared to be limited to the slight anticipation of the surface reduction at lower temperature. The same behaviour was also observed for both Ni supported catalysts, NiCZ80 and NidpCZ80. In particular, for the catalyst supported on the doped support, peaks ascribed to the direct reduction of NiO to Ni were shifted to lower temperatures.

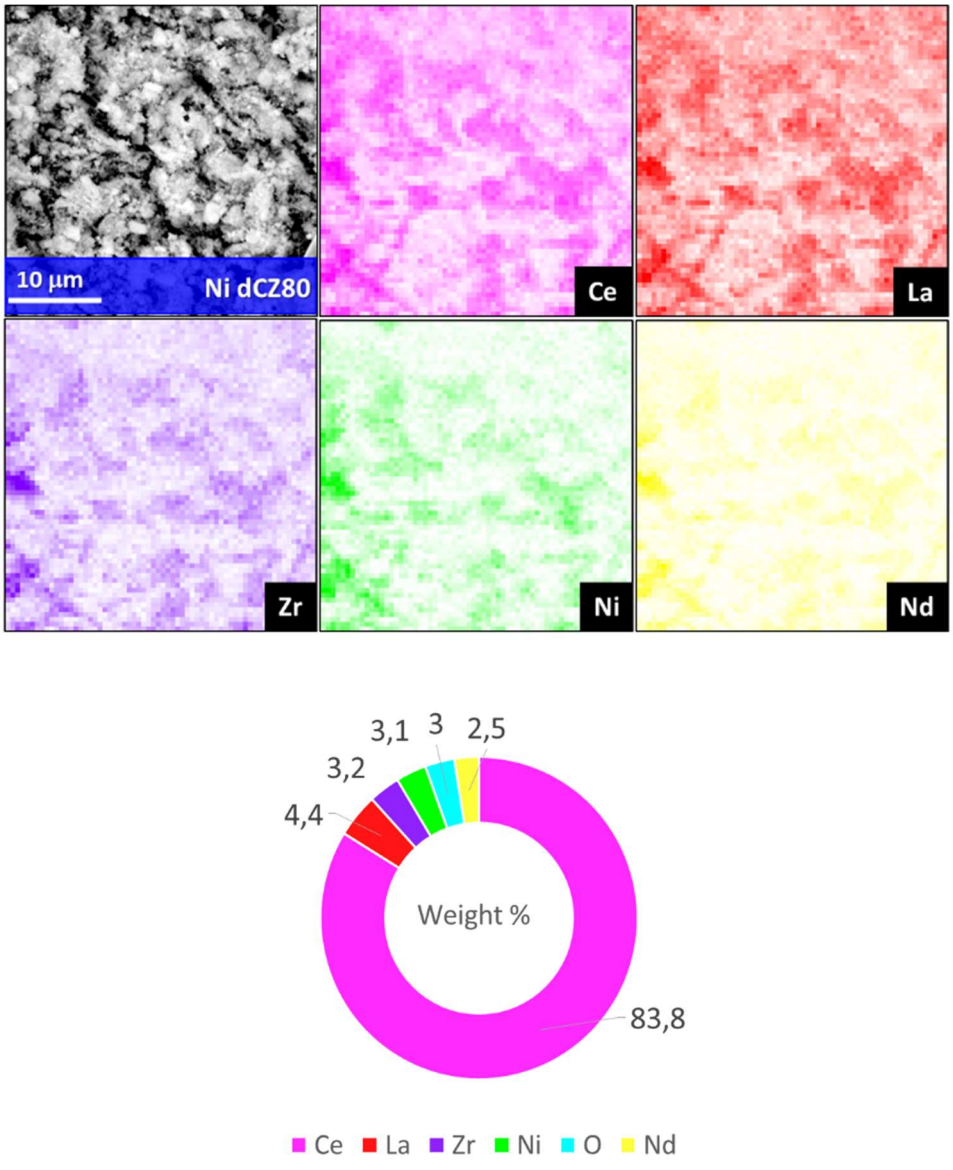

Figure 2.8. EDX mapping of element distribution over NidpCZ80 catalyst.

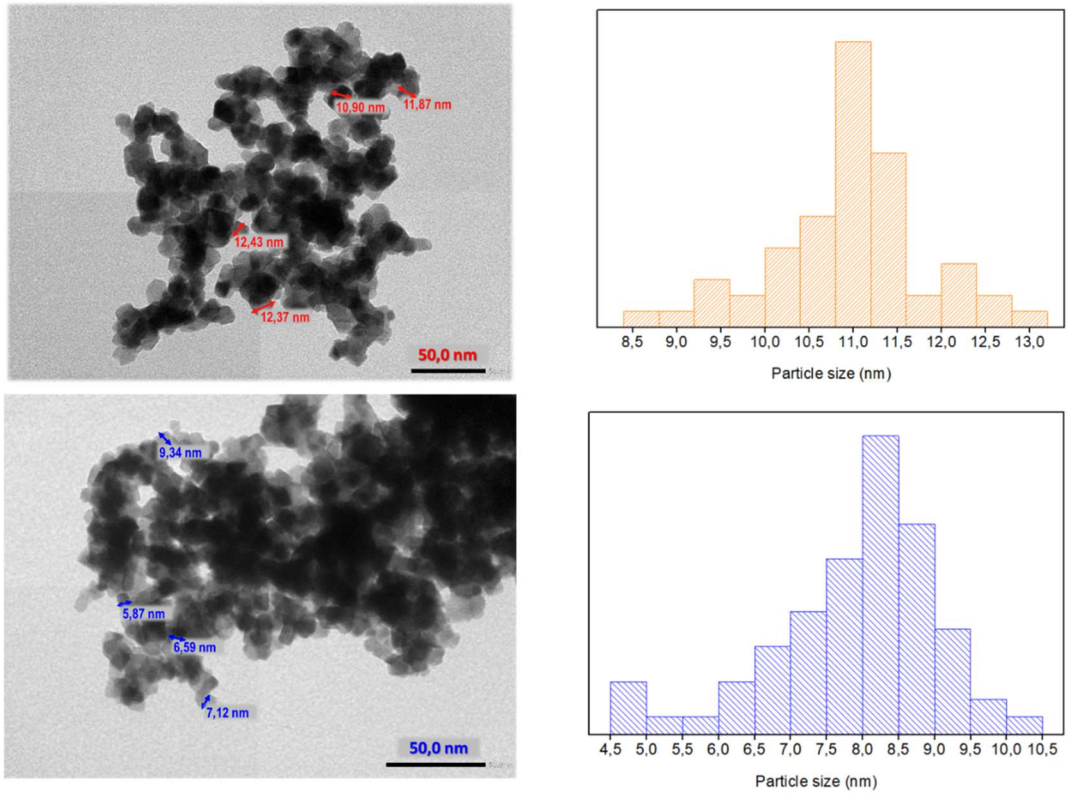

Figure 2.9. TEM images and particle size distribution of catalysts.

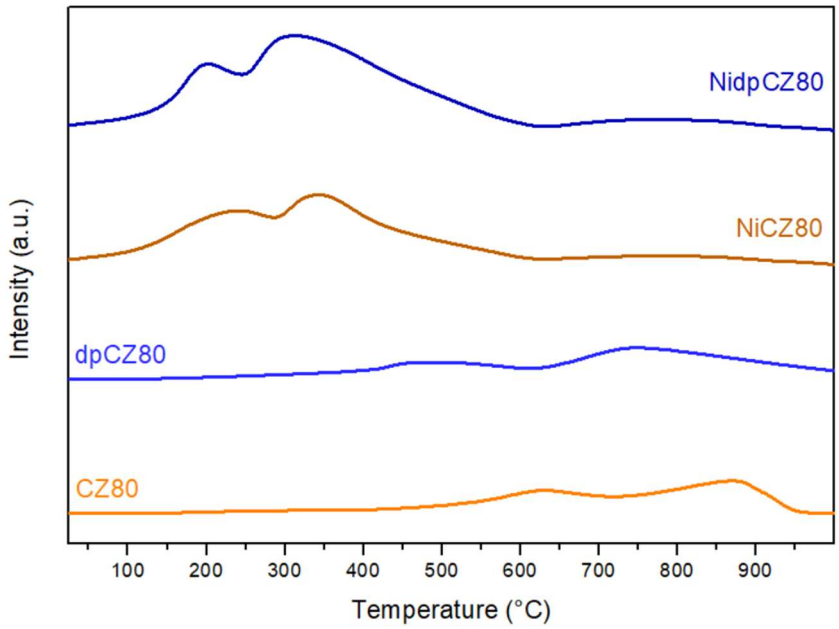

Figure 2.10. H_2-TPR profiles of supports, undoped CZ80 and doped dpCZ80, and Ni supported catalysts, NiCZ80 and NidpCZ80.

2.3.2 Experimental setup for the catalytic activity evaluation in reforming

Catalytic activity was evaluated in a quartz microreactor of internal diameter equal to 4mm, positioned in a ceramic tube furnace, at atmospheric pressure and at 800°C. All catalytic tests were performed at 120,000 h^{-1} space velocity (GHSV). The microreactor was operated in a down-flow mode with the gas inlet placed at the top of the reactor.

The gaseous mixture flows were adjusted for the different reactions: steam reforming (steam to carbon mole fraction S/C=2.5); partial oxidation (oxygen to carbon mole fraction O/C=0.5); autothermal reforming (mole fraction S/C=2.5 and O/C=0.5). In order to take into account the variation of the number of moles in the reactions, nitrogen was fed in the inlet stream and then was used as an internal standard. The outlet streams from the reactor were analyzed by a gas-chromatograph equipped with a TCD detector and columns appropriate for the gas identification. The time on stream was 10 hours and the catalytic activity results were generally registered 15 minutes after the start of the reaction. Overall, carbon and hydrogen balances were close to 100% in each experiment with standard deviation lower than 3%.

Conversion percentages were calculated as (Eq. 4):

$$\%Conversion = \frac{Fuel_{in} - Fuel_{out}}{Fuel_{in}} \qquad \text{(Eq. 4)}$$

Catalytic tests performed are reported in Table 2.1 together with related operational conditions.

Table 2.1. Experimental conditions adopted for ATR, SR and ATR reactions over undoped NiCZ80 and doped catalysts.

Reaction	Catalyst	Fuel	Experimental conditions			
Type			S/C	O/C	GHSV [h^{-1}]	T
ATR	3%NiCZ80	CH_4	2.5	0.5	120,000	800°C
SR			2.5	--		
POX			--	0.5		
ATR /100ppm H_2S			2.5	0.5		
ATR	3%NidpCZ80		2.5	0.5		
SR			2.5	--		
POX			--	0.5		
ATR /100ppm H_2S			2.5	0.5		
ATR	3%NiCZ80	C_3H_8	2.5	0.5		
SR			2.5	--		
POX			--	0.5		
ATR / 100ppm H_2S			2.5	0.5		
ATR	3%NidpCZ80		2.5	0.5		
SR			2.5	--		
POX			--	0.5		
ATR / 100ppm H_2S			2.5	0.5		
ATR	3%NiCZ80	CH_4/CO_2	2.5	0.5		
ATR/ 100ppm H_2S			2.5	0.5		
ATR	3%NidpCZ80	CH_4/CO_2	2.5	0.5		
ATR/ 100ppm H_2S			2.5	0.5		

2.4 Catalytic systems for CO_2 methanation

The development of effective and efficient CO_2 methanation catalytic systems is still a great challenge. Indeed, despite numerous metals are used as well-known active phases in CO_2 methanation reactions [24], the support of this phase plays a fundamental role, mainly improving the dispersion of active components and tuning the surface structure of catalysts. Therefore, the production of competitive and stable catalysts is based on the optimization of the couple metal/support.

Despite the several metals, nickel is regarded the best one due to its low cost and catalytic performance, while much wider is the choice of the support. Among these, SiO_2-based materials, such as zeolites, have been envisaged as good support materials due to peculiar features like ordered structures, high surface area, large pore volume, and affinity versus the CO_2, owing to the intrinsic basicity of the support [116].

The use of different zeolite-based catalysts and their potentiality for carbon dioxide methanation was reported by many authors. The type of zeolites more investigated were Y, A, X and ZSM-5 [117]. In this scenario few studies have employed the Engelhard Titanosilicate (ETS) as catalyst support. In particular, ETS-10 titanosilicate was proved to be an active and stable support for Ru species in the dry reforming of methane, it was reported to increase the selectivity when used as Pt support in the hexane reforming [118] and it was tested as a performant catalyst for the selective oxidation of CO in the presence of H_2, CO_2 and H_2O [119]. Successful results were also reported in the styrene functionalization reaction with Cu active phase [120].

However, these materials, due to their porosity features, need more in-depth investigation to improve their application in the catalysis field. In the

following, the suitability of ETS material as support for Ni catalyst in the methanation reaction will be presented and discussed.

2.4.1 Production and characterization of catalysts for CO_2 methanation

Engelhard titanium silicates, ETS-4 and ETS-10, are microporous materials composed of tetrahedral SiO_4^{4-} and octahedral TiO_6^{8-} units [121]. ETS-4 ($Na_9Si_{12}Ti_5O_{38}(OH)\oplus 12H_2O$) and ETS-10 ($M_2TiSi_5O_{13}$ H_2O with M=Na, K) have the same structure but differ from each other in the Si/Ti ratio and in the pore size. ETS-4 and ETS-10 were synthesized according to literature data [122,123]. Nickel was deposited over the two supports by incipient wetness impregnation method. The metal precursor, nickel nitrate hexahydrate $Ni(NO_3)_2$ $6H_2O$, was appropriately solubilized in an ethanol solution and dispersed on the ETS support with a total metal content of 5% by weight. After the impregnation process, the catalyst was dried at 120°C for 24 hours. Subsequently, using a mixture of 10 vol% H_2 in a He stream, the catalyst was reduced for 2 h at 500 °C using the same heating and cooling rates. Samples were characterized after each step of production.

The identification of phases in fresh, impregnated/dry, reduced and spent catalysts was performed by powder X-ray diffraction [124]. X-ray diffraction patterns of synthesized ETS-4 and ETS-10 are reported in Figure 2.11. As confirmed by literature, the synthesized carriers are pure ETS-4 and ETS-10. The impregnation process did not significantly alter the patterns of the tested materials, whereas reduction destroyed the structure of ETS-4. Indeed, in the related pattern, the only peak defined at about $2\theta = 44.6°$ corresponded to metallic nickel. For the reduced Ni/ETS-10, a peak associated with metallic nickel was detected too. It was found that the low thermal stability of ETS-4 was related to hydrogen bonding between the extra-framework water

molecules and the framework oxygen atoms, forming a glassy amorphous phase [125].

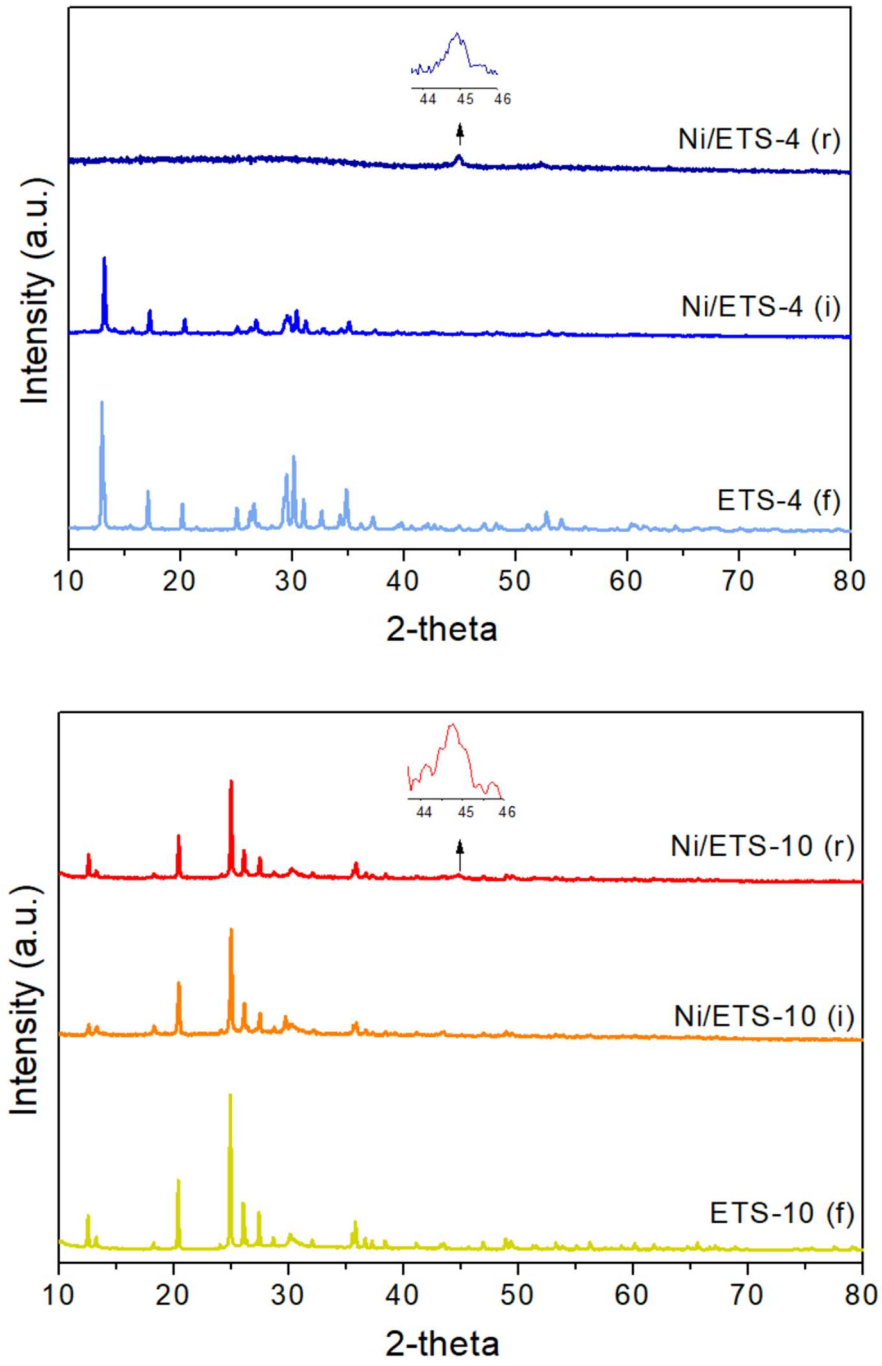

Figure 2.11. Diffraction pattern of: fresh ETS-4 (f), Ni/ETS-4 (i) after the impregnation treatment and Ni/ETS-4 (r) after the reduction treatment; fresh ETS-10 (f), Ni/ETS-10 (i) after the impregnation treatment and Ni/ETS-10 (r) after the reduction treatment, [124].

The porous features of the samples were determined by equilibrium adsorption and desorption isotherms of N_2 at 77 K. The pore volumes of the two supports were 0.12 and 0.15 cm^3/g for ETS-4 and ETS-10, respectively, close to typical values for other microporous materials. The contribution of internal surface area to total surface area was highly significant for both as-synthesized samples, 95% for ETS-10 and 90% for ETS-4. Since all isotherms were of type I, the deposition of Ni by impregnation of both structures did not significantly affect the specific surface area of the final sample or its pore volume. Indeed, after impregnation, samples showed a surface area reduction of ~13% for ETS-4 and ~9% for ETS-10. After the reduction, the internal surface area of Ni/ETS-10 decreased, whereas the external surface area increased. Moreover, the N_2 adsorption isotherm exhibited a hysteresis loop, at a relative pressure of 0.45–0.96, attributed to the presence of mesopores in the sample. Ni/ETS-4 showed a more important loss of internal surface area with respect to the pristine ETS-4, registering a decrease of the micropores volume almost to zero. The complete loss of the microporous area was explained by the incipient structure collapse, as also confirmed by XRD.

The sample ETS-4 exhibited a cuboid-like morphology, made of small plate crystals that measured approximately 2×20×5 μm (a×b×c). The treatment of impregnation did not modify the morphology of the support, but the reduction treatment promoted a "dissolution" of crystals, in agreement with the XRD observations. ETS-10 support was characterized by a more regular cubic shape that was not altered by the impregnation and the reduction steps, as evidenced in Figure 2.12. The distribution of nickel on the ETS-10 surface was regular as mapped by EDX and metal crystal size was estimated equal to 9.2 nm (±0.6 nm) through the Debye-Scherrer relation, Figure 2.13.

In Table 2.2 the main texture properties of supports and catalysts are reported [124]. The amount of deposited nickel was quite like the nominal content for both samples. The bare supports have microporous characteristics:

the internal surface area higher than the external one and are characterized by a monomodal distribution in the range of micropores.

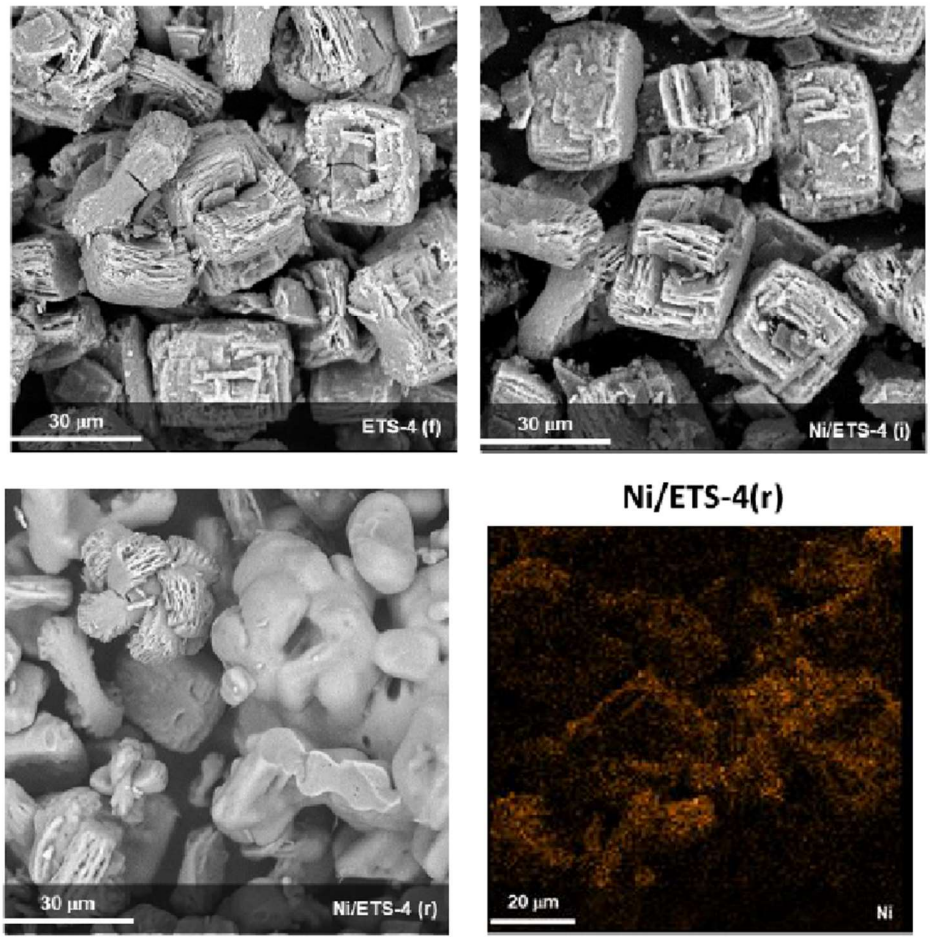

Figure 2.12. SEM and EDX of ETS-4 fresh (f), Ni/ETS-4 (i) after the impregnation treatment and Ni/ETS-4 (r) after the reduction treatment [124].

The TPR profiles, performed to study the reducibility of nickel precursor species and the metal–support interaction, showed for both samples, H_2 consumption peaks. In detail, peaks at 367°C for ETS-4 and 336°C for ETS-10 were attributed to more easily reducible Ni species located outside of the structure. The peaks located at higher temperature, 415°C for ETS-4 and 392°C for ETS-10, were instead correlated to the reduction of nickel species located within the zeolite super cages [126]. Being peaks of ETS-4 shifted to

higher temperature with respect to ETS-10, a greater interaction of Ni species with the ETS-4 support was inferred. At higher temperature, in the TPR profile of ETS-4, due to titanium reduction state from +4 to +3, a shoulder and broader peak at 500°C was registered [127] Figure 2.14.

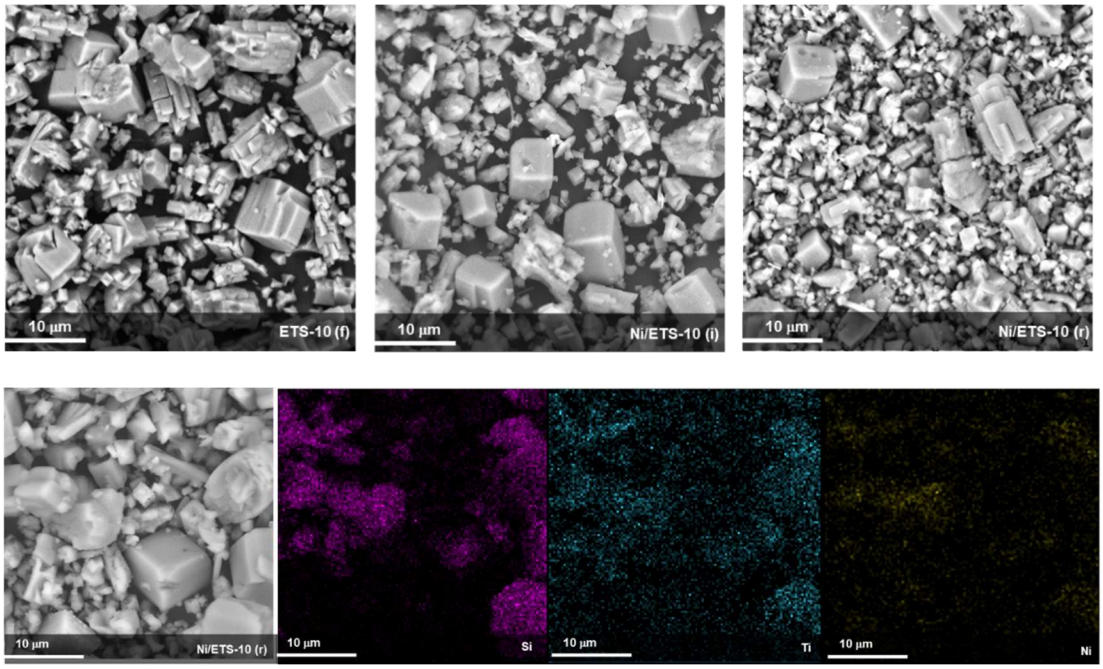

Figure 2.13. SEM of bare ETS-10 fresh (f), Ni/ETS-10 (i) after the impregnation treatment and Ni/ETS-10 (r) after the reduction treatment and EDX analysis on Ni/ETS-10 (r) [124].

Table 2.2. Textural and surface properties of impregnated supports and catalyst samples [124].

Sample	Si/Ti [a]	Ni [a] [*w*/*w*%]	SBET [b] m^2/g	Sint [c] m^2/g	Sext [c] m^2/g	Vmic [c] cm^3/g	Vmes [d] cm^3/g	Loss of Crystallinity [e] [%]
ETS-4 (f)	1.90	-	312	279	38	0.12	0.00	–
Ni/ETS-4 (i)	1.87	4.86	270	219	56	0.10	0.00	46
Ni/ETS-4 (r)	1.63	4.34	48	4	46	0.00	0.18	100
ETS-10 (f)	2.93	-	386	369	47	0.15	0.00	–
Ni/ETS-10 (i)	2.89	4.88	358	313	49	0.14	0.00	8
Ni/ETS-10 (r)	2.90	4.97	312	222	96	0.10	0.05	23

[a] Determined by EDX analysis considering at least 20 points of investigation for three different magnifications; [b] Valued by BET model; [c] Valued by "t-plot" approach (Harkins–Jura reference equation); [d] Valued as difference of the Vmic by Vtot; [e] Valued as loss of intensity of the main peak respect the fresh sample.

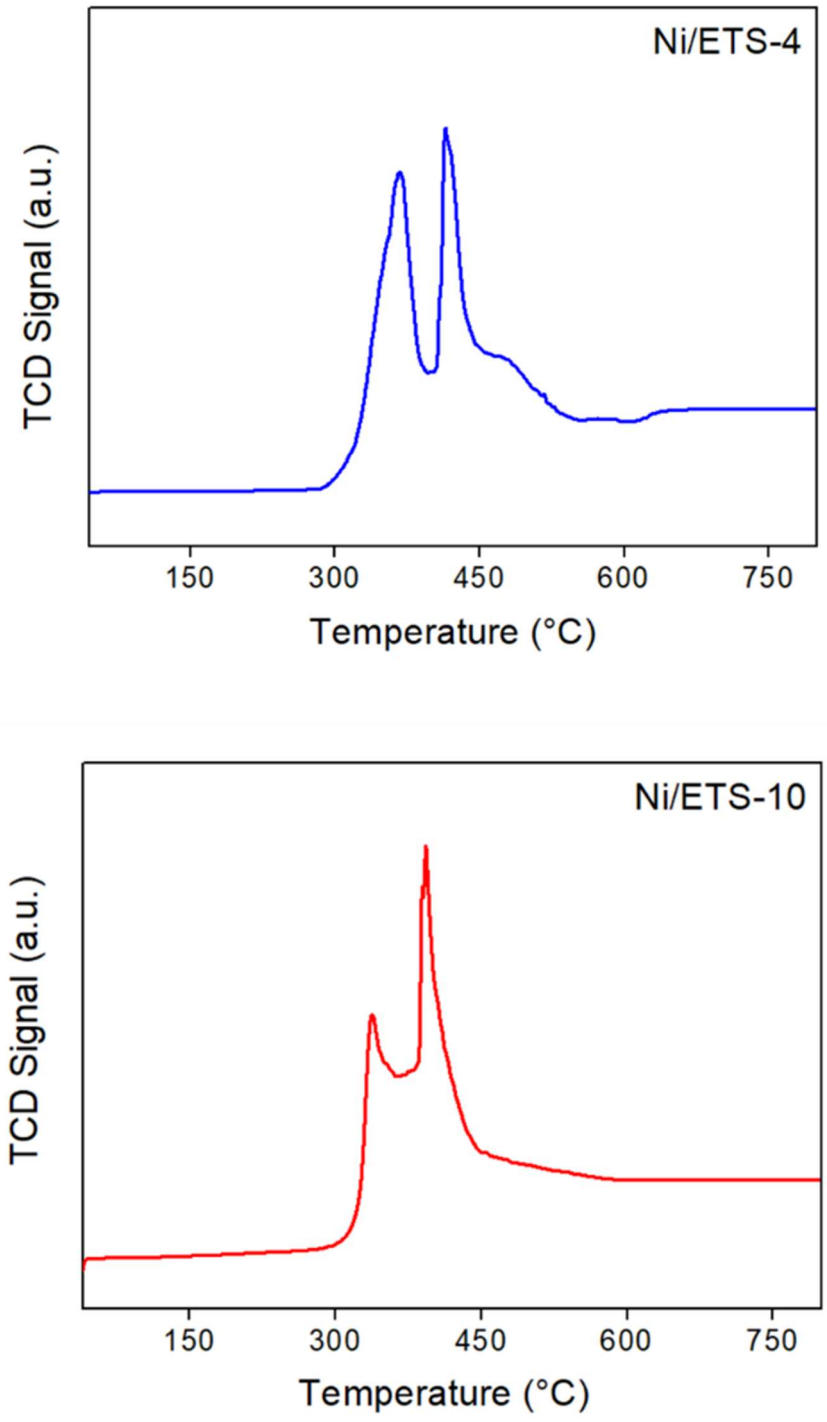

Figure 2.14. TPR-H_2 profiles of Ni/ETS-4 and Ni/ETS-10 catalysts [124].

2.4.2 Experimental setup for the catalytic activity evaluation in the CO_2 methanation

Catalytic methanation reactors are typically operated at temperatures between 200°C and 550°C and at pressures ranging from 1 to 100 bar, since CO_2 methanation is also a strongly exothermic reaction and increasing the temperature is unfavourable.

CO_2 methanation was carried out in a quartz tubular fixed-bed reactor (1 cm inner diameter, 25 cm length) horizontally placed in a furnace under atmospheric pressure. A mixture gas of $H_2/CO_2/N_2$ with fixed molar ratio 4/1/1 was fed into the reactor by mass flow-controllers. An Agilent 6890 Plus gas-chromatograph, equipped with thermal conductivity (TCD) and flame ionization (FID) detectors was used to on-line analyze reactants and products every 20 min. N_2 was used as an internal standard for mass balance calibration.

Activity tests of 8 hours each, were carried at fixed temperature in the range T = 300–500 °C and space velocity GHSV = 30000 h^{-1}. The total flow rate was 50 cc/min and GHSV was defined as:

GHSV = Volumetric flow velocity of gas/ Volume of catalyst

The CO_2 and H_2 conversion were calculated, on dry basis, by the following formula:

$$XCO_2 = (\text{moles } CO_2 \text{ in} - \text{moles } CO_2 \text{ out})/\text{moles } CO_2 \text{ in}$$

$$XH_2 = (\text{moles } H_2 \text{ in} - \text{moles } H_2 \text{ out})/\text{moles } H_2 \text{ in}$$

The selectivity of methane was defined as:

$$SCH_4 = \text{moles } CH_4 \text{ produced}/\text{moles of total products}$$

All reactions were repeated three times and the deviation measured for the results was ±4%. The conversion and selectivity were calculated referring to the stationary values registered when the profile of conversion/selectivity

versus time was stable, and the phenomenon of deactivation had not occurred yet. In Figure 2.15, the experimental setup for the CO_2 methanation reaction is schematized.

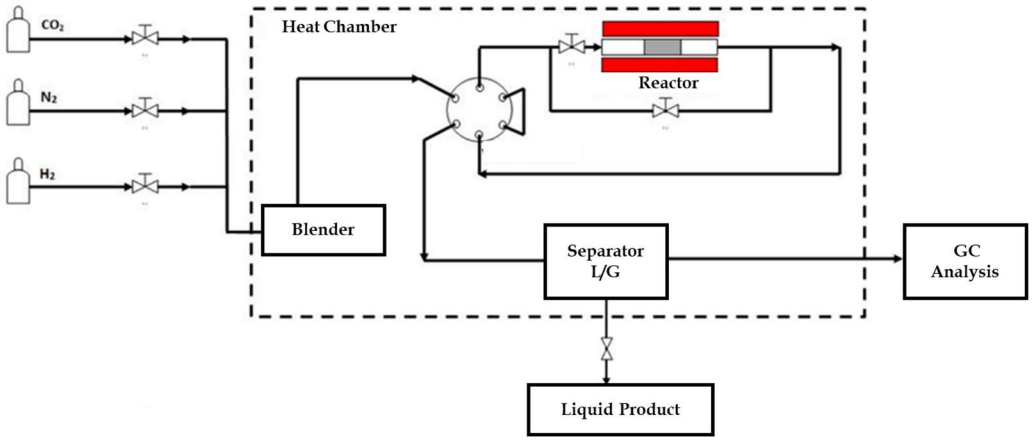

Figure 2.15. Experimental setup for the CO_2 methanation reaction.

2.5 Catalytic systems for the reductive upgrading of biomass-derived furfural

The black mass is the product resulting from the first step of the battery recycling process, generally based on the mechanical treatment of the different components of LIBs batteries, such as anode, cathode and separator. It contains mixtures of valuable metals such as lithium nickel/manganese/cobalt oxides and aluminium, derived from the cathodic part of LIBs, together with fluoride-based polymers due to the separator material, carbon and copper, derived instead from the anodic part of LIBs [128]. Chemical elements characterized BM are schematized in Figure 2.16.

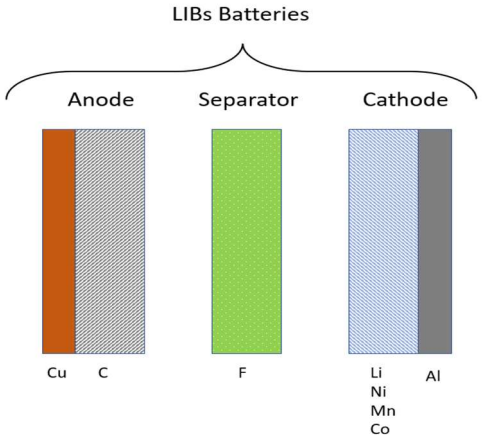

Figure 2.16. Chemical elements characteristic of black mass.

2.5.1 Production and characterization of catalytic systems for the reductive upgrading of biomass-derived furfural

Black mass, derived from a recycling facility, was opportunely treated before its application. In particular, it was first sieved using a sieve screen mesh (425 mm - 40 mesh) owing to homogenize the sample and to remove any

metallic solid residue and impurities. It was then grinded with a ball mill apparatus at 350 rpm for 10 min and calcined under atmospheric conditions at 600°C for 6 hours (BM*ox*) to remove traces of binder materials. It was finally reduced at 500 °C for 6 hours under 1ml/min H_2 flow (BM*red*). A schematic representation of mechano-thermal treatment of BM is sketched in Figure 2.17.

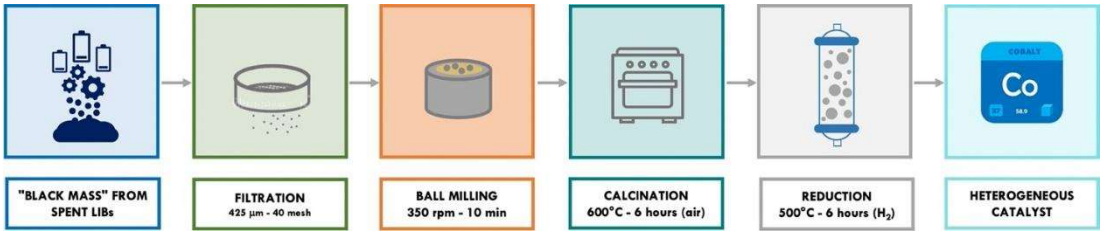

Figure 2.17. Schematic representation of mechano-thermal treatment of spent LIBs black mass for the preparation of co-based heterogeneous catalysts [129].

Black mass was fully characterized by complementary investigation techniques.

In Figure 2.18 the XRD spectra of all BM samples are reported. Together with carbon, other chemical elements of BM were arranged in the form of well-defined crystalline structures with $LiMeO_2$ oxides (Me = Co, Li and Mn) being the main phases present. The oxidation process led to a high decrease in the intensity of peaks at 26.5°, 43.3° and 54.9° because of the graphitic carbon oxidation to CO_2, following Eq. 5-Eq.7. After the reductive treatment at 500°C, the diffraction peaks of $LiMeO_2$ disappeared in favour of the formation of metallic Co and Ni as well as Li_2O, whereas the formation of metallic Mn and Li from the corresponding oxides requires higher temperatures [130,131] as a result of the following reactions:

$$2LiMeO_2 + 2C + 2O_2 \rightarrow 2LiMeO_2 + 2CO_2 [Me: Co, Ni, Mn] \quad \text{(Eq.5 - BM oxidation)}$$

$$2LiMeO_2 + 3H_2 \rightarrow Li_2O + 2Me + 3H_2O \ [Me: Co, Ni] \quad \text{(Eq.6 - BM reduction)}$$

$$LiMnO_2 + H_2 \rightarrow Li_2O + 2MnO + H_2O \quad \text{(Eq.7 – BM reduction)}$$

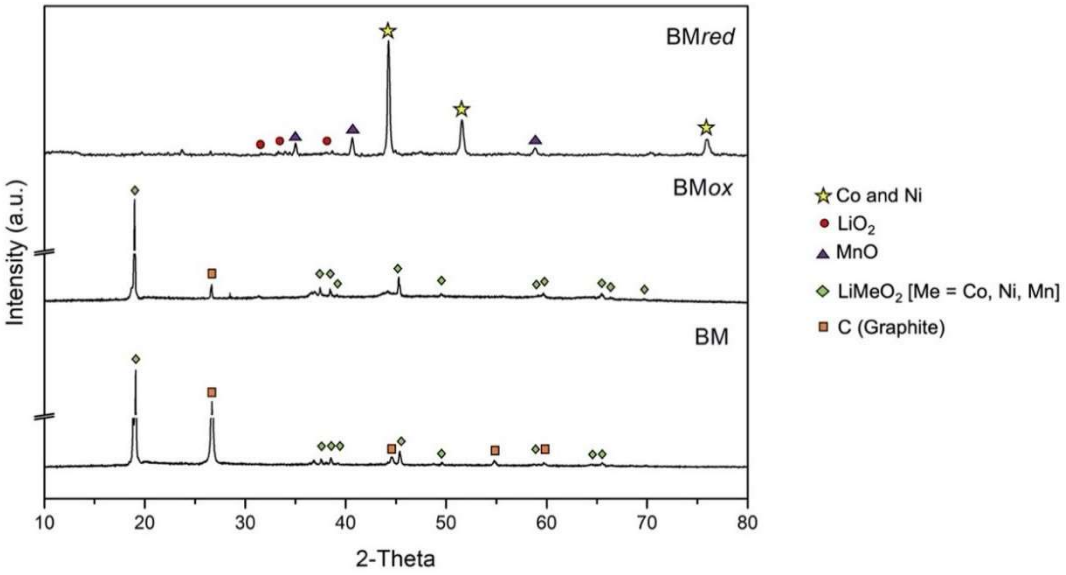

Figure 2.18. XRD patterns of BM, BM*ox* and BM*red* samples.

The TGA-DTA analysis, reported in Figure 2.19 was used to study the thermal behavior of BM. A gradual weight loss of BM until 600 °C was attributed to the decomposition of the residual polymer binder and the graphitic carbon [130]. Increasing the temperature up to 600 °C, a significant weight loss around 43% was detected, highlighting the high instability of BM at temperatures in the range of 600-1000°C.

The H_2 temperature programmed reduction (H_2-TPR) profile of the BM*ox* sample is reported in Figure 2.20. Three main hydrogen consumption peaks were registered at approximately 375, 550 and 600 °C and ascribed to the reduction of Ni, Co and Mn cations, respectively [131], in accordance with literature data [132]. Indeed, it was demonstrated that, in the reduction process of mixed Mn-Co oxides, the reduction of cobalt cations occurs in the range 300–450 °C while the formation of metallic Mn requires higher reduction temperatures (450–750 °C).

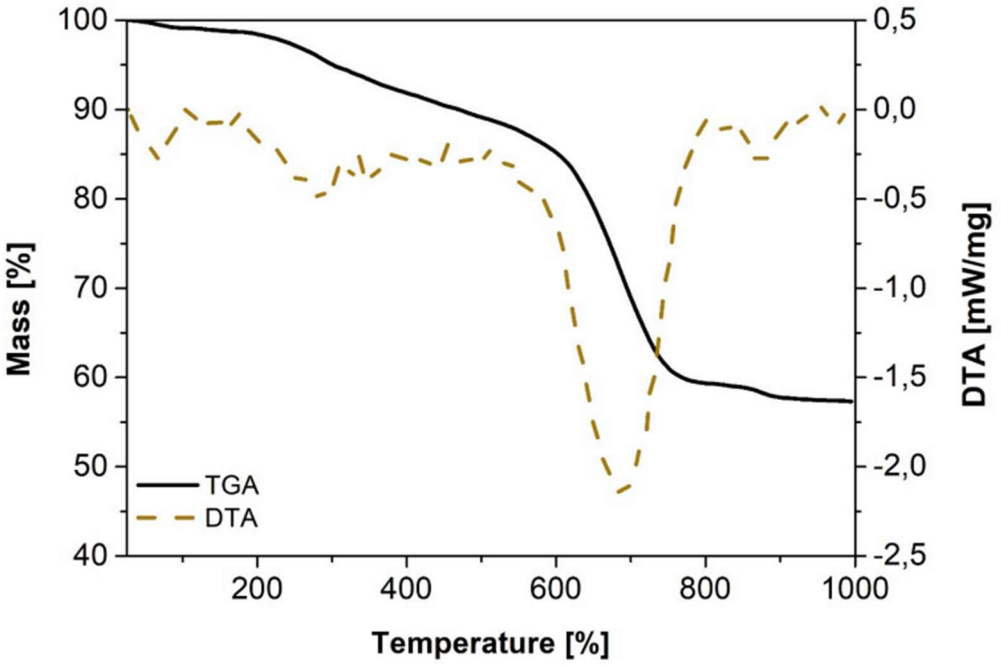

Figure 2.19. TGA and DTA spectra of black mass.

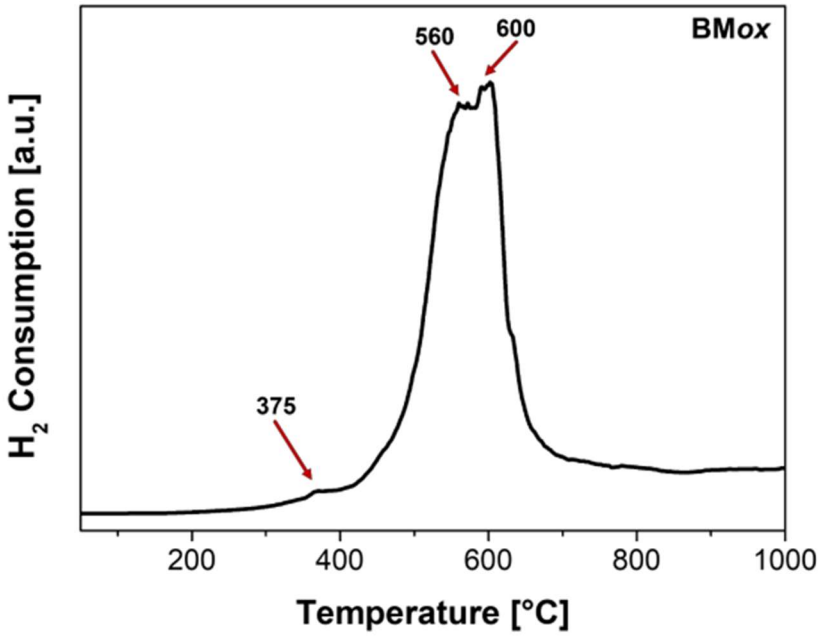

Figure 2.20. H_2-TPR profile of oxidized black mass.

SEM analysis, used to investigate samples morphology, are displayed in Figure 2.21 and Figure 2.22.

It was shown that BM*ox* and BM*red* samples consisted of irregular particles, mainly of cobalt species.

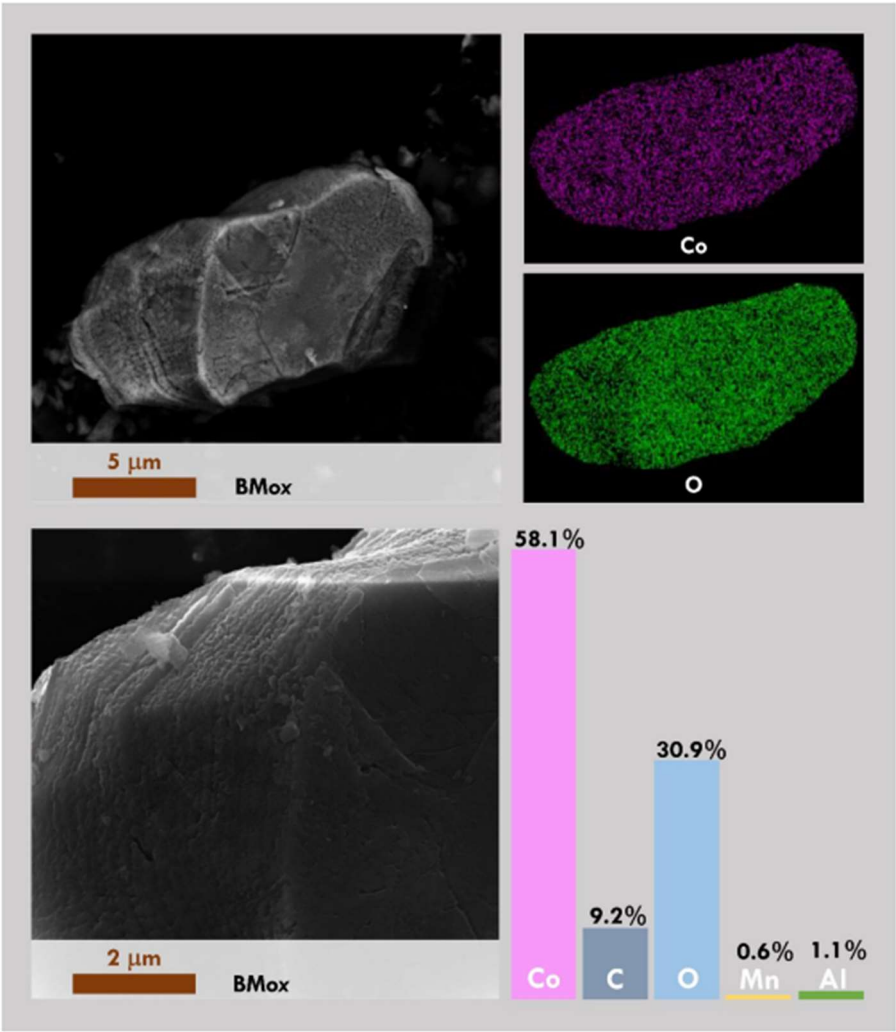

Figure 2.21. Low resolution and high resolution SEM-EDX images of BM*ox* sample [129].

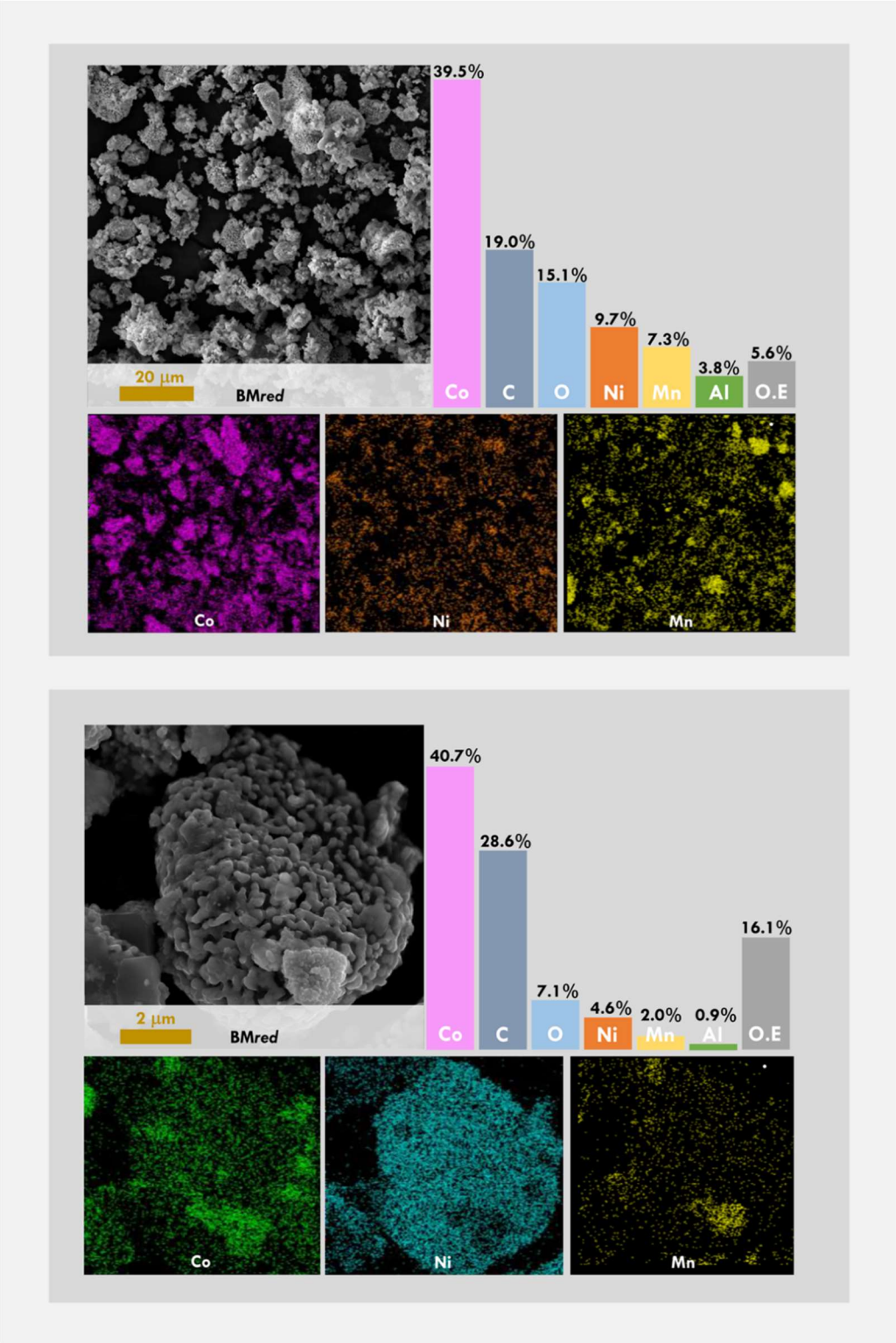

Figure 2.22. Low resolution and high resolution SEM-EDX images of BM*red* sample [129].

Indeed, as revealed by EDX analysis, the molar Co:O ratio of 1:2 confirmed that the mechanochemical and the calcination processes did not favor the conversion of $LiCoO_2$ particles into Li_2CO_3 and Co_3O_4.

In BM*red* sample, Co (39,5%), O (15,1%), Ni (9,7%) and Mn (7,8%), uniformly distributed on the surface together with some traces of Al, in the form of Al_2O_3, resulted the most abundant elements. SEM-EDX images, obtained at higher resolution, revealed both the presence of metallic cobalt characterized by rounded shapes as well as the persistence of MnO_2 species, in accordance with XRD and H_2-TPR analysis.

2.5.1 Experimental setup for the catalytic activity evaluation in the reductive upgrading of biomass-derived furfural

Catalytic tests were performed following a standard procedure [129]. In particular, tests were carried out in a 100 ml stainless steel autoclave at a stirring speed of 500 rpm. The reactor was loaded with a suspension of the catalyst (0.2 g) in a solution of the desired substrate in an alcoholic solvent (60 ml, 4% wt). The reactor was purged three times with N_2 and subsequently pressurized at the desired gas (N_2 or H_2) pressure and heated at the reaction temperature, monitored using a thermocouple fixed into the autoclave and connected to the reactor controller. The reaction time started after reaching the desired temperature (the heating rate was well reproduced in the experiments). At the end of the reaction, the reactor was cooled to room temperature, the pressure released, and the composition of the organic phase was analysed by gas chromatography.

For every recycling test, after each run, the catalyst was magnetically recovered, thoroughly washed with 2-propanol and reused with fresh reactants under the same reaction conditions. Gas chromatographic analyses were performed on a HP 5890 gas chromatograph equipped with a wide-bore

capillary column (CP- WAX 52CB, 60 m, i.d. 0.53 mm) and flame ionization detector.

The conversion, product selectivity and yield in the liquid phase were calculated on the basis of the following relations:

$$\text{Conversion [\%]} = \frac{\text{mol of reacted substrate}}{\text{mol of substrate feed}} \times 100$$

$$\text{Liquid phase selectivity [\%]} = \frac{\text{mol of specific product in liquid phase}}{\text{sum of mol of all products in liquid phase}} \times 100$$

$$\text{Product Yield [\%]} = \frac{\text{mol of specific product}}{\text{mol of substrate feed}} \times 100$$

Chapter 3

Catalytic performance of investigated catalytic systems

3.1 The reforming process for the H_2 fuel production

In this section it is reported the investigation of the reactivity of the nickel based catalytic systems with defined ceria-zirconia compositions, undoped Ni/$Ce_{0.8}Zr_{0.2}O_2$ (Ni/CZ80) and doped with lanthanum and neodymium Ni/$Ce_{0.8}Zr_{0.13}La_{0.5}Nd_{0.2}O_{2-x}$ (NidpCZ80), towards the reforming reactions: steam reforming (SR), partial oxidation (POX) and autothermal reforming (ATR) of different fuels, such as methane, biogas and propane.

Methane as fuel

The performance in terms of CH_4 conversion (average values), in different reaction conditions, is shown, for both undoped and doped catalysts, in Figure 3.1. The better performance in terms of conversion was related to the reaction under the ATR condition, for both catalysts. This could be probably due to the acknowledged indirect mechanism of ATR, according to which oxidation of methane takes place producing CO_2 and H_2O, and then synthesis gas is produced via carbon dioxide and steam-reforming reaction of the unreacted methane [112].

Moreover, it was already observed the better performance of ATR and POX conditions with respect to SR condition, in which the catalytic performance is highly depleted by hydration. At high temperatures, as well as 800°C, a high water saturation grade of reaction systems occurred, reducing the active sites accessibility (surface flooding), and furthermore reducing the reduction degree of metallic nickel with negative consequence on the catalytic performances [133].

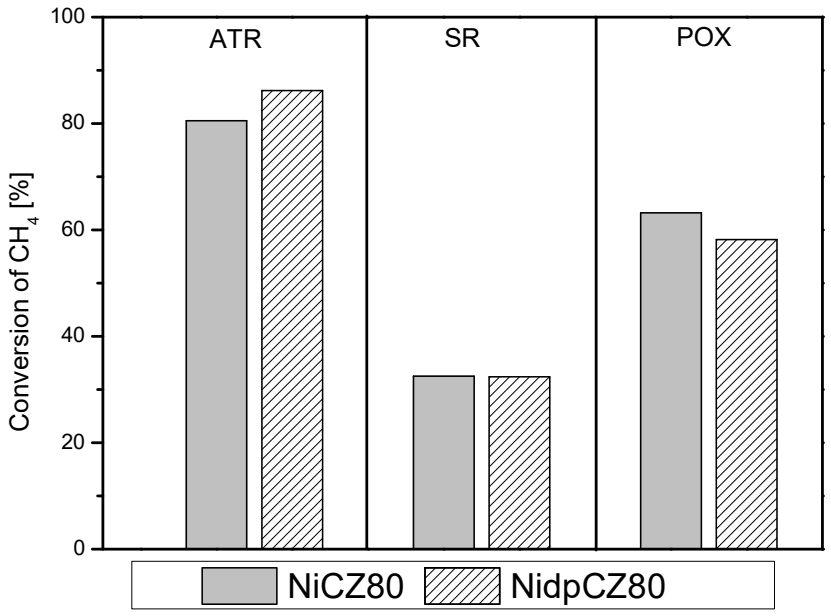

Figure 3.1. Conversion of Methane CH_4 for NiCZ80 and NidpCZ80 under ATR, SR and POX conditions at T=800°C GSVH=120000 h^{-1}.

The ATR conversion of methane on doped catalyst was slightly improved by the presence of the doping elements; on the other hand, no significant differences promoted by doping were observed for the SR of methane. Instead, in the POX condition, the doping seemed to have a detrimental effect.

Since the conversion of fuels was quite stable in the time on stream considered, as shown in Figure 3.2, it was possible to determine the average value of the products formed during the different reactions. From the data reported in Figure 3.2 it is possible to notice that the distribution of products depends on the reaction conditions. The largest amount of hydrogen was produced during the ATR reaction, instead the POX reaction produced the largest amount of carbon monoxide.

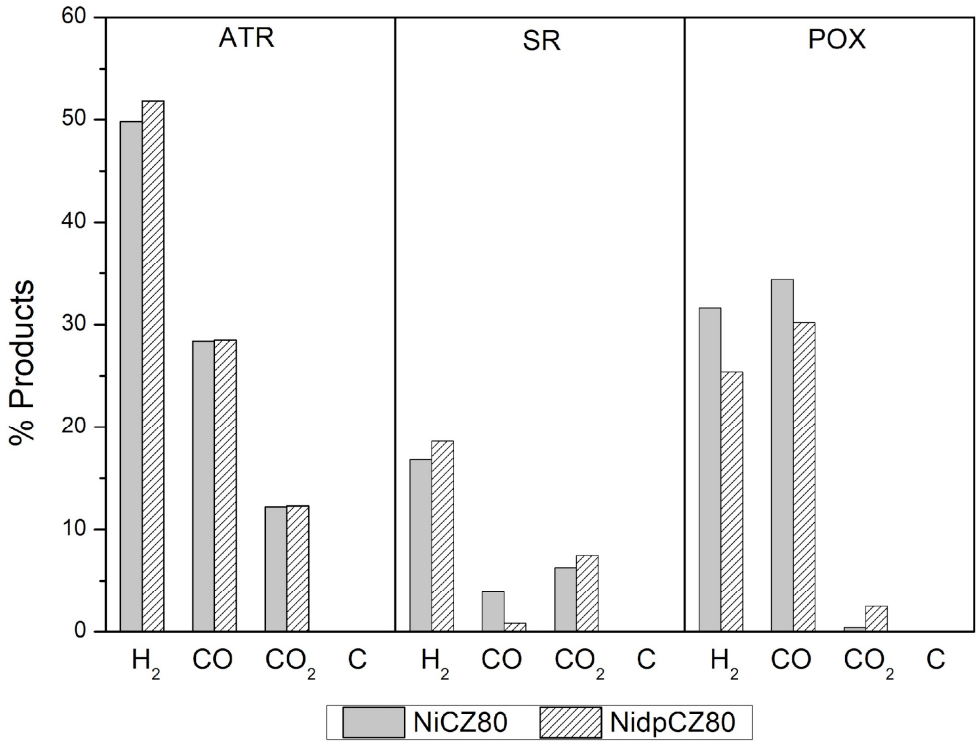

Figure 3.2. Products distribution for NiCZ80 and NidpCZ80 under ATR, SR and POX conditions at T=800°C, GSVH=120000 h^{-1}.

Propane as fuel

Propane auto thermal reforming proceeds combining the POX conditions, Eq. 4, and SR conditions, Eq. 5:

$$C_3H_8 + 3/2\ O_2 = 3\ CO + 4\ H_2\ \Delta H°= -227{,}6\ kJ/mol^{-1} \quad \text{(Eq. 4)}$$

$$C_3H_8 + 3\ H_2O = 3\ CO + 7\ H_2\ \Delta H°= 498\ kJ/mol^{-1} \quad \text{(Eq. 5)}$$

The catalytic behaviour of Ni supported catalysts, in terms of propane conversion vs reaction time at different reaction conditions is shown in Figure 3.3. Under ATR condition the propane conversion was very high for the two catalysts, suggesting that the combination of the steam and oxygen in the reagent stream played a decisive role in promoting catalyst activity and stability. In the SR and POX conditions the doped catalyst exhibited higher

conversion with respect to the undoped one. For both catalysts, products distribution, shown in Figure 3.3, was affected by operating conditions. According to literature data [133], in the POX condition, the production of H_2 is lower than ATR and SR conditions. Moreover, there was an enhanced production of CH_4 and C_2H_4 due to a significant decomposition of propane and other products (C +others), probably oxygenated molecules that could not be revealed by the analytical equipment used.

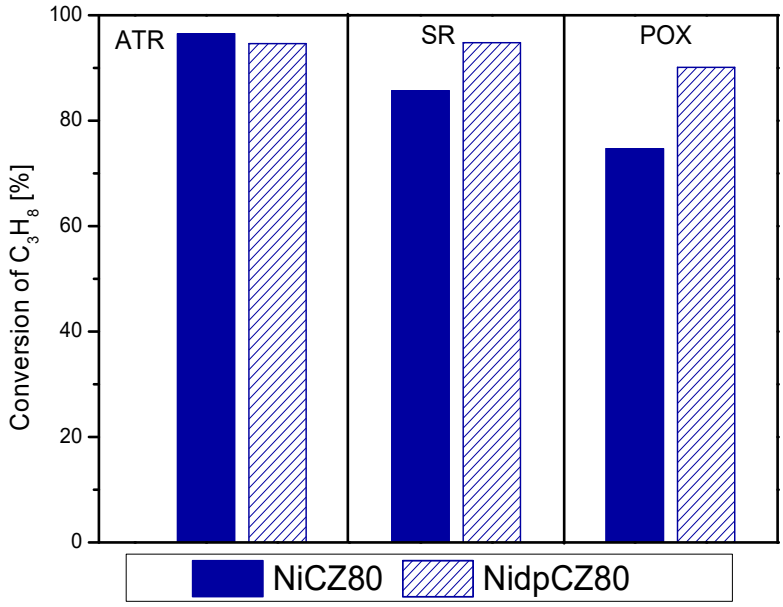

Figure 3.3. Conversion of Propane C_3H_8 for NiCZ80 and NidpCZ80 under ATR, SR and POX conditions at T=800°C, GSVH=120000 h^{-1}.

The distribution of products is presented in Figure 3.4. Under the ATR conditions the distribution of products was not substantially modified by the doping of the support. Both catalysts, undoped and doped, showed instead the highest H_2 content in the SR conditions. In addition, in the SR conditions the effect of doping was remarkable in the lower methane production and in the higher C_2H_6 content for the reaction catalysed by Ni catalyst with doped support. Probably, the formation of methane did not occur by

hydrogenation/decomposition of unsaturated species and methane could be formed by methanation of carbon oxides and/or hydrogenolysis of propane.

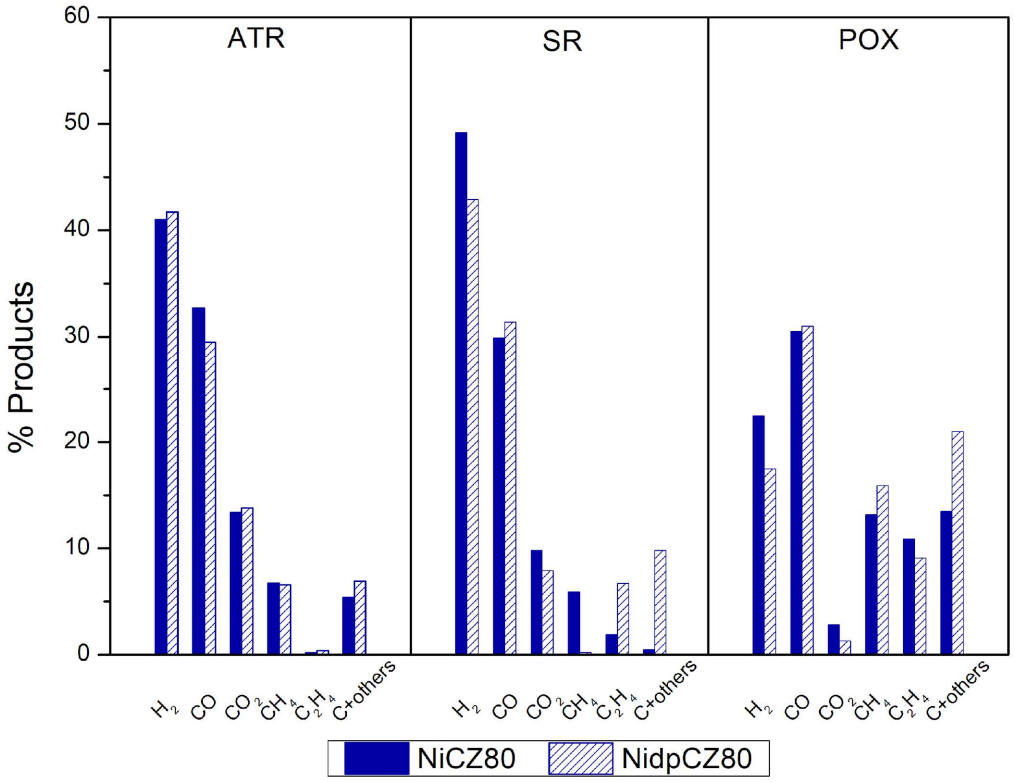

Figure 3.4. Products distribution for NiCZ80 and NidpCZ80 under ATR, SR and POX conditions at T=800°C, GSVH=120000 h^{-1}.

Odorized fuel with H_2S

The sulphur tolerance of reforming catalysts always represents a severe issue in determining the performance and stability in the reaction process, which is particularly relevant for biofuels.

Biogas contains CH_4 and CO_2 as main components and among other gases, hydrogen sulphide (e.g., H_2S, NH_3, and H_2) is a problematic contaminant because it can poison the reforming catalyst. The H_2S concentration is affected by the type of feedstocks/waste sources utilized to produce biofuel. Only 10 ppm of H_2S can deactivate the nickel catalyst, but

temperature, reaction time, and catalyst geometry have a significant impact on the stability of the catalyst [134]. The irreversible chemisorption of sulphur onto catalytic active sites is the primary cause of catalyst deactivation. Due to its high adsorption strength relative to other species competing for catalytic sites in the reaction media, sulphur has a poisonous effect. The direct use of odorized propane, particularly in non-conventional energy conversion technologies such as Solid Oxide Fuel Cells, causes particular problems [135]. In reality, conventional SOFCs cannot prevent coke formation from organic fuels nor are they resistant to sulphur poisoning. These restrictions can be circumvented by utilizing fuel processing consisting of a purification process in the first step and reforming of fuel to syngas in the second step, with an obvious increase in the system's complexity and cost; furthermore, the risk of poisoning cannot be eliminated entirely [136]. Using novel catalytic materials that simultaneously prevent the formation of coke and are resistant to sulphur poisoning is one possible response to such requirements. The promotion of supports with proper elements can increase the catalysts basicity and its poison resistance related to sulphur components.

With this background, catalytic tests of autothermal reforming were carried out over undoped and doped catalysts, in the presence of 100 ppm of H_2S.

A different catalytic activity was observed for the different fuels as shown in Figure 3.5. In particular, in the presence of H_2S, a dramatic collapse in the conversion was detected using methane and biogas as fuels for both catalytic systems. This phenomenon could be ascribed to the formation of sulphides on the catalyst surface, in particular of Ni sulphide species that somehow led to a decrease of the number of catalytic sites available for the main process. In the case of propane, the loss of conversion was moderate for both catalysts.

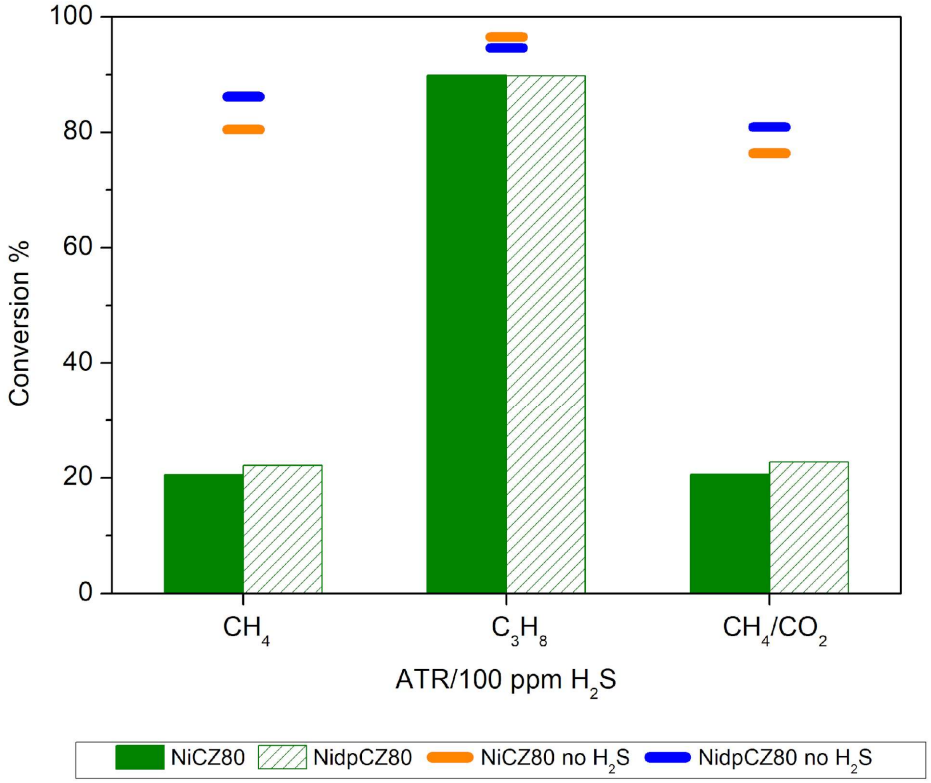

Figure 3.5. Conversion of different fuels in ATR conditions at T=800°C GSVH=12000 h^{-1} over undoped and doped catalysts.

The different behavior in the loss of conversion for different fuels was explained considering that the addition of H_2S, that, as stated above, tended to block the catalytic sites, made the oxidation reaction of fuels less favored than in the case of the ATR carried out in the absence of H_2S and. Instead, the catalytic cracking process became the most favoured reaction. This find was also confirmed by the highest yield of H_2 and CO, obtained for the reaction carried out in the absence of H_2S (around three times higher). The addition of H_2S in the ATR of propane causes an increase of the production of CO_2, CH_4 and C_2H_4 for both doped and undoped catalytic systems.

Despite the sulphur presence affected the products distribution, however no severe catalysts deactivation occurred:

The spent catalysts were characterized by XRD in order to identify possible structural modifications and/or formation of surface carbon species. No evident modifications of the support structure were observed, all patterns were similar to those reported for fresh catalysts (Figure 3.6), probably due to a limit of detection of the instrument used. Then, to investigate more in-depth the presence and the amount of coke, thermogravimetric analysis was employed to estimate the amount of deposited carbon.

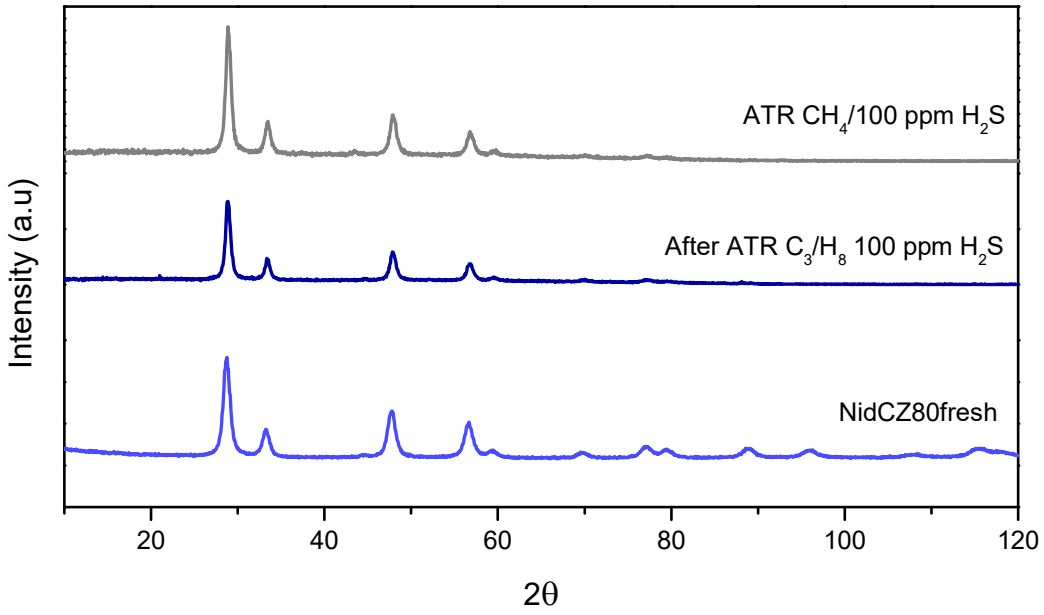

Figure 3.6. X-Ray patterns of NidCZ80 fresh and after ATR reactions of methane and propane with 100 ppm of H_2S at T=800°C and GSVH=120000 h^{-1}.

The content of carbon for all catalytic systems was lower than 3%. The higher amount of coke (2,8% wt) was detected for the undoped catalyst after ATR of odorized propane with respect to the doped catalysts (0,39 % w). The amount of carbon detected on the catalysts used for the other reactions resulted lower than 0.2 %.

TEM image (Figure 3.7) confirmed the absence of coke for the catalytic system tested under the ATR of methane on doped catalyst and highlighted the high sintering of the catalyst that probably produced the loss of conversion

in undoped and doped catalysts. The random presence of carbon nanotubes (Figure 3.8) was detected in the ATR of propane with undoped catalysts, confirming the low content of carbon detected by thermogravimetric analysis and the preserved activity in the considered time of reaction.

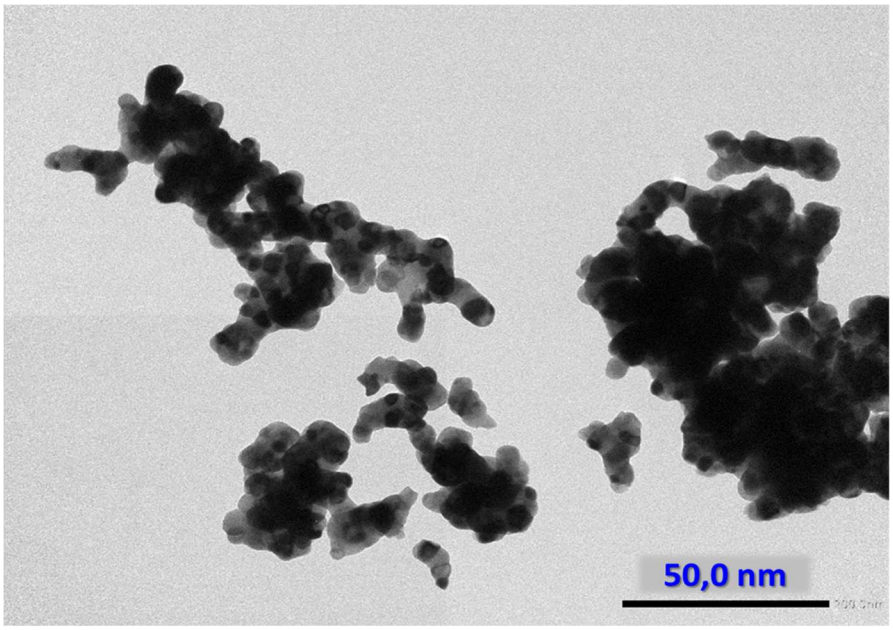

Figure 3.7. TEM image of doped catalysts after ATR of methane at T=800°C and GSHV=120000 h^{-1}.

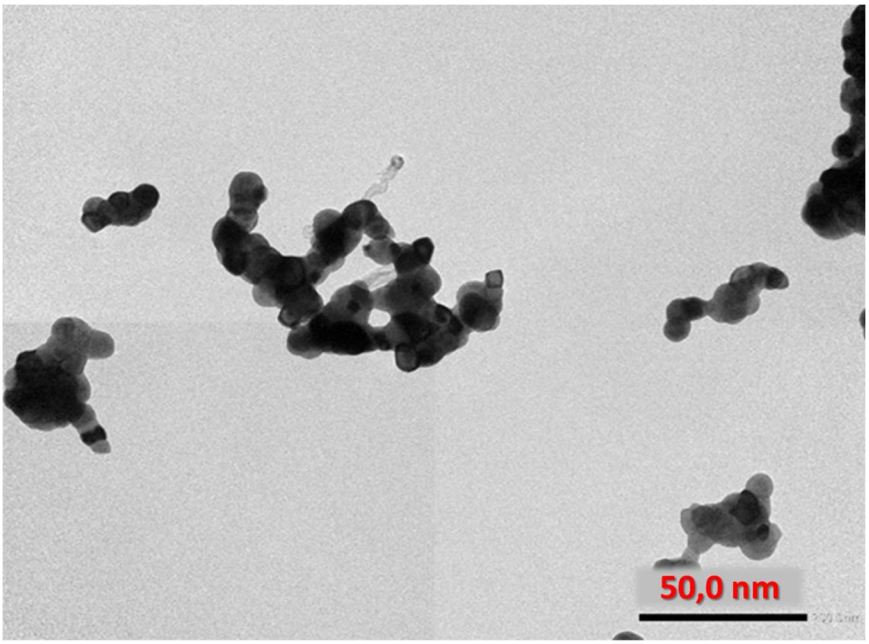

Figure 3.8. TEM image of undoped catalysts after ATR of propane at T=800°C and GSHV=120000 h^{-1} .

On the basis of this observation, the catalytic system obtained over the doped catalyst resulted high resistant to deactivation, being characterized by a higher concentration of defect groups and oxygen vacancies (due to the doping of neodymium and lanthanum), thereby preventing the formation of deactivating species (amorphous carbon and nickel sulphide).

Endurance test

Endurance tests of undoped NiCZ80 and doped NidpCz80 catalysts were carried under ATR of C_3H_8 conditions in presence of 100 ppm of H_2S. The profiles of conversion are reported in Figure 3.9. As shown, the undoped catalyst exhibited catalytic activity for around 55 hours. After that, a dramatic loss of conversion was registered, probably due to the coke formation that hindered the gas flow, causing the block of the reaction. In effect, as shown in Figure 3.10, the reactor was full of coke.

Instead, the doped catalyst showed a stable catalytic activity for over 100 hours.

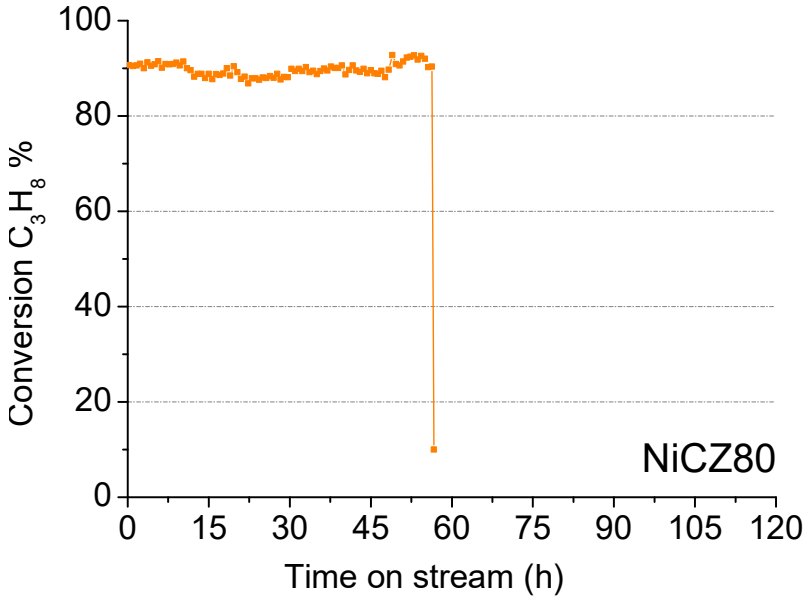

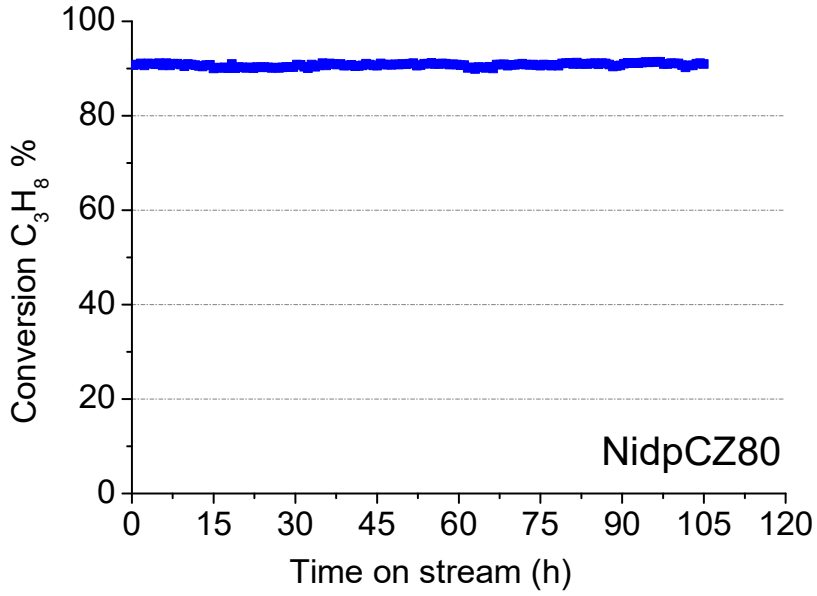

Figure 3.9. Profiles of C_3H_8 conversion for NiCZ80 and NidpCZ80 under ATR conditions at T=800°C and GSHV=120000 h^{-1}.

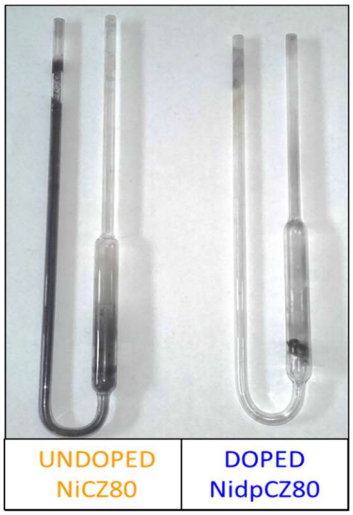

Figure 3.10. Photographs of reactors after the endurance test.

The characterization of spent catalysts was carried out by XRD, and TG-DSC analysis in order to identify the coke formed during reactions. XRD

results of spent catalysts doped and undoped are shown in Figure 3.11 and Figure 3.12, respectively. For both catalysts, peaks attributable to the carbon formation in the 2θ range 25-27° were clearly observed, even if they were characterized by different profiles. In the case of undoped NiCZ80 catalyst, the peak was more sharp than that of doped NidpCZ80 and the corresponding d_{002} value (3.432 Å) approaches the theoretical value of standard graphite (3.354 Å) [137]. The value of d_{002} (3.395 Å) for the peak of the doped catalyst was far from the theoretical value, so amorphous carbon instead of ordered graphite was obtained. As well known, the nature of coke formed during the reaction influences the deactivation of catalysts [138]. Therefore, some forms of carbon reduce the catalytic activity and others do not. For high temperatures (> 650°C) graphitic carbon species were formed over the undoped catalyst, encapsulating the metallic surface [138]. The above observation on coke formation led to the conclusion that doping addresses the methanation to be a coke-insensitive reaction. The catalytic activity of doped catalyst was not affected even when appreciable quantities of "coke" were deposited on its surface, as proved by thermogravimetry curve, Figure 3.13. Probably, it was due to the promotion effect of La and Nd, able to maintain the surface sufficiently reactive [139].

In TGA-DSC profiles (Figure 3.13) the weight loss under 150° C was associated with the desorption of moisture. The weight loss at high temperatures, up to 600°C, could be attributed instead to the oxidation of deposited carbon. The related exothermic peak for NiCz80 catalyst was centred at 665°C, whereas for the doped catalyst was centred at 780°C. This was due to the different nature of the coke deposited on catalysts, in fact amorphous carbon is known to oxidize easily with respect to more ordered carbon species [140].

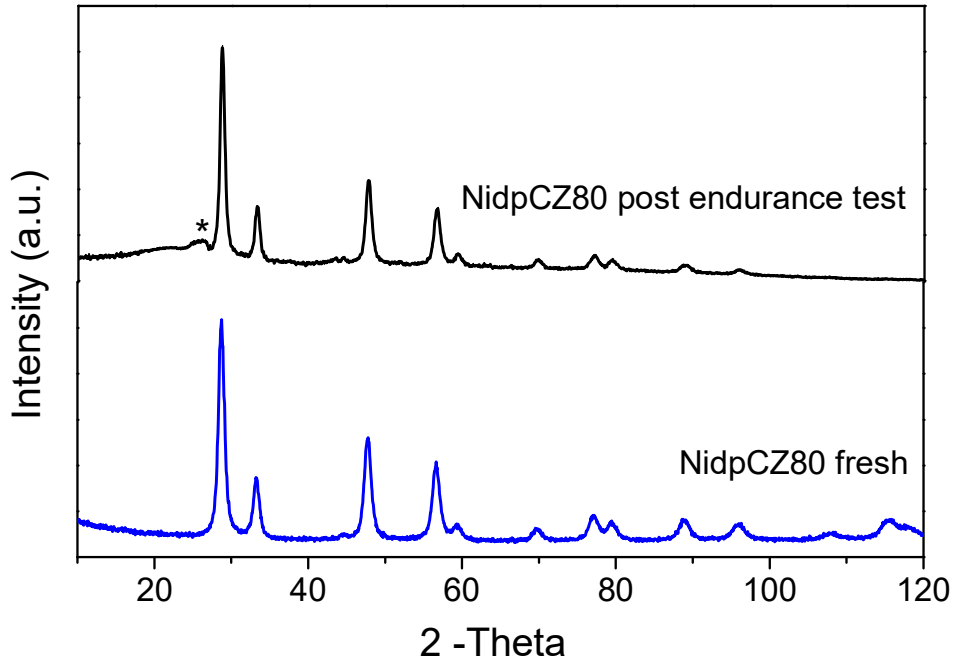

Figure 3.11. X-ray diffraction spectra of NidpCZ80 catalyst, fresh and after the endurance test.

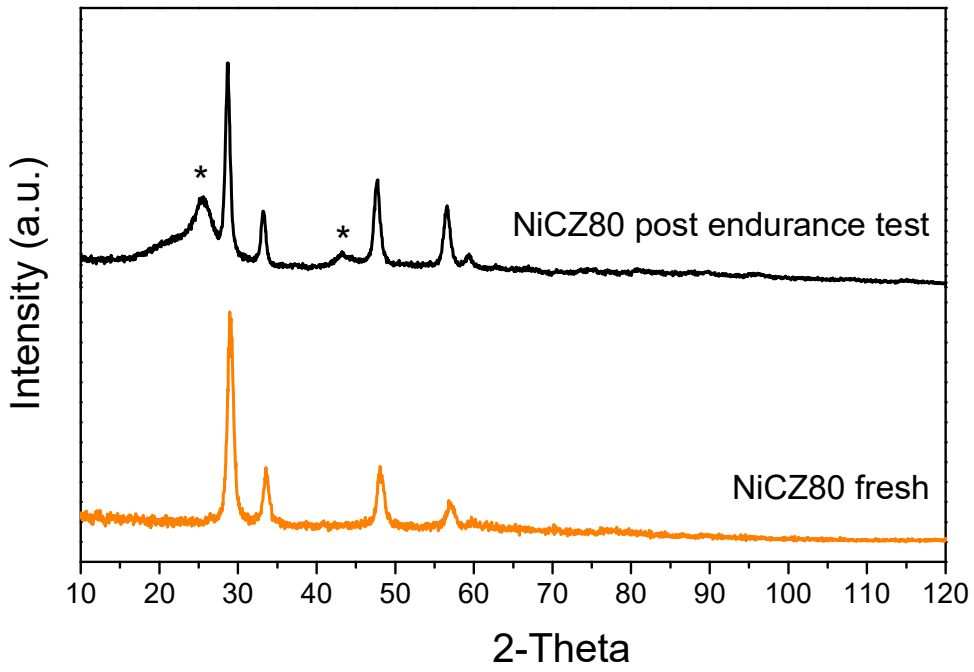

Figure 3.12. X-ray diffraction spectra of NiCZ80 catalyst, fresh and after the endurance test.

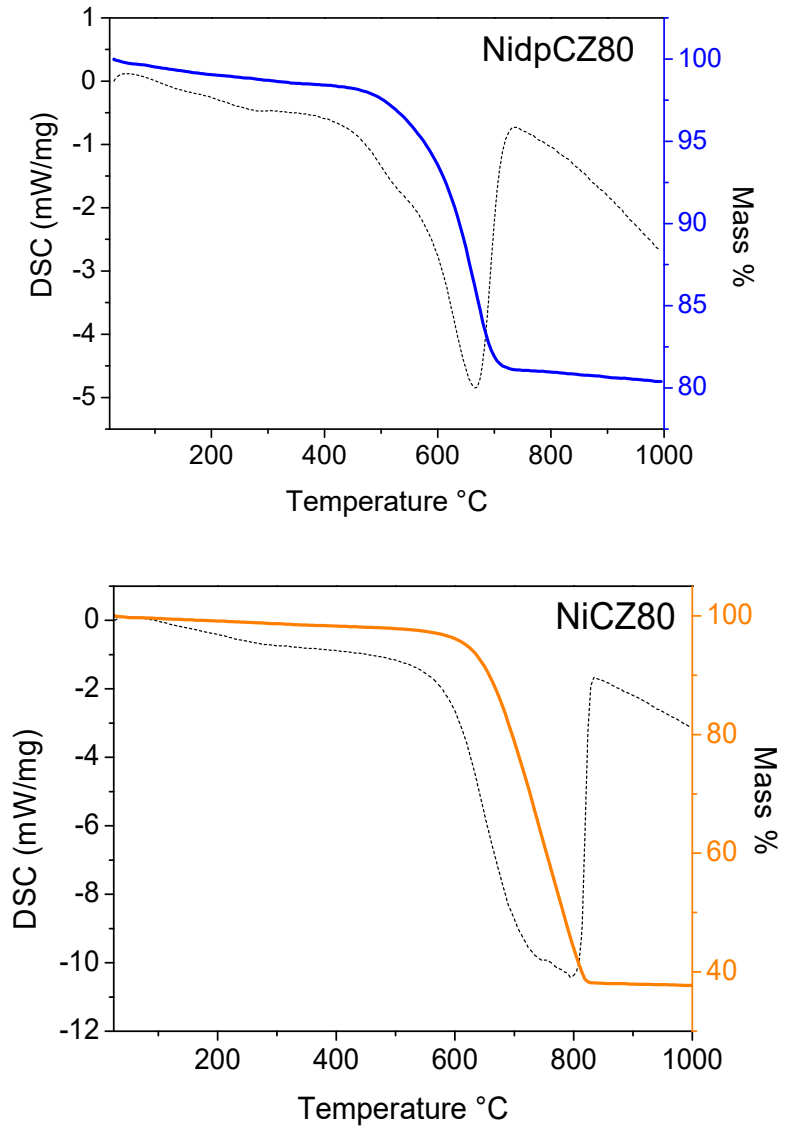

Figure 3.13. TGA-DSC profiles of NidpCZ80 and NiCZ80 catalysts after endurance test.

3.2 CO_2 methanation promoted by Nickel supported catalysts

The carbon dioxide methanation was performed in the temperature range 300-500°C, over pristine ETS supports, ETS-4 and ETS-10, and both Ni/ETS catalysts.

ETS-4 and ETS-10 supports did not exhibit any catalytic activity due to the absence of the active catalytic phase, whereas results of Ni based catalysts are reported in Figure 3.14. Methane and carbon monoxide were the only products observed in the outlet gas stream, evaluated on a dry basis. At the lowest temperatures no catalytic activity or in small percentage was registered. The optimum conversion of CO_2 and H_2 was reached at 400°C for both catalysts Ni/ETS-4 and Ni/ETS-10. Temperature increments up to 500°C showed instead the reduction of CO_2 and H_2 conversions due to the thermodynamic limitations of CO_2 methanation. In detail, the Ni/ETS-4 catalyst showed ca. 11% of CO_2 conversion at 300 °C, that increased to ca. 62% at 400 °C whereas Ni/ETS-10 showed ca. 29% of CO_2 conversion at 300 °C, that increased up to ca. 67% at 400 °C, remaining below the thermodynamic limits; this could be due to the greater kinetic barrier for the full reduction of CO_2 (+4) to CH_4 (-4), an eight-electron process which obviously requires high activation energy [141]. Further increase in the reaction temperature at 500°C led to a slight decrease in the CO_2 conversion due to thermodynamic limit of methanation reaction and to the occurrence of RWGS (Reverse water gas shift) reaction [141]. The registered values of CO_2 conversion were 55% for Ni/ETS-4 and 60% for Ni/ETS-10.

In Figure 3.15 the CH_4 selectivity results are displayed. For Ni/ETS-4 the CH_4 selectivity increased from ca. 29% at 300°C to 42% at 400°C and then

decreased to ca. 2% at 500°C. Instead, the CH_4 selectivity of Ni/ETS-10 varied from ca. 56% at 300°C to 98% at 400°C and then decreased to 35.4 % at 500°C. The obtained results seemed apparently not thermodynamically consistent, because methane concentration should decrease by increasing the temperature, due to the methanation equilibrium; therefore, this suggested that the methanation on the Ni/ETS catalysts at relatively low temperatures (T< 400 °C) was probably a kinetic controlled reaction [142].

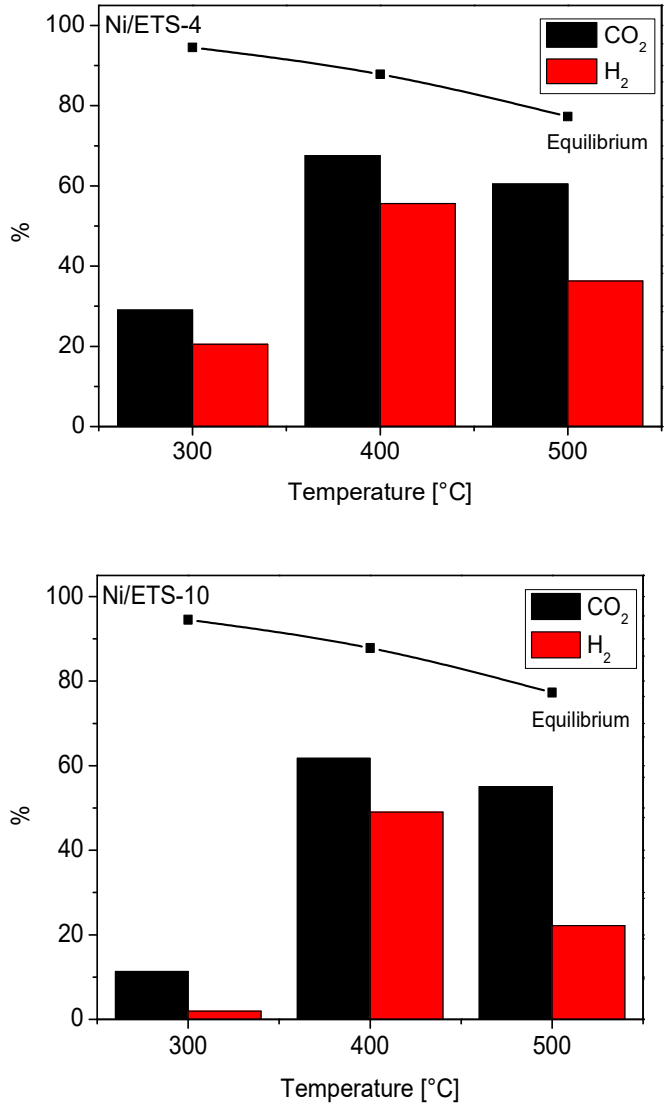

Figure 3.14. CO_2 and H_2 Conversion of samples Ni/ETS-4 (a) and Ni/ETS-10 (b) in the temperature range 300-500°C [124].

As shown in Figure 3.15, even if the profiles of CH_4 selectivity were similar for both catalysts, it should be highlighted that, in the range of temperatures examined, selectivity values were actually very different. Indeed, Ni/ETS-10 allowed obtaining a selectivity close to 100% at 400°C, instead, at the same temperature, the CH_4 selectivity of Ni/ETS-4 was scarcely above 40%.

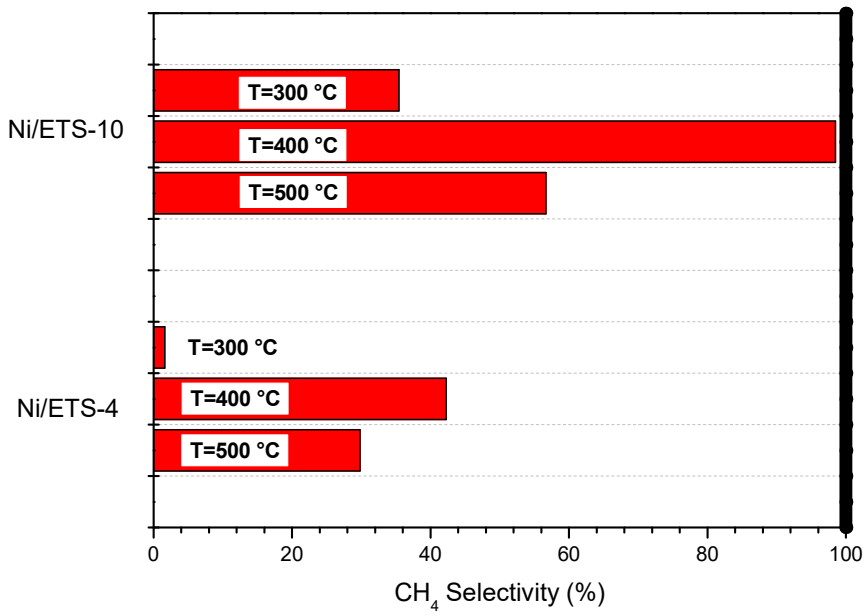

Figure 3.15. CH_4 selectivity of the Ni/ETS-4 and Ni/ETS-10 catalysts in the temperature range 300-500°C [124].

The different behaviour of ETS-4 and ETS-10 catalysts was ascribed to the content of titanium in the framework of the zeolitic structure of the two supports. To clarify the results of catalytic tests, methanation reactions were carried out using silicon dioxide and titanium dioxide as nickel supports, loaded with the same metal content and tested at the same operative conditions at 400°C. In this way the effect of nickel supported on titaniumsilicate was evaluated. Conversion and selectivity values for all catalysts, tested at T=400°C, were analysed and reported in

Figure 3.16. A higher value of CO_2 conversion was exhibited by both catalysts with respect to Ni/ETS, but the CH_4 selectivity for Ni catalyst supported on titanium dioxide was consistently lower than all other catalysts. Then, it was confirmed that the catalyst based on titaniumsilicate ETS-4 performed worse in terms of CH_4 selectivity because it was characterized by a higher titanium content that determined the low thermal stability of the sample, as verified by XRD diffraction results. Indeed, despite the dispersion of the active metal was observed, as confirmed by the EDX-analysis, during the reduction procedure, with the collapse of zeolites structure, there was a leaching of titanium from the framework and at the same time the titania underwent a reduction to TiO_x ($x<2$). This titanium species covered the nickel particles that, although remained in their metallic state, were encapsulated by Ti suboxides (TiO_x), as also reported in literature [143]. TiO_x species addressed the CO_2 dissociation, decreased the hydrogen dissociation and then probably caused the change in the selectivity of products [144].

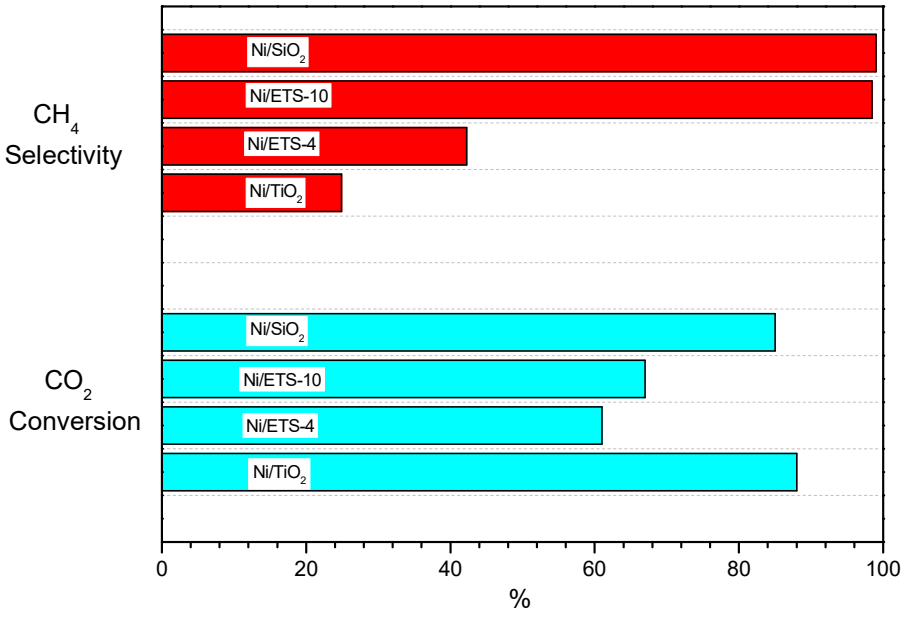

Figure 3.16. Comparison of different supports for Ni catalysts in the methanation reaction at T=400°C and GHSV 30000 h^{-1}.

A different behavior was instead displayed by catalysts supported on ETS-10, that maintained the zeolitic structure and the featuring morphology, as shown in Figure 3.17. The catalytic activity of the ETS-10 catalyst was compared with those obtained over other zeolites materials used as Ni support for CO_2 methanation, as evidenced in Table 3.1. In similar reaction conditions, it resulted that ETS-10 appears a promising support for Ni catalyst in the methanation reaction.

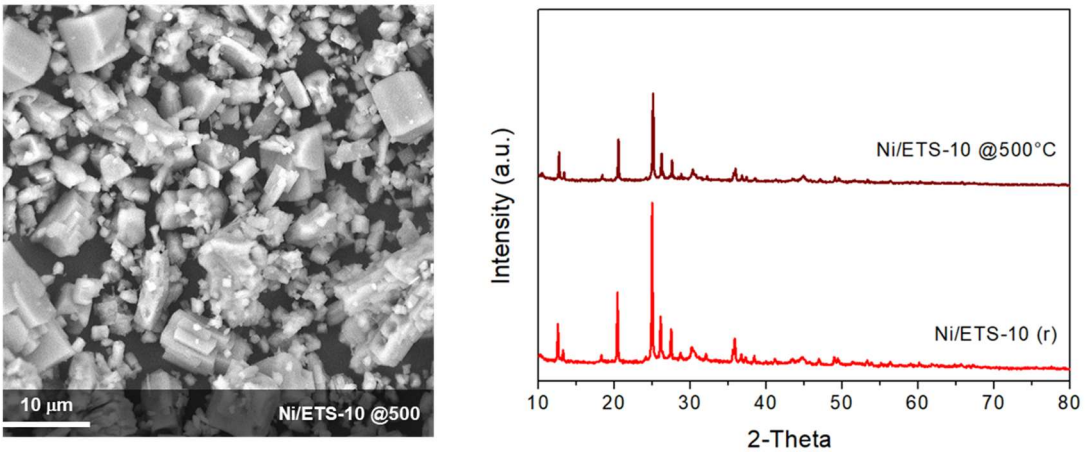

Figure 3.17. SEM and XRD analysis of Ni/ETS-10 catalyst after reaction at 500°C.

In particular, it was interesting to compare Ni catalyst supported on ETS-10 and zeolite Beta, being characterized by topological similarities. Both these materials have three-dimensional pore systems, almost identical, although the zeolite Beta is an aluminosilicate composed of tetrahedral SiO_4^{4-} and AlO_4^{5-} units, whereas ETS-10 is a titanosilicate composed of tetrahedral SiO_4^{4-} and octahedral TiO_6^{8-} units [122,145,146]. The comparison of the catalytic activity of Ni/ETS-10 and Ni/Beta highlighted that Ni/ETS-10 exhibited better catalytic activity as compared to Ni/Beta catalyst despite the lower metal loading and the higher GHSV employed in the experiment.

Table 3.1. Summary of CO2 methanation performance of Ni/zeolites catalysts at high temperature reaction (T>350°C) [124].

Catalyst composition	H_2/CO_2	GHSV [h^{-1}]	T [°C]	CO_2 conversion	CH_4 selectivity	Ref.
5%NiY	4:1	43000	450	50	95	26
5%NiSilicalite	4:1	60000	450	57	91	27
5%Ni/ETS-10	4:1	30000	400	68	98	This work
5%Ni/ETS-10	4:1	30000	350	52	90	This work
10%NiHY	4:1	10000	350	15	88	21
10%NiNaY	4:1	10000	350	30	82	21
10%NiHBeta	4:1	10000	350	23	82	21
10%NiNaBeta	4:1	10000	350	33	88	21
15%NiHbeta	4:1	16000	350	80	79	28
15%NiHbeta	4:1	16000	400	76	75	28

For this material, each TiO_6 unit contributes two minus charges to the framework, leading to the framework oxygen atoms in TiO_6 unit bearing negative charges, referred to as the basic sites [123,147]. These basic sites on the catalyst surface likely improve CO_2 uptake via acid-base interaction, that in turn, can increase in the presence of oxygen vacancies on the support [148], easily formed within reducible supports (TiO_2, CeO_2, ZrO_2, etc.) since the oxygen vacancy can be mobile inside the lattice and plays an important role in the redox process. The presence of defected sites on Ni/ETS-10 was probably due to the incipient support mesoporosity, indirectly confirmed by the loss of crystallinity introduced after the reduction treatment.

The differences in the catalytic performance between the different Ni based zeolite supports was then ascribed to the different zeolite framework, both from a compositional and topological point of view, that influences: i) the interaction and affinity with CO_2 and ii) the metal support interactions, affected by the spatial arrangement and bond angles present in the microporous materials [124].

3.3 Reductive Upgrading of Biomass-Derived Furfural promoted by Spent LIBs derived Ni-Co based catalyst

BM_{red}, the black mass powder obtained from the recovery of spent lithium-ion batteries mainly consists of a mixture of metals, mostly cobalt and nickel. Since Co and Ni are widely known as metals able to catalyse the transfer hydrogenation and hydrogenolysis of furfural and other biomass-derived molecules it has been used as heterogeneous catalyst. The effect of parameters, such as reaction time, temperature and pressure was investigated to evaluate BM_{red} catalytic performance in the hydrogenation reaction of furfural, in the presence of gaseous H_2 as well as under CTH conditions.

Effect of reaction time

By using 2-propanol as a hydrogen source, the conversion of FUR into FAL was very high after 90 minutes and it arrived at a quantitative conversion in 3 hours of reaction at low temperature (120 °C). Data in Figure 3.18 show that at the same temperature, in the presence of gaseous H_2 (10 bar) as a reducing agent, it is possible to obtain FAL yield of 100% in a shorter reaction time (90 minutes). The hydrogenation of FUR proceeds without formation of any other products related to undesired side reactions that may occur in CTH processes (e.g., etherification, acetalization, and aldol condensation).

Effect of reaction temperature and pressure

The influence of reaction temperature on the CTH process was subsequently investigated in the range from 120 to 210 °C maintaining constant the reaction time of 90 minutes, both in the presence as well as in the

absence of added hydrogen. In Figure 3.18 the values of FAL yield % at different temperatures are reported. As expected, in all cases, the conversion of FUR increased by increasing the reaction temperature. Similar trends were observed at a fixed set temperature as a function of H_2 pressure. The quantitative yield of FAL with selectivity of 100% was reached after 150 °C. It was interesting to note that the change of reaction conditions did not affect the >99% selectivity of the catalyst, indicating that the catalyst had a high selectivity for the C=O bond in the CTH of FUR.

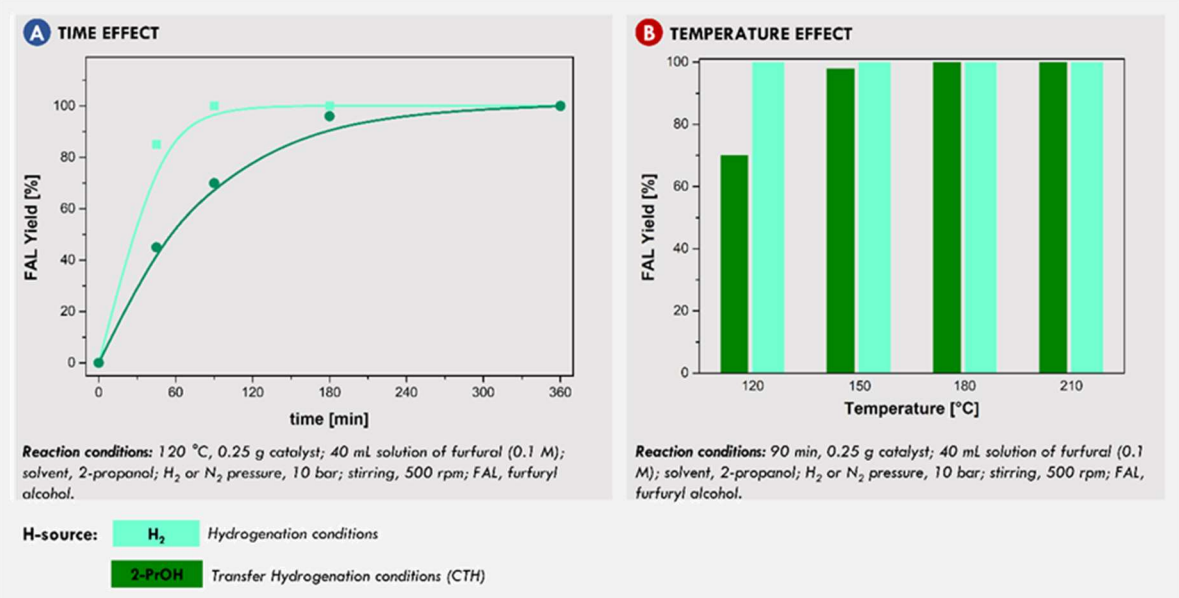

Figure 3.18. Hydrogenation of furfural promoted by the heterogeneous BMred catalyst: effect of reaction time (A) and reaction temperature (B) [129].

Effect of hydrogen donor/ solvent

The catalytic activity of BM_{red} in the transfer hydrogenation of furfural was evaluated at 120 °C using various hydrogen donor alcohols: methanol, ethanol and 2-propanol. Furfural conversion depends strongly on the alcohol and increases following the order: methanol < ethanol < 2-propanol. In particular, the conversion of FUR resulted very low in the presence of either ethanol (5%) or in methanol (1%). This result was not surprising because it is

well known that secondary alcohols are better H-donors than primary alcohols since their electron-releasing inductive effect is smaller, they have a higher reduction potential and are more polar. In addition, it was observed that, by using ethanol and methanol, the values of FUR conversion continued to remain low (12.6% and 8.3%, respectively) also in presence of H_2 (10 bar) as reducing agent. These experimental data implied that the direct transfer of hydrogen from the 2-propanol (H-donor) to FUR (H-acceptor) proceeds faster than C=O hydrogenation via metal hydride mechanism and, consequently, the conversion of FUR into FAL, in CTH conditions, occured via the Meerwein−Ponndorf−Verley (MPV) mechanism with the formation of a six-membered intermediate state.

Catalyst stability

Catalyst stability was examined carrying out catalyst recycling experiments. For each recycling test, after reaction, the catalyst was magnetically recovered with the assistant of a magnet, washed several times with 2-propanol to remove the organics adsorbed on the surface and reused after drying overnight at 80 °C. The results of recycling tests carried out at 120°C for 90 minutes demonstrated that the furfural conversion over the spent catalyst did not decrease significantly after consecutive five reaction cycles.

Based on these results, that made the black mass a promising catalyst for the hydrogenation reactions, other catalytic tests were carried out using several aldehyde and ketone substrates derived from biomass such as 5-Hydroxymethylfurfural, benzaldehyde, acetophenone, and cyclohexanone.

Data in Table 3.2 show the following results:

- 5-Hydroxymethylfurfural and acetophenone were converted after 90 min at 120 °C (100% in the presence of H_2, 98% under CTH conditions), with a selectivity of 100% to 2,5-bis(hydroxymethyl)furan and benzyl alcohol.

- ketonic derivatives (acetophenone and cyclohexanone), exhibit lower conversions than aldehydes but similar selectivity (>99%) toward the corresponding alcohols at higher temperatures (180 °C).

Table 3.2. Hydrogenation of biomass derived aldehydes and ketones promoted by the BM*red* catalyst. Reaction conditions: 0.25 g of BM*red* catalyst, 40 ml solution of desired substrate (0.1 M), solvent: 2-propanol; H_2 or N_2 pressure: 10 bar; stirring: 500 rpm

HYDROGENATION REACTION	TEMP. [°C]	TIME (min)	CONVERSION [%]	
			H_2	2-PrOH
	120	90	100	98
	120	90	100	98
	180	90	90	60
	180	90	75	35

The results of this study clearly show how the black mass derived from spent LIBs, after a proper oxidative-reductive thermal process, is a promising heterogeneous catalyst for the reductive upgrading of biomass-derived aldehydes and ketones [129].

Chapter 4

Conclusions and future perspectives

In summary, this thesis was aimed at providing a contribution to the development of heterogeneous catalytic systems for chemical and environmental engineering processes.

Catalysts, that enable reactions to be carried out in the most effective, economical, and environmentally friendly manner, are a very important part of green chemistry and sustainable processes. Actually, products can be obtained more quickly while using less resources and most of all producing less wastes, since catalysts remain unchanged after reactions and can be cyclically reused. Therefore, catalysts represent a key component in a broad range of reactions, covering very different fields. In this study the development of heterogeneous catalysts for selected processes was considered. In particular, the reforming of fuels, the methanation reaction of carbon dioxide and the reductive upgrading of biomass-derived furfural were considered.

The reactivity of the nickel catalytic systems with defined ceria zirconia compositions, undoped and doped with lanthanum and neodymium $Ce_{0.8}Zr_{0.2}O_2$ (CZ80) and $Ce_{0.8}Zr_{0.13}La_{0.5}Nd_{0.2}O_{2-x}$ (dpCZ80), was tested towards the reforming reactions: steam reforming (SR), partial oxidation (POX) and autothermal reforming (ATR) of different fuels, such as methane, biogas and propane. Catalysts were extensively characterized by various analytical techniques highlighting that: i) the insertion of lanthanum and neodymium into the fluorite structure, ii) the homogeneity distribution of the different elements in the catalysts, iii) the loading of metallic phase is very close to nominal content (3.5 ±0.2 %). Undoped and doped catalysts showed both a well-defined cubic nanomorphology with slightly reduced dimension for the doped sample, together with the absence of the segregation related to lanthanum and neodymium doping. The effect of doping on the reducibility

of the catalyst seemed to be limited to the slight anticipation of the surface reduction at low temperatures. As shown, doped catalyst just slightly improved the ATR conversion of methane, while no significant differences were promoted by doping elements for the SR of methane and in the POX condition, where the doping seemed to have a detrimental effect. As regards propane conversion, under ATR condition, it was very high for both catalysts suggesting that the combination of steam and oxygen in the reagent stream plays a decisive role in promoting catalyst activity and stability. In the SR and POX condition, higher conversions were registered for the doped catalyst compared to undoped one. The doped catalyst dispersed nickel species on the surface with a higher concentration of defect groups and oxygen vacancies (due to neodymium and lanthanum doping), thereby preventing the formation of deactivating species (amorphous carbon and nickel sulphide) and resulting in a higher resistance to deactivation.

Endurance catalytic tests confirmed the beneficial effect of the doped catalysts. Further development will interest the scale up of powdered catalysts on structured form that will be tested as anode catalysts for SOFCs/SOECs systems.

Methanation reaction of carbon dioxide is a facile solution for the storage and transportation of low-grade energies, contributing at the same time to the mitigation of CO_2 emissions. To this purpose a nickel catalyst impregnated over an innovative support, Engelhard Titanium Silicates, was tested towards the CO_2 methanation reaction. Two catalysts, ETS-4 and ETS-10, being characterized by a different titanium amount, were loaded with 5% of Nickel and their catalytic performance tested in the temperature range of 300-500°C. Multiple characterizations were performed by XRD, SEM-EDX, N_2 adsorption-desorption and H_2-TPR, that highlighted some differences in the catalysts structure. The ETS-4 was demonstrated to be not a suitable support for the Ni catalyst because of the collapse of the structure, while results

showed a potential catalytic activity of the Ni/ETS-10 catalyst, that retained its framework zeolitic structures and was characterized by the 68% of CO_2 conversion and the 98% of CH_4 selectivity at T=400°C. The comparison of catalytic performance of Ni/ETS-10 with those obtained by other Ni-zeolites catalysts confirms that Ni/ETS-10 catalyst is a promising one for the CO_2 methanation reaction.

The encouraging results obtained over ETS materials, due to their porosity features, consolidated their application in the catalysis field and further improved applications.

An outstanding example of environmental sustainability regarded the possibility to obtain benign heterogeneous catalysts from abundant and readily available spent lithium-ion batteries. In this study, it was demonstrated that black mass derived from spent batteries, after a proper oxidative-reductive thermal process, was used as an efficient cobalt based heterogeneous catalyst for the reductive upgrading of furfural and other biomass derived substrates. In particular, it was proved the full conversion of furfural in furfuryl alcohol as the only reaction product after 90 min at 120°C in the presence of molecular hydrogen under batch conditions. Under transfer hydrogenation conditions indeed, the same reactions, performed in 2-propanol, provided similar furfural conversion as well as 100 % of selectivity to furfuryl alcohols. The hydrogenation of furfural was found to be much less efficient when reactions were carried out in ethanol and methanol even in the presence of molecular hydrogen as reducing agent thus implying that the reduction of the C=O bond likely occured via the Meerwein–Ponndorf–Verley (MPV) mechanism when 2-propanol was used as solvent/H-source.

Future attempts will be aimed to better understand the physico-chemical properties of the BM reduced to highlight the nature of the active catalytic

species involved in the hydrogenation process and its recycling performance under different reaction conditions in the presence of various solvents.

References

1. Backes, J.G.; Traverso, M. Life Cycle Sustainability Assessment as a metrics towards SDGs Agenda 2030. *Curr. Opin. Green Sustain. Chem.* **2022**, 100683, doi:10.1016/j.cogsc.2022.100683.

2. Schwager, P.; Decker, N.; Kaltenegger, I. Exploring Green Chemistry, Sustainable Chemistry and innovative business models such as Chemical Leasing in the context of international policy discussions. *Curr. Opin. Green Sustain. Chem.* **2016**, *1*, 18–21, doi:10.1016/j.cogsc.2016.07.005.

3. Chen, T.L.; Kim, H.; Pan, S.Y.; Tseng, P.C.; Lin, Y.P.; Chiang, P.C. Implementation of green chemistry principles in circular economy system towards sustainable development goals: Challenges and perspectives. *Sci. Total Environ.* **2020**, *716*, 136998, doi:10.1016/j.scitotenv.2020.136998.

4. Khajuria, A.; Atienza, V.A.; Chavanich, S.; Henning, W.; Islam, I.; Kral, U.; Liu, M.; Liu, X.; Murthy, I.K.; Oyedotun, T.D.T.; et al. Accelerating circular economy solutions to achieve the 2030 agenda for sustainable development goals. *Circ. Econ.* **2022**, *1*, 100001, doi:10.1016/j.cec.2022.100001.

5. Doni, F.; Gasperini, A.; Soares, J.T. What is the SDG 13?", SDG13 – Climate Action: Combating Climate Change and its Impacts. *Concise Guid. to United Nations Sustain. Dev. Goals* **2020**, 21–30.

6. Shyu, C.W. A framework for 'right to energy' to meet UN SDG7: Policy implications to meet basic human energy needs, eradicate energy poverty, enhance energy justice, and uphold energy democracy. *Energy Res. Soc. Sci.* **2021**, *79*, 102199, doi:10.1016/j.erss.2021.102199.

7. Martins, F.F.; Felgueiras, C.; Caetano, N.S. Macro modeling of electricity price towards SDG7. *Energy Reports* **2022**, *8*, 614–622, doi:10.1016/j.egyr.2022.04.055.

8. Beach, E.S.; Cui, Z.; Anastas, P.T. Green Chemistry: A design framework for sustainability. *Energy Environ. Sci.* **2009**, *2*, 1038–1049, doi:10.1039/b904997p.

9. Vanegas Cantarero, M.M. Of renewable energy, energy democracy, and sustainable development: A roadmap to accelerate the energy transition in developing countries. *Energy Res. Soc. Sci.* **2020**, *70*, 101716, doi:10.1016/j.erss.2020.101716.

10. Sharma, S.K.; Chaudhary, A.; Singh, R. V. Gray chemistry verses green chemistry: Challenges and opportunities. *Rasayan J. Chem.* **2008**, *1*, 68–92.

11. Anastas, P.; Eghbali, N. Green Chemistry: Principles and Practice. *Chem. Soc. Rev.* **2010**, *39*, 301–312, doi:10.1039/b918763b.

12. Sheldon, R.A. The: E factor 25 years on: The rise of green chemistry and sustainability.

Green Chem. **2017**, *19*, 18–43, doi:10.1039/c6gc02157c.

13. Kirchhoff, M.M. Promoting sustainability through green chemistry. *Resour. Conserv. Recycl.* **2005**, *44*, 237–243, doi:10.1016/j.resconrec.2005.01.003.

14. Parrino, F.; Bellardita, M.; García-López, E.I.; Marcì, G.; Loddo, V.; Palmisano, L. Heterogeneous Photocatalysis for Selective Formation of High-Value-Added Molecules: Some Chemical and Engineering Aspects. *ACS Catal.* **2018**, *8*, 11191–11225, doi:10.1021/acscatal.8b03093.

15. Dosa, M.; Piumetti, M.; Bensaid, S.; Andana, T.; Galletti, C.; Fino, D.; Russo, N. Photocatalytic Abatement of Volatile Organic Compounds by TiO2 Nanoparticles Doped with Either Phosphorous or Zirconium. *Materials (Basel).* 2019, *12*.

16. Rodríguez-Padrón, D.; Puente-Santiago, A.R.; Balu, A.M.; Muñoz-Batista, M.J.; Luque, R. Environmental Catalysis: Present and Future. *ChemCatChem* **2019**, *11*, 18–38, doi:https://doi.org/10.1002/cctc.201801248.

17. Liu, L.; Corma, A. Metal Catalysts for Heterogeneous Catalysis: From Single Atoms to Nanoclusters and Nanoparticles. *Chem. Rev.* **2018**, *118*, 4981–5079, doi:10.1021/acs.chemrev.7b00776.

18. Frontera, P.; Malara, A.; Stelitano, S.; Leonardi, S.G.; Bonavita, A.; Fazio, E.; Antonucci, P.; Neri, G.; Neri, F.; Santangelo, S. Characterisation and H2O2 sensing properties of TiO2-CNTs/Pt electro-catalysts. *Mater. Chem. Phys.* **2016**, *170*, 129–137, doi:10.1016/j.matchemphys.2015.12.030.

19. Kisszékelyi, P.; Nagy, S.; Fehér, Z.; Huszthy, P.; Kupai, J. Membrane-Supported Recovery of Homogeneous Organocatalysts: A Review. *Chemistry (Easton).* 2020, *2*.

20. Xu, C.; Paone, E.; Rodríguez-Padrón, D.; Luque, R.; Mauriello, F. Reductive catalytic routes towards sustainable production of hydrogen, fuels and chemicals from biomass derived polyols. *Renew. Sustain. Energy Rev.* **2020**, *127*, 109852, doi:https://doi.org/10.1016/j.rser.2020.109852.

21. Malara, A.; Paone, E.; Bonaccorsi, L.; Mauriello, F.; Macario, A.; Frontera, P. Pd/Fe3O4 nanofibers for the catalytic conversion of lignin-derived benzyl phenyl ether under transfer hydrogenolysis conditions. *Catalysts* **2020**, *10*, 1–14, doi:10.3390/catal10010020.

22. Ren, Y.; Li, H.; Yang, W.; Shi, D.; Wu, Q.; Zhao, Y.; Feng, C.; Liu, H.; Jiao, Q. Alkaline Ionic Liquids Immobilized on Protective Copolymers Coated Magnetic Nanoparticles: An Efficient and Magnetically Recyclable Catalyst for Knoevenagel Condensation. *Ind. {\&} Eng. Chem. Res.* **2019**, *58*, 2824–2834, doi:10.1021/acs.iecr.8b05933.

23. Wang, D.; Astruc, D. Fast-Growing Field of Magnetically Recyclable Nanocatalysts. *Chem. Rev.* **2014**, *114*, 6949–6985, doi:10.1021/cr500134h.

24. Miceli, M.; Frontera, P.; Macario, A.; Malara, A. Recovery/Reuse of Heterogeneous Supported Spent Catalysts. *Catal.* 2021, *11*.

25. Johnson, C.; Ruiz Sierra, A.; Dettmer, J.; Sidiropoulou, K.; Zicmane, E.; Canalis, A.; Llorente, P.; Paiano, P.; Mengal, P.; Puzzolo, V. The Bio-Based Industries Joint

Undertaking as a catalyst for a green transition in Europe under the European Green Deal. *EFB Bioeconomy J.* **2021**, *1*, 100014, doi:10.1016/j.bioeco.2021.100014.

26. Lange, L.; Connor, K.O.; Arason, S.; Bundgård-Jørgensen, U.; Canalis, A.; Carrez, D.; Gallagher, J.; Gøtke, N.; Huyghe, C.; Jarry, B. Developing a sustainable and circular bio-based economy in EU: by partnering across sectors, upscaling and using new knowledge faster, and for the benefit of climate, environment & biodiversity, and people & business. *Front. Bioeng. Biotechnol.* **2021**, *8*, 619066.

27. Mengal, P.; Wubbolts, M.; Zika, E.; Ruiz, A.; Brigitta, D.; Pieniadz, A.; Black, S. Bio-based Industries Joint Undertaking: The catalyst for sustainable bio-based economic growth in Europe. *N. Biotechnol.* **2018**, *40*, 31–39, doi:10.1016/j.nbt.2017.06.002.

28. Subotić, V.; Hochenauer, C. Analysis of solid oxide fuel and electrolysis cells operated in a real-system environment: State-of-the-health diagnostic, failure modes, degradation mitigation and performance regeneration. *Prog. Energy Combust. Sci.* **2022**, *93*, 101011.

29. Oni, A.O.; Anaya, K.; Giwa, T.; Di Lullo, G.; Kumar, A. Comparative assessment of blue hydrogen from steam methane reforming, autothermal reforming, and natural gas decomposition technologies for natural gas-producing regions. *Energy Convers. Manag.* **2022**, *254*, 115245.

30. Steele, B.C.H.; Heinzel, A. Materials for fuel-cell technologies. In *Materials for sustainable energy: a collection of peer-reviewed research and review articles from Nature Publishing Group*; World Scientific, 2011; pp. 224–231.

31. Jacobson, A.J. Materials for solid oxide fuel cells. *Chem. Mater.* **2010**, *22*, 660–674.

32. Sengodan, S.; Lan, R.; Humphreys, J.; Du, D.; Xu, W.; Wang, H.; Tao, S. Advances in reforming and partial oxidation of hydrocarbons for hydrogen production and fuel cell applications. *Renew. Sustain. Energy Rev.* **2018**, *82*, 761–780.

33. Hecht, E.S.; Gupta, G.K.; Zhu, H.; Dean, A.M.; Kee, R.J.; Maier, L.; Deutschmann, O. Methane reforming kinetics within a Ni–YSZ SOFC anode support. *Appl. Catal. A Gen.* **2005**, *295*, 40–51.

34. Douvartzides, S.L.; Coutelieris, F.A.; Demin, A.K.; Tsiakaras, P.E. Electricity from ethanol fed SOFCs: the expectations for sustainable development and technological benefits. *Int. J. Hydrogen Energy* **2004**, *29*, 375–379.

35. Vohs, J.M.; Gorte, R.J. High-performance SOFC cathodes prepared by infiltration. *Adv. Mater.* **2009**, *21*, 943–956.

36. Gorte, R.J.; Vohs, J.M. Nanostructured anodes for solid oxide fuel cells. *Curr. Opin. Colloid Interface Sci.* **2009**, *14*, 236–244.

37. Qiu, P.; Sun, S.; Yang, X.; Chen, F.; Xiong, C.; Jia, L.; Li, J. A review on anode on-cell catalyst reforming layer for direct methane solid oxide fuel cells. *Int. J. Hydrogen Energy* **2021**, *46*, 25208–25224.

38. Liese, E.A.; Gemmen, R.S. Performance comparison of internal reforming against

external reforming in a solid oxide fuel cell, gas turbine hybrid system. *J. Eng. Gas Turbines Power* **2005**, *127*, 86–90.

39. Noureldin, M.M.B.; Elbashir, N.O.; El-Halwagi, M.M. Optimization and selection of reforming approaches for syngas generation from natural/shale gas. *Ind. Eng. Chem. Res.* **2014**, *53*, 1841–1855.

40. Zhang, H.; Sun, Z.; Hu, Y.H. Steam reforming of methane: Current states of catalyst design and process upgrading. *Renew. Sustain. Energy Rev.* **2021**, *149*, 111330.

41. Raju, A.S.K.; Park, C.S.; Norbeck, J.M. Synthesis gas production using steam hydrogasification and steam reforming. *Fuel Process. Technol.* **2009**, *90*, 330–336.

42. Teh, L.P.; Setiabudi, H.D.; Timmiati, S.N.; Aziz, M.A.A.; Annuar, N.H.R.; Ruslan, N.N. Recent progress in ceria-based catalysts for the dry reforming of methane: A review. *Chem. Eng. Sci.* **2021**, *242*, 116606.

43. Wang, M.; Zhao, T.; Dong, X.; Li, M.; Wang, H. Effects of Ce substitution at the A-site of LaNi0. 5Fe0. 5O3 perovskite on the enhanced catalytic activity for dry reforming of methane. *Appl. Catal. B Environ.* **2018**, *224*, 214–221.

44. Adijanto, L.; Padmanabhan, V.B.; Küngas, R.; Gorte, R.J.; Vohs, J.M. Transition metal-doped rare earth vanadates: a regenerable catalytic material for SOFC anodes. *J. Mater. Chem.* **2012**, *22*, 11396–11402.

45. Zanganeh, R.; Rezaei, M.; Zamaniyan, A. Dry reforming of methane to synthesis gas on NiO–MgO nanocrystalline solid solution catalysts. *Int. J. Hydrogen Energy* **2013**, *38*, 3012–3018.

46. Wei, T.; Jia, L.; Zheng, H.; Chi, B.; Pu, J.; Li, J. LaMnO3-based perovskite with in-situ exsolved Ni nanoparticles: a highly active, performance stable and coking resistant catalyst for CO2 dry reforming of CH4. *Appl. Catal. A Gen.* **2018**, *564*, 199–207.

47. Irvine, J.T.S.; Neagu, D.; Verbraeken, M.C.; Chatzichristodoulou, C.; Graves, C.; Mogensen, M.B. Evolution of the electrochemical interface in high-temperature fuel cells and electrolysers. *Nat. Energy* **2016**, *1*, 1–13.

48. Hua, B.; Li, M.; Sun, Y.; Li, J.; Luo, J. Enhancing perovskite electrocatalysis of solid oxide cells through controlled exsolution of nanoparticles. *ChemSusChem* **2017**, *10*, 3333–3341.

49. Araújo, P.M.; da Costa, K.M.; Passos, F.B. Hydrogen production from methane autothermal reforming over CaTiO3, BaTiO3 and SrTiO3 supported nickel catalysts. *Int. J. Hydrogen Energy* **2021**, *46*, 24107–24116.

50. Angeli, S.D.; Monteleone, G.; Giaconia, A.; Lemonidou, A.A. State-of-the-art catalysts for CH4 steam reforming at low temperature. *Int. J. Hydrogen Energy* **2014**, *39*, 1979–1997.

51. Elbadawi, A.H.; Ge, L.; Li, Z.; Liu, S.; Wang, S.; Zhu, Z. Catalytic partial oxidation of methane to syngas: review of perovskite catalysts and membrane reactors. *Catal. Rev.* **2021**, *63*, 1–67.

52. Ruiz, J.A.C.; Passos, F.B.; Bueno, J.M.C.; Souza-Aguiar, E.F.; Mattos, L. V; Noronha, F.B. Syngas production by autothermal reforming of methane on supported platinum catalysts. *Appl. Catal. A Gen.* **2008**, *334*, 259–267.

53. Mazza, A.; Bompard, E.; Chicco, G. Applications of power to gas technologies in emerging electrical systems. *Renew. Sustain. Energy Rev.* **2018**, *92*, 794–806.

54. Frontera, P.; Macario, A.; Ferraro, M.; Antonucci, P. Supported Catalysts for CO2 Methanation: A Review. *Catalysts* 2017, *7*.

55. Gao, R.; Zhang, C.; Jun, K.-W.; Kim, S.K.; Park, H.-G.; Zhao, T.; Wang, L.; Wan, H.; Guan, G. Green liquid fuel and synthetic natural gas production via CO2 hydrogenation combined with reverse water-gas-shift and co-based Fischer-Tropsch synthesis. *J. CO2 Util.* **2021**, *51*, 101619.

56. Malara, A.; Frontera, P.; Antonucci, P.; Macario, A. Smart recycling of carbon oxides: Current status of methanation reaction. *Curr. Opin. Green Sustain. Chem.* **2020**, *26*, doi:10.1016/j.cogsc.2020.100376.

57. Frontera, P.; Miceli, M.; Mauriello, F.; De Luca, P.; Macario, A. Investigation on the Suitability of Engelhard Titanium Silicate as a Support for Ni-Catalysts in the Methanation Reaction. *Catalysts* **2021**, *11*, 1225.

58. Dannesboe, C.; Hansen, J.B.; Johannsen, I. Catalytic methanation of CO 2 in biogas: Experimental results from a reactor at full scale. *React. Chem. Eng.* **2020**, *5*, 183–189.

59. Butera, G.; Jensen, S.H.; Clausen, L.R. A novel system for large-scale storage of electricity as synthetic natural gas using reversible pressurized solid oxide cells. *Energy* **2019**, *166*, 738–754, doi:10.1016/j.energy.2018.10.079.

60. Gorre, J.; Ruoss, F.; Karjunen, H.; Schaffert, J.; Tynjälä, T. Cost benefits of optimizing hydrogen storage and methanation capacities for Power-to-Gas plants in dynamic operation. *Appl. Energy* **2020**, *257*, 113967, doi:10.1016/J.APENERGY.2019.113967.

61. Götz, M.; Lefebvre, J.; Mörs, F.; Koch, A.M.; Graf, F.; Bajohr, S.; Reimert, R.; Kolb, T. Renewable Power-to-Gas: A technological and economic review. *Renew. energy* **2016**, *85*, 1371–1390.

62. Jürgensen, L.; Ehimen, E.A.; Born, J.; Holm-Nielsen, J.B. Dynamic biogas upgrading based on the Sabatier process: Thermodynamic and dynamic process simulation. *Bioresour. Technol.* **2015**, *178*, 323–329.

63. Lee, W.J.; Li, C.; Prajitno, H.; Yoo, J.; Patel, J.; Yang, Y.; Lim, S. Recent trend in thermal catalytic low temperature CO2 methanation: A critical review. *Catal. Today* **2020**, doi:https://doi.org/10.1016/j.cattod.2020.02.017.

64. Hillestad, M. Systematic generation of a once-through staged reactor design for direct methanation of biogas. *Chem. Eng. Process. Intensif.* **2022**, 109112.

65. Gutiérrez-Martín, F.; Rodríguez-Antón, L.M. Power-to-SNG technologies by hydrogenation of CO2 and biomass resources: a comparative chemical engineering process analysis. *Int. J. Hydrogen Energy* **2019**, *44*, 12544–12553.

66. Stangeland, K.; Kalai, D.; Li, H.; Yu, Z. CO2 methanation: the effect of catalysts and reaction conditions. *Energy Procedia* **2017**, *105*, 2022–2027.

67. Mohd Ridzuan, N.D.; Shaharun, M.S.; Anawar, M.A.; Ud-Din, I. Ni-Based Catalyst for Carbon Dioxide Methanation: A Review on Performance and Progress. *Catalysts* **2022**, *12*, 469.

68. Wang, W.; Wang, S.; Ma, X.; Gong, J. Recent advances in catalytic hydrogenation of carbon dioxide. *Chem. Soc. Rev.* **2011**, *40*, 3703–3727.

69. Younas, M.; Loong Kong, L.; Bashir, M.J.K.; Nadeem, H.; Shehzad, A.; Sethupathi, S. Recent advancements, fundamental challenges, and opportunities in catalytic methanation of CO2. *Energy & Fuels* **2016**, *30*, 8815–8831.

70. Su, X.; Xu, J.; Liang, B.; Duan, H.; Hou, B.; Huang, Y. Catalytic carbon dioxide hydrogenation to methane: A review of recent studies. *J. energy Chem.* **2016**, *25*, 553–565.

71. Rönsch, S.; Schneider, J.; Matthischke, S.; Schlüter, M.; Götz, M.; Lefebvre, J.; Prabhakaran, P.; Bajohr, S. Review on methanation–From fundamentals to current projects. *Fuel* **2016**, *166*, 276–296.

72. Vita, A.; Italiano, C.; Pino, L.; Frontera, P.; Ferraro, M.; Antonucci, V. Activity and stability of powder and monolith-coated Ni/GDC catalysts for CO2 methanation. *Appl. Catal. B Environ.* **2018**, *226*, 384–395, doi:10.1016/j.apcatb.2017.12.078.

73. Petrus, L.; Noordermeer, M.A. Biomass to biofuels, a chemical perspective. *Green Chem.* **2006**, *8*, 861–867, doi:10.1039/b605036k.

74. Besson, M.; Gallezot, P.; Pinel, C. Conversion of biomass into chemicals over metal catalysts. *Chem. Rev.* **2014**, *114*, 1827–1870, doi:10.1021/cr4002269.

75. Mika, L.T.; Cséfalvay, E.; Németh, Á. Catalytic Conversion of Carbohydrates to Initial Platform Chemicals: Chemistry and Sustainability. *Chem. Rev.* **2018**, *118*, 505–613, doi:10.1021/acs.chemrev.7b00395.

76. Serrano-Ruiz, J.C.; Luque, R.; Sepúlveda-Escribano, A. Transformations of biomass-derived platform molecules: From high added-value chemicals to fuels via aqueous-phase processing. *Chem. Soc. Rev.* **2011**, *40*, 5266–5281, doi:10.1039/c1cs15131b.

77. He, J.; Schill, L.; Yang, S.; Riisager, A. Catalytic Transfer Hydrogenation of Bio-Based Furfural with NiO Nanoparticles. *ACS Sustain. Chem. Eng.* **2018**, *6*, 17220–17229, doi:10.1021/acssuschemeng.8b04579.

78. Xu, C.; Paone, E.; Rodríguez-Padrón, D.; Luque, R.; Mauriello, F. Recent catalytic routes for the preparation and the upgrading of biomass derived furfural and 5-hydroxymethylfurfural. *Chem. Soc. Rev.* **2020**, *49*, 4273–4306, doi:10.1039/d0cs00041h.

79. Deng, W.; Feng, Y.; Fu, J.; Guo, H.; Guo, Y.; Han, B.; Jiang, Z.; Kong, L.; Li, C.; Liu, H.; et al. Catalytic conversion of lignocellulosic biomass into chemicals and fuels. *Green Energy Environ.* **2022**, doi:10.1016/j.gee.2022.07.003.

80. Wang, F.; Ouyang, D.; Zhou, Z.; Page, S.J.; Liu, D.; Zhao, X. Lignocellulosic biomass as sustainable feedstock and materials for power generation and energy storage. *J. Energy Chem.* **2021**, *57*, 247–280, doi:10.1016/j.jechem.2020.08.060.

81. Singh, S.K. Heterogeneous Bimetallic Catalysts for Upgrading Biomass-Derived Furans. *Asian J. Org. Chem.* **2018**, *7*, 1901–1923, doi:10.1002/ajoc.201800307.

82. He, J.; Qiang, Q.; Liu, S.; Song, K.; Zhou, X.; Guo, J.; Zhang, B.; Li, C. Upgrading of biomass-derived furanic compounds into high-quality fuels involving aldol condensation strategy. *Fuel* **2021**, *306*, 121765, doi:10.1016/j.fuel.2021.121765.

83. Amalina, F.; Syukor Abd Razak, A.; Krishnan, S.; Sulaiman, H.; Zularisam, A.W.; Nasrullah, M. Advanced techniques in the production of biochar from lignocellulosic biomass and environmental applications. *Clean. Mater.* **2022**, *6*, 100137, doi:10.1016/j.clema.2022.100137.

84. Gupta, K.; Rai, R.K.; Singh, S.K. Metal Catalysts for the Efficient Transformation of Biomass-derived HMF and Furfural to Value Added Chemicals. *ChemCatChem* **2018**, *10*, 2326–2349, doi:10.1002/cctc.201701754.

85. Yang, Z.; Zhang, J.; Qian, G.; Duan, X.; Zhou, X. Production of biomass-derived monomers through catalytic conversion of furfural and hydroxymethylfurfural. *Green Chem. Eng.* **2021**, *2*, 158–173, doi:10.1016/j.gce.2020.11.001.

86. Liu, B.; Zhang, Z. One-pot conversion of carbohydrates into furan derivatives via furfural and 5-hydroxylmethylfurfural as intermediates. *ChemSusChem* **2016**, *9*, 2015–2036, doi:10.1002/cssc.201600507.

87. Valekar, A.H.; Lee, M.; Yoon, J.W.; Kwak, J.; Hong, D.Y.; Oh, K.R.; Cha, G.Y.; Kwon, Y.U.; Jung, J.; Chang, J.S.; et al. Catalytic Transfer Hydrogenation of Furfural to Furfuryl Alcohol under Mild Conditions over Zr-MOFs: Exploring the Role of Metal Node Coordination and Modification. *ACS Catal.* **2020**, *10*, 3720–3732, doi:10.1021/acscatal.9b05085.

88. Wang, Y.; Zhao, D.; Rodríguez-Padrón, D.; Len, C. Recent advances in catalytic hydrogenation of furfural. *Catalysts* **2019**, *9*, doi:10.3390/catal9100796.

89. Gilkey, M.J.; Xu, B. Heterogeneous Catalytic Transfer Hydrogenation as an Effective Pathway in Biomass Upgrading. *ACS Catal.* **2016**, *6*, 1420–1436, doi:10.1021/acscatal.5b02171.

90. Chuah, G.; Jaenicke, S.; Zhu, Y.; Liu, S. Meerwein-Ponndorf-Verley Reduction over Heterogeneous Catalysts. *Curr. Org. Chem.* **2006**, *10*, 1639–1654, doi:10.2174/138527206778249621.

91. Tabanelli, T.; Vásquez, P.B.; Paone, E.; Pietropaolo, R.; Dimitratos, N.; Cavani, F.; Mauriello, F. Improved Catalytic Transfer Hydrogenation of Levulinate Esters with Alcohols over ZrO2 Catalyst. **2020**, 28, doi:10.3390/eccs2020-07585.

92. Li, S.; Fan, Y.; Wu, C.; Zhuang, C.; Wang, Y.; Li, X.; Zhao, J.; Zheng, Z. Selective hydrogenation of furfural over the co-based catalyst: A subtle synergy with Ni and Zn

dopants. *ACS Appl. Mater. Interfaces* **2021**, *13*, 8507–8517, doi:10.1021/acsami.1c01436.

93. Wang, G.; Deng, X.; Gu, D.; Chen, K.; Tüysüz, H.; Spliethoff, B.; Bongard, H.; Weidenthaler, C.; Schmidt, W.; Schüth, F. Co3O4 Nanoparticles Supported on Mesoporous Carbon for Selective Transfer Hydrogenation of α, β-Unsaturated Aldehydes. *Angew. Chemie Int. Ed.* **2016**, *55*, 11101–11105.

94. Deutschmann, O.; Knözinger, H.; Kochloefl, K.; Turek, T. Heterogeneous catalysis and solid catalysts, 1. Fundamentals. *Ullmann's Encycl. Ind. Chem.* **2000**.

95. Moulijn, J.A.; van Leeuwen, P.W.N.M.; van Santen, R.A. *Catalysis: an integrated approach to homogeneous, heterogeneous and industrial catalysis*; Elsevier, 1993; ISBN 0080886981.

96. Goldstein, J.I.; Newbury, D.E.; Michael, J.R.; Ritchie, N.W.M.; Scott, J.H.J.; Joy, D.C. *Scanning electron microscopy and X-ray microanalysis*; Springer, 2017; ISBN 1493966766.

97. Chauhan, A.; Chauhan, P. Powder XRD technique and its applications in science and technology. *J Anal Bioanal Tech* **2014**, *5*, 1–5.

98. Loganathan, S.; Valapa, R.B.; Mishra, R.K.; Pugazhenthi, G.; Thomas, S. Thermogravimetric analysis for characterization of nanomaterials. In *Thermal and Rheological Measurement Techniques for Nanomaterials Characterization*; Elsevier, 2017; pp. 67–108.

99. Hurst, N.W.; Gentry, S.J.; Jones, A.; McNicol, B.D. Temperature programmed reduction. *Catal. Rev. Sci. Eng.* **1982**, *24*, 233–309.

100. Walton, K.S.; Snurr, R.Q. Applicability of the BET method for determining surface areas of microporous metal− organic frameworks. *J. Am. Chem. Soc.* **2007**, *129*, 8552–8556.

101. Gregg, S.J.; Sing, K.S.W.; Salzberg, H.W. Adsorption surface area and porosity. *J. Electrochem. Soc.* **1967**, *114*, 279Ca.

102. Macario, A.; Frontera, P.; Candamano, S.; Crea, F.; Luca, P. De; Antonucci, P.L. Nanostructured catalysts for dry-reforming of methane. *J. Nanosci. Nanotechnol.* **2019**, *19*, 3135–3147.

103. Song, Y.; Ozdemir, E.; Ramesh, S.; Adishev, A.; Subramanian, S.; Harale, A.; Albuali, M.; Fadhel, B.A.; Jamal, A.; Moon, D. Dry reforming of methane by stable Ni–Mo nanocatalysts on single-crystalline MgO. *Science (80-.).* **2020**, *367*, 777–781.

104. Cheekatamarla, P.K.; Finnerty, C.M. Reforming catalysts for hydrogen generation in fuel cell applications. *J. Power Sources* **2006**, *160*, 490–499.

105. Ni, M.; Leung, D.Y.C.; Leung, M.K.H. A review on reforming bio-ethanol for hydrogen production. *Int. J. Hydrogen Energy* **2007**, *32*, 3238–3247.

106. Dhanala, V.; Maity, S.K.; Shee, D. Roles of supports (γ-Al 2 O 3, SiO 2, ZrO 2) and performance of metals (Ni, Co, Mo) in steam reforming of isobutanol. *RSC Adv.* **2015**, *5*, 52522–52532.

107. Frontera, P.; Macario, A.; Aloise, A.; Crea, F.; Antonucci, P.L.; Nagy, J.B.; Frusteri, F.;

Giordano, G. Catalytic dry-reforming on Ni–zeolite supported catalyst. *Catal. Today* **2012**, *179*, 52–60.

108. Profeti, L.P.R.; Ticianelli, E.A.; Assaf, E.M. Production of hydrogen via steam reforming of biofuels on Ni/CeO2–Al2O3 catalysts promoted by noble metals. *Int. J. Hydrogen Energy* **2009**, *34*, 5049–5060.

109. Pawelec, B.; Damyanova, S.; Arishtirova, K.; Fierro, J.L.G.; Petrov, L. Structural and surface features of PtNi catalysts for reforming of methane with CO2. *Appl. Catal. A Gen.* **2007**, *323*, 188–201.

110. Frontera, P.; Macario, A.; Candamano, S.; Crea, F.; Barberio, M.; Antonucci, P.L. Alkaline-promoted zeolites for methane dry-reforming catalyst preparation. *Adv. Sci. Lett.* **2017**, *23*, 5883–5885.

111. Frontera, P.; Macario, A.; Aloise, A.; Antonucci, P.L.; Giordano, G.; Nagy, J.B. Effect of support surface on methane dry-reforming catalyst preparation. *Catal. Today* **2013**, *218–219*, 18–29, doi:https://doi.org/10.1016/j.cattod.2013.04.029.

112. Nguyen, T.G.H.; Sakamoto, M.; Uchida, T.; Doan, D.C.T.; Dang, M.C.; Tu, P.H.; Sasaki, K.; Shiratori, Y. Development of paper-structured catalyst for application to direct internal reforming solid oxide fuel cell fueled by biogas. *Int. J. Hydrogen Energy* **2019**, *44*, 10484–10497.

113. Wang, Y.; Zhang, R.; Yan, B. Ni/Ce0. 9Eu0. 1O1. 95 with enhanced coke resistance for dry reforming of methane. *J. Catal.* **2022**, *407*, 77–89.

114. Sartoretti, E.; Novara, C.; Chiodoni, A.; Giorgis, F.; Piumetti, M.; Bensaid, S.; Russo, N.; Fino, D. Nanostructured ceria-based catalysts doped with La and Nd: How acid-base sites and redox properties determine the oxidation mechanisms. *Catal. Today* **2022**, *390*, 117–134.

115. Pappacena, A.; Schermanz, K.; Sagar, A.; Aneggi, E.; Trovarelli, A. Development of a modified co-precipitation route for thermally resistant, high surface area ceria-zirconia based solid solutions. In *Studies in Surface Science and Catalysis*; Elsevier, 2010; Vol. 175, pp. 835–838 ISBN 0167-2991.

116. Zhang, Q.; Yu, J.; Corma, A. Applications of zeolites to C1 chemistry: recent advances, challenges, and opportunities. *Adv. Mater.* **2020**, *32*, 2002927.

117. Westermann, A.; Azambre, B.; Bacariza, M.C.; Graça, I.; Ribeiro, M.F.; Lopes, J.M.; Henriques, C. The promoting effect of Ce in the CO2 methanation performances on NiUSY zeolite: A FTIR In Situ/Operando study. *Catal. Today* **2017**, *283*, 74–81, doi:https://doi.org/10.1016/j.cattod.2016.02.031.

118. Philippou, A.; Naderi, M.; Pervaiz, N.; Rocha, J.; Anderson, M.W. n-hexane reforming reactions over basic Pt-ETS-10 and Pt-ETAS-10. *J. Catal.* **1998**, *178*, 174–181.

119. Medrano, J.A.; Garofalo, A.; Donato, L.; Basile, F.; De Santo, M.P.; Gallucci, F.; Cofone, F.; Ciuchi, F.; Algieri, C. CO selective oxidation using catalytic zeolite membranes. *Chem. Eng. J.* **2018**, *351*, 40–47.

120. Fu, W.; Yin, C.; Feng, Y.; Zhang, L.; Cheng, F.; Fang, Z.; Zhu, C.; Tang, T. Synergistic catalysis of the Brönsted acid and highly dispersed Cu on the mesoporous Beta zeolite in the intermolecular aminoazidation of styrene. *Appl. Catal. A Gen.* **2021**, *609*, 117907.

121. Anderson, M.W.; Terasaki, O.; Ohsuna, T.; Malley, P.J.O.; Philippou, A.; MacKay, S.P.; Ferreira, A.; Rocha, J.; Lidin, S. Microporous titanosilicate ETS-10: a structural survey. *Philos. Mag. B* **1995**, *71*, 813–841.

122. Aziz, M.A.A.; Jalil, A.A.; Triwahyono, S.; Mukti, R.R.; Taufiq-Yap, Y.H.; Sazegar, M.R. Highly active Ni-promoted mesostructured silica nanoparticles for CO2 methanation. *Appl. Catal. B Environ.* **2014**, *147*, 359–368.

123. Tang, T.; Zhang, L.; Fu, W.; Ma, Y.; Xu, J.; Jiang, J.; Fang, G.; Xiao, F.-S. Design and synthesis of metal sulfide catalysts supported on zeolite nanofiber bundles with unprecedented hydrodesulfurization activities. *J. Am. Chem. Soc.* **2013**, *135*, 11437–11440.

124. Cruciani, G.; De Luca, P.; Nastro, A.; Pattison, P. Rietveld refinement of the zorite structure of ETS-4 molecular sieves. *Microporous mesoporous Mater.* **1998**, *21*, 143–153.

125. Wei, L.; Haije, W.; Kumar, N.; Peltonen, J.; Peurla, M.; Grenman, H.; de Jong, W. Influence of nickel precursors on the properties and performance of Ni impregnated zeolite 5A and 13X catalysts in CO2 methanation. *Catal. Today* **2021**, *362*, 35–46.

126. Bal, R.; Chaudhari, K.; Srinivas, D.; Sivasanker, S.; Ratnasamy, P. Redox and catalytic chemistry of Ti in titanosilicate molecular sieves: an EPR investigation. *J. Mol. Catal. A Chem.* **2000**, *162*, 199–207.

127. Hu, X.; Mousa, E.; Tian, Y.; Ye, G. Recovery of Co, Ni, Mn, and Li from Li-ion batteries by smelting reduction-Part I: A laboratory-scale study. *J. Power Sources* **2021**, *483*, 228936.

128. Paone, E.; Miceli, M.; Malara, A.; Ye, G.; Mousa, E.; Bontempi, E.; Frontera, P.; Mauriello, F. Direct Reuse of Spent Lithium-Ion Batteries as an Efficient Heterogeneous Catalyst for the Reductive Upgrading of Biomass-Derived Furfural. *ACS Sustain. Chem. Eng.* **2022**, *10*, 2275–2281.

129. Pinegar, H.; Marthi, R.; Yang, P.; Smith, Y.R. Reductive Thermal Treatment of LiCoO2 from End-of-Life Lithium-Ion Batteries with Hydrogen. *ACS Sustain. Chem. Eng.* **2021**, *9*, 7447–7453.

130. Jung, D.-H.; Umirov, N.; Kim, T.; Bakenov, Z.; Kim, J.S.; Kim, S.S. Thermal and structural stabilities of LixCoO2 cathode for Li secondary battery studied by a temperature programmed reduction. **2019**.

131. Bulavchenko, O.A.; Gerasimov, E.Y.; Afonasenko, T.N. Reduction of double manganese–cobalt oxides: in situ XRD and TPR study. *Dalt. Trans.* **2018**, *47*, 17153–17159.

132. Lo Faro, M.; Modafferi, V.; Frontera, P.; Antonucci, P.; Aricò, A.S. Catalytic behavior of Ni-modified perovskite and doped ceria composite catalyst for the conversion of

odorized propane to syngas. *Fuel Process. Technol.* **2013**, *113*, 28–33, doi:10.1016/j.fuproc.2013.03.010.

133. Frontera, P.; Antonucci, P.L.; Macario, A. Focus on Materials for Sulfur-Resistant Catalysts in the Reforming of Biofuels. *Catalysts* **2021**, *11*, 1029.

134. Faro, M. Lo; Antonucci, V.; Antonucci, P.L.; Aricò, A.S. Fuel flexibility: A key challenge for SOFC technology. *Fuel* **2012**, *102*, 554–559.

135. Pino, L.; Vita, A.; Cipitì, F.; Lagana, M.; Recupero, V. Performance of Pt/CeO2 catalyst for propane oxidative steam reforming. *Appl. Catal. A Gen.* **2006**, *306*, 68–77.

136. Feret, F.R. Determination of the crystallinity of calcined and graphitic cokes by X-ray diffraction. *Analyst* **1998**, *123*, 595–600.

137. Menon, P.G. Coke on catalysts-harmful, harmless, invisible and beneficial types. *J. Mol. Catal.* **1990**, *59*, 207–220.

138. Argyle, M.D.; Bartholomew, C.H. Heterogeneous Catalyst Deactivation and Regeneration: A Review. *Catalysts* 2015, *5*.

139. Illeková, E.; Csomorová, K. Kinetics of oxidation in various forms of carbon. *J. Therm. Anal. Calorim.* **2005**, *80*, 103–108.

140. Xu, L.; Yang, H.; Chen, M.; Wang, F.; Nie, D.; Qi, L.; Lian, X.; Chen, H.; Wu, M. CO2 methanation over Ca doped ordered mesoporous Ni-Al composite oxide catalysts: The promoting effect of basic modifier. *J. CO2 Util.* **2017**, *21*, 200–210.

141. Lu, H.; Yang, X.; Gao, G.; Wang, J.; Han, C.; Liang, X.; Li, C.; Li, Y.; Zhang, W.; Chen, X. Metal (Fe, Co, Ce or La) doped nickel catalyst supported on ZrO2 modified mesoporous clays for CO and CO2 methanation. *Fuel* **2016**, *183*, 335–344.

142. Pan, J.-M.; Madey, T.E. The encapsulation of Fe on TiO2 (110). *Catal. Letters* **1993**, *20*, 269–274.

143. Van de Loosdrecht, J.; Van Der Kraan, A.M.; Van Dillen, A.J.; Geus, J.W. Metal-support interaction: titania-supported and silica-supported nickel catalysts. *J. Catal.* **1997**, *170*, 217–226.

144. Goodarzi, F.; Kang, L.; Wang, F.R.; Joensen, F.; Kegnæs, S.; Mielby, J. Methanation of Carbon Dioxide over Zeolite-Encapsulated Nickel Nanoparticles. *ChemCatChem* **2018**, *10*, 1566–1570.

145. Liang, C.; Zhang, L.; Zheng, Y.; Zhang, S.; Liu, Q.; Gao, G.; Dong, D.; Wang, Y.; Xu, L.; Hu, X. Methanation of CO2 over nickel catalysts: Impacts of acidic/basic sites on formation of the reaction intermediates. *Fuel* **2020**, *262*, 116521.

146. Yu, Q.; Zhang, L.; Guo, R.; Sun, J.; Fu, W.; Tang, T.; Tang, T. Catalytic performance of CoMo catalysts supported on mesoporous ZSM-5 zeolite-alumina composites in the hydrodesulfurization of 4, 6-dimethyldibenzothiophene. *Fuel Process. Technol.* **2017**, *159*, 76–87.

147. Varilla, L.A.; Seriani, N.; Montoya, J.A. Molecular adsorption and dissociation of CO2

on TiO2 anatase (001) activated by oxygen vacancies. *J. Mol. Model.* **2019**, *25*, 1–8.

Other activities

Scientific production

- **Miceli M**, Frontera P, Macario A, Malara A. **Recovery/Reuse of Heterogeneous Supported Spent Catalysts**. *Catal* . 2021;11(5). doi:10.3390/catal11050591.

- Frontera P, **Miceli M**, Mauriello F, De Luca P, Macario A. **Investigation on the Suitability of Engelhard Titanium Silicate as a Support for Ni-Catalysts in the Methanation Reaction**. *Catalysts*. 2021;11(10):1225.

- Paone E, **Miceli M**, Malara A, Ye G, Mousa E, Bontempi E, Frontera P and Mauriello F, **Direct Reuse of Spent Lithium-Ion Batteries as an Efficient Heterogeneous Catalyst for the Reductive Upgrading of Biomass-Derived Furfural**. *ACS Sustain Chem Eng*. 2022;10(7):2275-2281.

- Malara A, **Miceli M**, Frontera P e Macario A, **CO_2 methanation process over Ni supported titanolicate catalyst**, Proceedings by Springer in the ASTI series 2021, (under publishing).

- Frontera P, Malara A, Macario A, Miceli M, Bonaccorsi L, Antonucci PL and Boaro M, **Performance and stability of doped Ceria-Zirconia catalyst for a multifuel reforming,** submitted to International Journal of Hydrogen Energy.

Attendance at conferences

- "*SICHEM WINTER SCHOOL 2020"- Sustainable Industrial Chemistry,* dal 4 al 6 febbraio 2020 presso l'Università di Bologna- Dipartimento di Chimica Industriale Toso Montanari.

- XII Congresso AICIng, Reggio Calabria 5-8 Settembre 2021. Poster: "***Ex-solved Ni perovskite as catalyst for ethanol reforming*", M. Miceli**, Angela Malara, Marta Boaro, Patrizia Frontera.

- XXVII Congresso Nazionale della Società Chimica Italiana", dal 14 al 23 settembre 2021. Oral: "***Titaniosilicalite as Nickel Support for Methanation Reaction*" M. Miceli**, A. Malara, P. Frontera, A. Macario

- Co-author **"Catalytic performance of Ni-supported on ETS-silicates for CO_2 methanation reaction"**, P.Frontera, A. Malara, **M. Miceli**, P. De Luca, A. Macario), XVI Convegno Nazionale AIMAT 2021, Cagliari, Italia 15-18 Settembre 2021

- Co-author **"Spent Lithium-Cobalt Batteries: Efficient Heterogeneous Catalyst for the Reductive Upgrading of Biomass Derived Furan"** (E. Paone, **M. Miceli**, P. Frontera, F. Mauriello, G. Ye, E. Mousa, E. Bontempi e A. Malara), New-Times – New Trends in Materials Science and Engineering, Virtual Conference

- Co-author **"CO_2 methanation process over Ni supported Titaniosilicate catalyst"** (A. Malara, **M. Miceli**, P. Frontera e A. Macario), 10-13 giugno 2021. 3rd Euro-Mediterranean Conference for Environmental Integration (EMCEI-2021), Virtual Conference

- Co-author **"Spent Lithium-Ion batteries: from waste to an efficient heterogeneous catalyst for the reductive upgrading of biomass-derived furfural"** E. Paone, **M. Miceli**, A. Malara, G.Ye, E. Mousa, E. Bontempi, P. Frontera, F. Mauriello. SUM2022, sixth symposium on circular economy and urban mining, 18-20 May 2022, Capri, Italy

- Co-author **"From Spent Lithium-Ion Batteries to a Heterogeneous Co-Ni Catalyst for the Reductive Upgrading of Biomass-derived furanics"** E. Paone, **M. Miceli**, A. Malara, G. Ye, E. Mousa, E. Bontempi, P. Frontera, F. Mauriello, CORFU 2022, 9th International Conference on Sustainable Solid Waste Management, 15-18 June 2022, Corfù